MECHANICAL DEFORMATION OF APERIODIC ORGANIC SYSTEMS IN RESPONSE TO ELECTROSTATIC FIELDS: MOLECULAR PIEZOELECTRICITY

by

Keith Werling

B.S. in Chemistry,

University of Pittsburgh

Submitted to the Graduate Faculty of

the Dietrich School of Arts and Sciences in partial fulfillment

of the requirements for the degree of

Doctor of Philosophy

University of Pittsburgh

2019

UNIVERSITY OF PITTSBURGH

DIETRICH SCHOOL OF ARTS AND SCIENCES

This dissertation was presented

by

Keith Werling

It was defended on

June 3, 2019

and approved by

D. Lambrecht, Ph.D., Assistant Professor

G. Hutchison, Ph.D., Associate Professor

K. Jordan, Ph.D., Richard King Mellon Professor and Distinguished Professor of Computational Chemistry

D. Yaron, Ph.D., Professor

Dissertation Director: D. Lambrecht, Ph.D., Assistant Professor

MECHANICAL DEFORMATION OF APERIODIC ORGANIC SYSTEMS IN RESPONSE TO ELECTROSTATIC FIELDS: MOLECULAR PIEZOELECTRICITY

Keith Werling, PhD

University of Pittsburgh, 2019

Piezoelectricity as a bulk phenomenon in crystals is well understood from scientific, mathematical and engineering perspectives and has found wide use in many devices that convert electrical to mechanical energy or vice versa. Many strong piezoelectric compounds are inorganic, stiff ceramics that possess large piezoelectric coefficients but may have non-ideal properties for some applications e.g. related to cost, toxicity, biocompatibility, and incidence of fracture over time. Currently work is being done to create flexible and soft piezoelectric materials from organic compounds to make new, smart materials that could be used in medical, industrial, robotic and other technological applications. To this end the ability to screen for good organic piezoelectrics is necessary and requires a fundamental understanding of piezoelectricity at the molecular and nanoscale level. At the heart of macroscopic piezoelectric properties are inter- and intramolecular interactions and the different deformation response properties of these interactions in an applied electric field. This thesis investigates the linear response properties of molecules and small (aperiodic) systems the building blocks for macroscopic and nano-scale piezoelectric materials and develops methods and formalisms with roots in strain theory to help better understand which types of inter- and intramolecular interactions are best suited to yield piezoelectric systems with specifically tailored responses to applied electric fields. At the same time, the methods and formalism presented here have potential applications in the control of nanomachines via electric fields.

TABLE OF CONTENTS

LIST OF TABLES

LIST OF FIGURES

LIST OF EQUATIONS

1.0 INTRODUCTION: GOAL OF THIS WORK

There is a growing need to utilize energy more efficiently and recover "wasted" energy from common daily activities–such as from driving, industrial processes, ambient background vibrations, heat dissipation, among others. This motivation is commonly posed in the vein of reducing the shared carbon footprint of our growing technological society and to limit our negative impact on the environment. At the same time, there is an increased need in medical, industrial, educational, and entertainment industries, among others, for stimuli-responsive materials with new properties like biocompatibility, flexibility, low weight, and high durability to tackle the challenges and demands of modern society. A major part of nearly any large scale process or delicate procedure is the use of mechanical energy to perform useful work. Piezoelectric materials, as will be discussed in the coming sections, offer an exciting opportunity to take advantage of different mechanical processes to generate electrical potentials which may be used as signals (such as in artificial cochleas) or in energy harvesting[2–6]. Conversely, they can convert applied electrical potentials into useful mechanical work as actuators, which can be used to control the motion of microelectromechanical machines (MEMS), nanomachines, and artificial muscles or organs[7–12].

Piezoelectricity is inherently a bulk phenomenon usually ascribed to crystals with no inversion symmetry and polar order, and piezolectrics are currently used widely in many different applications. Quartz crystals may be cut into different shapes and sizes and the "breathing" of these crystals can produce an electrical signal of such reliable frequency that digital watches keep time this way. Piezoelectric pickups on guitars are used either when the strings are not metal (and so, cannot work with magnetic pickups) or to avoid the background "hum" from local magnetic fields that are not produced by the vibrations of the strings. Piezoelectric transducers are used to control the position of tips in scanning

tunneling microscopes and other imaging technology. Other currrent work is to convert ambient background vibrations into stored electrical energy[13,14]. These are just some of a vast number of applications already in use or being considered for piezoelectric materials[15–19].

Many of the "strong" (ie. high piezoelectric coefficient) piezoelectric materials are inorganic ceramics like barium titanate, lead zirconate titanate (PZT), and zinc oxide, among many more[20–22]. The main goal of this work is to explore the microscopic causes of piezoelectricity from inter- and intramolecular interactions primarily for the use in screening for "good" organic piezoelectric materials – though much of this work can be extended to general systems. The last section of this chapter discusses why organic piezoelectric systems are interesting to study and their possible advantages over inorganics. We would like to be able to qualitatively and semi-quantitatively predict the piezoelectric response of a material computationally using modern quantum chemistry approaches to identify organic compounds and which molecular interactions (hydrogen bonding, dipole-dipole, dipole-induced dipole, etc.) yield high response to help guide the design of materials. To this end, we explore the viability of using quantum chemistry software to predict electromechanical properties of molecules and finite systems to identify which features (ie. types of bonds or molecular inter- or intramolecular interactions) convey strong piezoelectricity. But moreover, from this work we can accurately (within the confines of the wave function or density functional theory method) predict the deformation properties of molecules and finite systems under applied electric fields, which should have wide applicability in the control of nanomachines and other aperiodic nanoscale systems.

1.1 WHAT IS PIEZOELECTRICITY?

Piezoelectric materials are a class of materials that exhibit coupling between electrical and mechanical stimuli[23]. More specifically, the piezoelectric coefficients quantify the linear coupling of electroelastic materials – i.e. small deformations in the limit of small electric fields as opposed to large deformations in finite fields. Piezoelectric compounds are ubiquitous in nature, for example bone, collagen, proteins, crystals, and a multitude of human tissues and

in industry, for example zinc oxide, lead zirconate titanate (PZT), and polyvinylidene difluoriede (PVDF)[24–26]. Piezoelectrics have long been used in a number of devices: transducers for the interconversion of electrical and mechanical energy, resonators and filters for very precise timings and general frequency control, and also as acoustic wave sensors[23].

When piezoelectric materials are compressed or deformed in some manner, they become polarized and a difference in electrical potential can be measured as a voltage across opposing surfaces. This is known as the direct piezoelectric effect. This process is due to either the reorientation of dipoles and their corresponding Weiss domains (local areas of similar dipole density) under applied stress or a local change in the environment surrounding the domains. Conversely, piezoelectric materials are also deformed in response to an applied electric field. This deformation is due to the field interacting with the molecular electrostatic moments (both static and induced). This is known as the converse piezoelectric effect. The direct and converse piezoelectric effect are illustrated for a material in Fig. 1 and Fig. 2 respectively. For a more thorough introduction into piezoelectricity, we refer the reader to Refs.[23] and [27].

1.1.1 Microscopic origins of piezoelectricity

All physical bodies of interest to the discussion of piezoelectric materials are polarizable within an electric field. This is a natural consequence of the atomistic nature of all materials (i.e. the positive nuclei and negative electrons of molecules experience opposite forces in an electric field).

At the microscopic level, there are a number of types of polarizations possible in chemical systems – as shown in Fig. 3[23]. In the case of piezoelectricity, by polarization, we refer to the dipole moment density, which is a vector field in the material that can be viewed as the sum of individual dipole moments in the material per given unit of volume at a point in the material. The field causes charges to separate and induces local dipole moments in addition to the permanent dipole moments. Any of the types of polarization are the result of the fact that negative and positive charges experience opposite forces when placed in an electric field. The *electronic polarization* of atoms refers to the distortion of the electron "cloud"

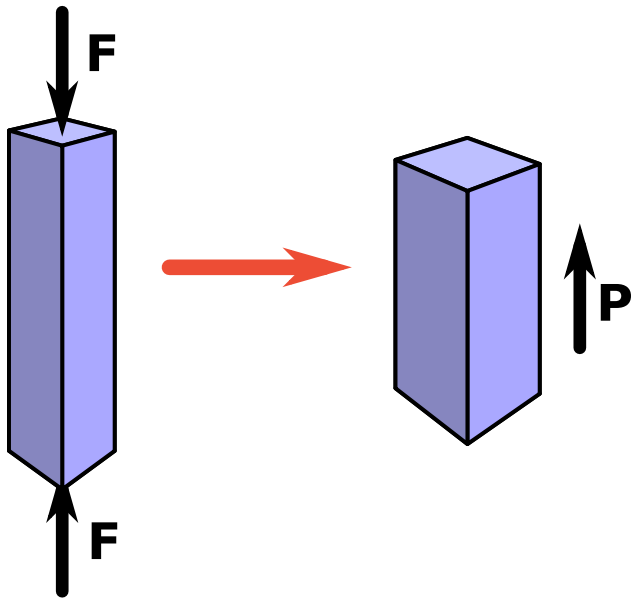

Figure 1: The direct piezoelectric effect. Deformation of a piezoelectric crystal (via force **F**) results in a net polarization (**P**) that can be measured as a voltage or charge separation accross opposing faces.

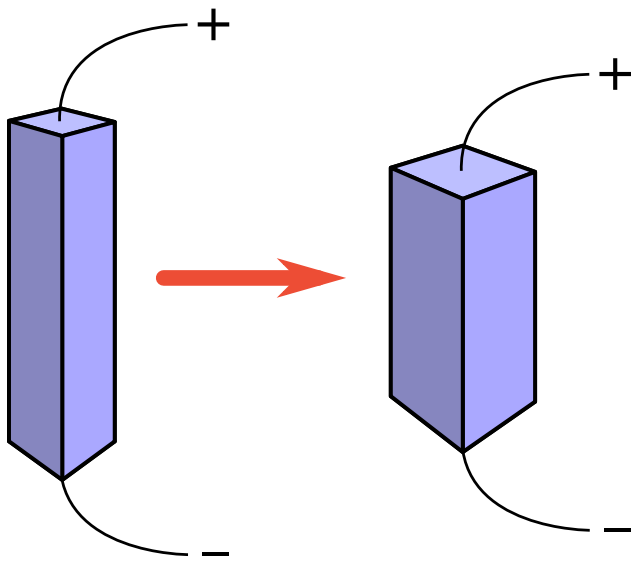

Figure 2: The converse piezoelectric effect. The application of an applied electric field leads to the deformation of the piezoelectric crystal.

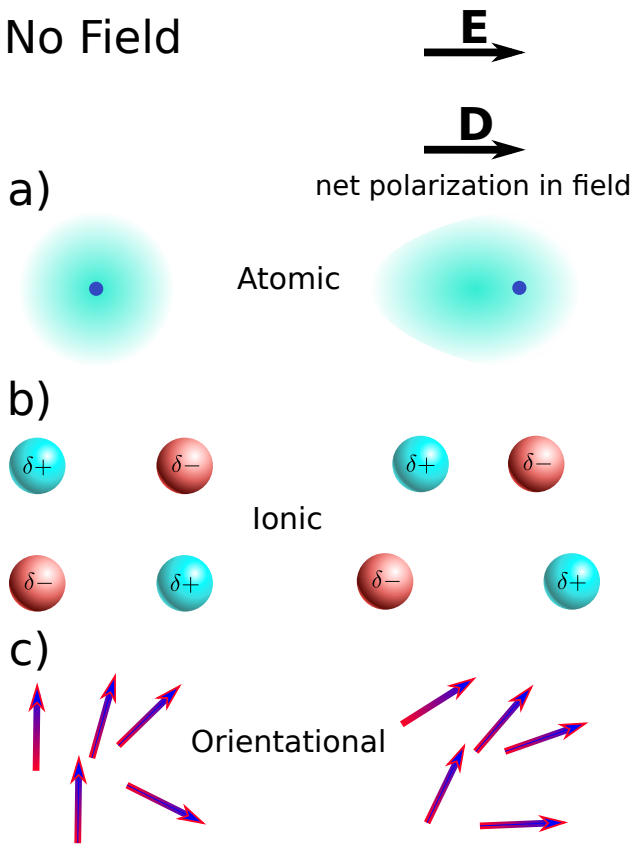

Figure 3: Types of microscopic polarization a) electronic polarization of atoms, b) polarization of ions within ionic crystal, c) orientational polarization[23]. The net polarization vector and electric field vector are given by **D** and **E** respectively.

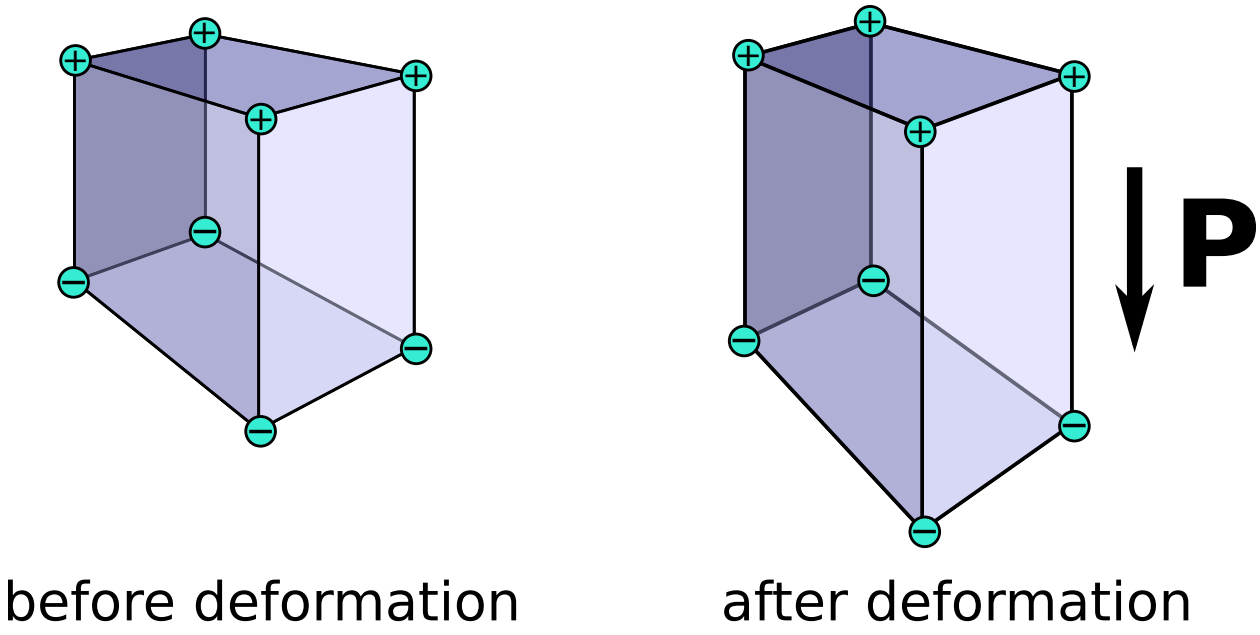

Figure 4: Upon deformation, typically a small polarization vector, $\mathbf{P}$,(relative to undeformed) is created due to charge separation[23].

around the nucleus and is possible in any system composed of atoms. *Ionic polarization* refers to the relative distortion of entire ions in an electric field. This type of polarization is of course possible in ionic systems, but is also possible in systems where electron density is "shared" asymmetrically between atoms due to differences in electronegativity. *Orientational polarization* describes the tendency of dipoles within a system to align themselves with an electric field.

For a material to be piezoelectric, it must also be polarizable upon deformation [23]. This is the result of the material's natural charge distribution. Fig. 4 depicts how the deformation of a theoretical system changes the net polarization.

For the purposes of this dissertation, we will be concerned with the linear piezoelectric equations, which describe deformations and polarizations in the limit of infinitesimally small applied fields or stresses, respectively. The theory of piezoelectric response is well-established for crystalline (bulk) systems. For more information on piezoelectricity we refer the reader to Refs.[27–29]

In Fig. 4, the polarization shown is perpendicular to the applied load, but this is not always the case; the direction of the polarization depends on the specific aniosotropy of the material. The piezoelectric tensor fully describes the anisotropy of the piezoelectric effect that we will consider in this work. That being said, we note that we will not consider time dependent properties of the piezoelectric effect in this work.

1.1.2 The constituitive equations

The linear piezoelectric equations are given by the constituitive equations for a body. The *direct* piezoelectric effect (Eq. (1.1)) describes the *polarization* (electric charge density displacement) D_i of the crystal in terms of an applied stress T_{jk} and electric field f_j. Here

$$\begin{aligned} D_i &= d_{ijk}T_{jk} + \epsilon_{ij}f_j \\ \mathbf{D} &= \mathbf{dT} + \boldsymbol{\epsilon}\mathbf{f}. \end{aligned} \tag{1.1}$$

and in the rest of this work, Einstein sum convention is implied for repeated indices. Here the second-rank tensor, $\mathbf{T}$, is the stress tensor, which describes the individual components of pricipal and shear stress (think pressure) that act on a differential volume element of a continuum body (see B.1). Stress is not discussed in any length here, but we refer the reader to Ref.[1]. $\mathbf{f}$ is the familiar electric field vector that is useful for describing the forces acting on electrically charged bodies. The third rank tensor, $\mathbf{d}$, is the piezolectric tensor which is discussed in greater depth in chapter 4 and appendix B. In this constituitive equation, it has the definition $d_{ijk} = \frac{\partial D_i}{\partial T_{jk}}$. The transpose of this tensor has another definition (see below) which we will be using mostly in this work. The second-rank tensor $\boldsymbol{\epsilon}$ is the permittivity and has the definition $\epsilon_{ij} = \frac{\partial D_i}{\partial f_j}$ and describes the free-body dielectric constant for the material.

The *converse* piezoelectric effect (Eq. (1.2)) describes the strain E_{ij} induced in the material when an external field is applied. Here the tensor $\mathbf{E}$ is the strain tensor, and in this work, we will refer to the Green strain tensor in particular. The strain tensor describes the fractional change in the physical dimensions (length, width, height) of a body and is

$$
\begin{aligned}
E_{ij} &= \sigma_{ijkl} T_{kl} + d_{ijk} f_k \\
\mathbf{E} &= \boldsymbol{\sigma}\mathbf{T} + \mathbf{df}
\end{aligned}
\tag{1.2}
$$

discussed more in chapter 4 and appendix B. The stress tensor, $\mathbf{T}$, is linked to the strain tensor by the rank-4 compliance tensor, $\boldsymbol{\sigma}$, at zero field. The compliance tensor then has the form $\sigma_{ijkl} = \frac{\partial E_{ij}}{\partial T_{kl}}$ and describes the ability of the body to deform in response to applied stresses (pressure). The piezoelectric tensor is then given by Eq. (1.3). We note that the

$$
d_{ijk} = \left(\frac{\partial E_{ij}}{\partial f_k} \right)_{\mathbf{T}=\mathbf{0}} \tag{1.3}
$$

indices pertaining to strain, ij, depend on the coordinate system used as a reference frame for measuring strain (which can be e.g. unit cell parameters or cartesian coordinates, etc.), whereas the index contracted with the field, k, depends on the external (laboratory) reference frame of the applied field.

The piezoelectric effect is described fully by the spatially dependent piezoelectric tensor for a material. The tensor is generally of third-rank, although it is often written as a matrix, and many forms have been deduced for different crystallographic groups[23,27]. For the work presented here, we will stick to the third-rank tensor form for convenience.

1.2 REASONS TO CONSIDER APERIODIC RESPONSE

Since piezoelectric materials are usually crystalline, it might seem unconventional/surprising to approach screening for piezoelectric materials from the point of view of aperiodic calcula-

tions. The recent advancement of nanomachines[5,30,31] is a clear area where the systems are aperiodic and might be controlled via an electric field[32]. To achieve precision control of these systems, it is useful to develop formalisms and methods to describe the relative motions of different parts of the machines accurately. Much of this work is dedicated to understanding the anisotropy of response in finite molecular systems.

Even for periodic systems though, there are different types of interactions which might give rise to significant piezoelectricity. Adequately describing these interactions might be difficult for periodic calculations. DFT methods might not adequately describe these interactions between molecules and is not as systematically improveable as wavefunction methods. Periodic wave function methods may have other shortcomings such as expense and are generally not as well-developed for electric field interactions. There is progress being made in this direction, though, with methods like periodic-local MP2 developed for crystal systems[33]. As we will see in the chapters to come, semi-empirical methods seem to have difficulty describing more exotic types of intermolecular interactions.

But to this end, local interactions of molecules and small systems can be described in a systematically improveable way with modern wavefunction methods, and when tailoring piezolectric "smart" materials or nanomachines, describing these interactions well is of utmost importance. In this work we create methods to understand the anisotropic response of molecular interactions in order to better predict the types chemical species to use in desired applications.

1.3 ORGANIC PIEZOELECTRIC MATERIALS

Currently synthetic ceramics, which are widely used due to their very large piezocoefficients but may be toxic, for example may contain lead, have a negative environmental impact in production, may require heavy metals for production, or are costly to produce. Ceramics in general are stiff and brittle as well which may make them ill-suited for some applications[34]. More flexible organic-inorganic composites have been develeoped with piezoelectric coefficients that rival those of ceramics and could have applications in flexible sensors with uses in

medicine, robotics, and biomechanical devices[35]. Even fully organic electroactive polymers have been developed, which exhibit fast response speeds as actuators, low hysteresis, and strain levels far above those of traditional piezoelectric materials. They also have elastic energy densities surpassing those of ceramics[36–38]. These are promising targets for example in the production of artificial muscles. Recent work has also demonstrated that many synthetic organic crystals and even single layers of molecules can possess notable piezoelectricity[39,40]. This work offers exciting alternatives to the current inorganic materials being commonly used for piezoelectric devices. Most notably we expect that organic alternatives can be highly tunable owing to the rich functional groups and diversity of organic compounds.

There is also a breadth of established work in the self assembly of polar organic crystals which may be useful in efficiently producing organic piezoelectrics. Work is also being done to create piezoelectric films or foams to create flexible and piezoelectric poymers, which all rely on the current synthetic methods of organic chemistry. A large portion of the work presented here deals with the deformation properties of hydrogen bonds. An electromechanically-responsive hydrogen bond is interesting from both a materials design and a chemistry perspective. Hydrogen bonds are ubiquitous in chemistry and biology, and have been frequently used to drive self-assembly in polar organic materials [41–46]. Consequently, piezo-response should be widespread in molecular materials[39,47,48] which suggests that the details of electromechanical response in hydrogen bonds should be investigated further. Furthermore, there are a large number of other polar interactions that exist in nature that also should exhibit electromechanical response and that should be considered when screening for organic piezoelectrics.

2.0 PIEZOELECTRIC EFFECTS OF APPLIED ELECTRIC FIELDS ON HYDROGEN-BOND INTERACTIONS: FIRST PRINCIPLES ELECTRONIC STRUCTURE INVESTIGATION OF WEAK ELECTROSTATIC INTERACTIONS

This work has been published in the *Journal of Physical Chemistry Letters* 2013, 4, 1365-1370. My contributions to this work include implementing the many-body expansion and the eletrostatically-embedded many body expansion methods for calculations involving the tetramer system of 2-mtheyl-4-nitroaniline (MNA). I am also responsible for all geometry optimizations both with and without applied electric fields in order to obtain d_{33} for all small systems (monomer, dimer, tetramer etc.). Moreover, I performed the optimizations with constraints and implementing a self-written optimizer for use in these calculations. I did not perform the periodic boundary calculations and non-covalent bonding analysis.

2.1 SUMMARY

In this chapter the piezoelectric properties of 2-methyl-4-nitroaniline (MNA) crystals are explored qualitatively and quantitatively using an electrostatically embedded many-body expansion (EE-MB) scheme for the correlation energies of a system of monomers within the crystal. The goal of this work is to demonstrate that hydrogen bonds can give rise to significant piezoelectricity, and more specifically that the deformation of the hydrogen bond is primarily responsible for the piezoelectric properties of 2-methyl-4-nitroaniline (MNA). The results demonstrate that hydrogen bonding is an inherently piezoelectric interaction, deforming in response to the electrostatic environment. We obtain piezo-coefficients in excellent

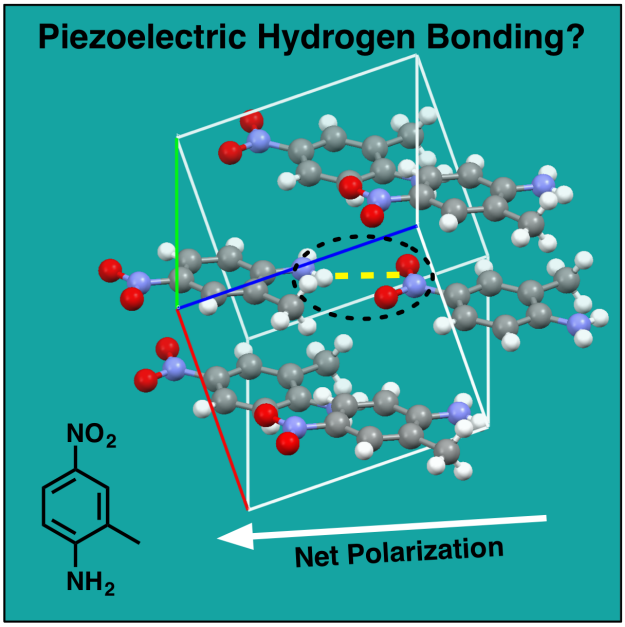

Figure 5: The unit cell of MNA is displayed, and the hydrogen bond is highlighted.

agreement with the experimental values. This approach reduces computational cost and reproduces the total Resolution of the Identity (RI)-Møller-Plesset second order perturbation theory (RI-MP2) energy for the system to within 1.3×10^{-5} %. Furthermore, the results suggest novel ways to self-assemble piezoelectric solids and that accurate treatment of hydrogen bonds requires precise electrostatic evaluation. Considering the ubiquity of hydrogen bonds across chemistry, materials, and biology, a new electromechanical view of these interactions is required.

2.2 2-METHYL-4-NITROANILINE AND PIEZOELECTRIC HYDROGEN-BONDS

As mentioned in section 1.1.1, piezoelectric distortion only requires polar order, and polarizable, deformable interactions. Consequently, piezoresponse should be ubiquitous in molecular chemistry, and common non-covalent interactions such as polar hydrogen bonding and

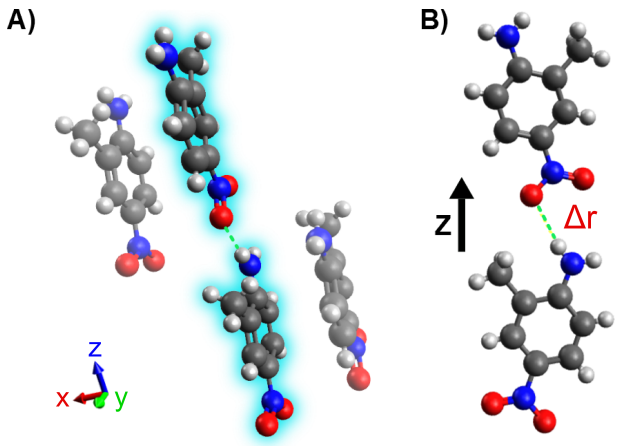

Figure 6: (A) MNA tetramer (contains hydrogen-bond and π- π stacking) (B) The dimer (highlighted in A) in planar view, with hydrogen-bond indicated.

π-stacking should deform in response to applied electrostatic potentials. A few examples of polar, piezoelectric organic crystals are known, including 2-methyl-4-nitroaniline.[40] The intrinsic unit cell includes a simple NH_2 - NO_2 hydrogen bonding motif, surrounded by π-stacking interactions, as illustrated in Fig. 5. We will use this system as a test of the hypothesis that hydrogen bonds exhibit measurable piezoelectric activity, since the experimentally determined response of the crystal is 13.8 pm/V[40]. We utilize first-principles calculations as a test of modern chemistry software's ability to describe the deformation of hydrogen bonds in electric fields.

2.3 METHODS

We test the deformation of the hydrogen bond in the presence of an applied electric field using first-principles calculations. This represents an interesting, challenging test of electronic structure methods, since accurately representing the binding strength of hydrogen bonds is difficult[49], and to accurately treat the piezoresponse, the methods must also accurately treat the polarization of the molecule and hydrogen bond due to the applied field.

We present quantum chemical calculations to model the geometry of 2-methyl-4-nitroaniline in response to a homogeneous external electric field, using a 76-atom tetramer representative of the crystal structure,[40] which we generated using Avogadro[50]. The initial geometry is aligned using Avogadro such that the interior hydrogen bond for the system (Fig. 6) lies primarily along the z-axis. Changes in this hydrogen bond length will later be used to determine the piezoelectric properties of the crystal. Analysis of geometries was routinely implemented using Avogadro. The field is applied in the z direction (as defined by Q-Chem[51]) and varied between -1 to +1 V/nm. While these values appear large on a macroscopic scale, they correspond to a field on the order of one anion or cation at a distance of 1.0 nm or about 1.95×10^{-3} atomic units of field. Such fields are ubiquitous on the molecular scale. Consequently, we believe the electromechanical response illustrated in this work is commonplace throughout chemistry and biology.

We present density functional calculations using the popular B3LYP functional[52–55] in a 6-31G(d) basis as well as resolution of the identity second-order Møller-Plesset perturbation theory (RI-MP2)[56] in a 6-31G(d) basis[57,58]. The RI-MP2 tetramer calculations use the frozen core approximation, and we employ a development version of Q-Chem[51] throughout. Both methods were initially explored on dimer and tetramer subunits for the system, and the RI-MP2 method was chosen for the subsequent calculations, because B3LYP underestimates the π- π stacking interactions that are essential for describing the stacking of the monomers[59].

A full RI-MP2 optimization on the tetramer subunit is quite costly due to the $O(N^5)$ scaling of MP2 and the fact that the geometry optimization requires many cycles (typically 100-400) because of the shallow potential energy surface. At the same time the major correlation contributions for the intermolecular interactions, i.e., to leading order, dispersion, are dominated by two-body effects. We therefore approximated the RI-MP2 correlation energy and gradients using a many-body (MB) expansion, truncated after two-body terms (MB2). The Hartree-Fock (HF) energy and gradients are calculated for the full system. The cost is thus reduced to $O(N^2)$ scaling for the correlation energy. In addition, we use electrostatic embedding (EE) to accelerate the convergence of the expansion (EE-MB2). For the EE, we use ChelPG charges as implemented in Q-Chem[51]. Our approach is similar to that by Dahlke et al. with only small differences in the implementation[60]. Details on many

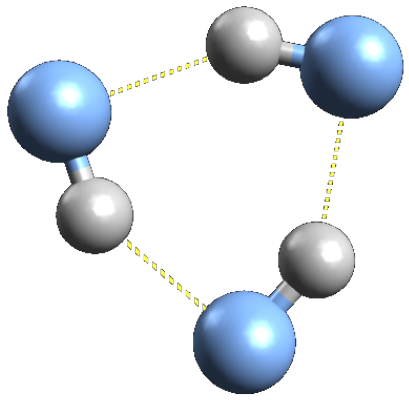

Figure 7: The optimized geometry for the HF trimer is shown.

body expansions and our (EE-)MB2 implementation are presented in A.1.

2.3.1 EE-MB2 calibration for the HF trimer

We tested the accuracy of the (EE-)MB2 approach by investigating errors in energies and optimized geometries as compared to full RI-MP2 results. As a first test we compared the optimized geometries and energies for a hydrogen fluoride trimer, $(HF)_3$ Fig. 7. The full RI-MP2, the MB2, and the EE-MB2 geometry optimizations were performed and very similar results were obtained; cc-pVDZ[61] was the chosen basis set for the calculations. Fig. 7 shows the optimized trimer for the full RI-MP2 calculation (the others are not included because they are visually indistinguishable). The hydrogen bond lengths are of particular interest because they play an important role for the piezoelectric analysis of our representative unit (Fig. 6) of the 2-methyl-4-nitroaniline crystal later. At 0.25 mHartree (0.04%), the (percent) error for the energy is very small. The relative error in the hydrogen bond length is 0.01 Å(0.6%) compared with the full calculation, which is also acceptable. Hydrogen bond length will be the main factor in analyzing piezoelectric properties in the crystal, so these results

are promising for use of the many body expansion methods for analysis in electric fields. Benchmarks for the tetramer are described below in Tab. 1.

Tab. 1 reports the final energies and lengths of possible interest obtained from all three optimizations and compares the MB2 and MB2-EE calculations with that of the full RI-MP2 calculations.

2.3.2 Dimer calculations

Both the hydrogen bond and π- π stacking interactions in MNA play an important role in crystal formation and its geometric response to an external field. The hydrogen bond length is of major importance for the deformation of this shape in an applied electric field and is responsible for forming the crystal along the z-direction (as defined in Fig. 6). Secondly, the π- π stacking interactions play important roles in the crystal formation along the other axis (here the x-axis). In addition to the direct polarization of hydrogen-bonded monomers, charge reorganization (polarization, induction) in the πsystem can screen the H-bond from the applied external field. This decreases the local field strength as compared to the isolated H-bond. For these reasons, we investigated both effects by considering the isolated dimer as well as the tetramer as the smallest meaningful units of the system.

To investigate the direct response of the hydrogen bond to the electric field, we first performed calculations on the dimer as highlighted in Fig. 8. After an initial geometry optimization, the dimer was aligned so that its dipole was parallel with the z-axis. Multiple electric field strengths of -1.0 V/nm to 1.0 V/nm in 0.25 V/nm increments, were applied along the z-axis, and the dimer geometries were optimized unconstrained. The calculations were performed at the B3LYP/6-31G(d) level. Results are shown in Fig. 9 (blue circles).

For the negative electric fields (see Fig. 8 for orientation), the hydrogen bond is polarized, and strengthened, maintaining the dimers overall form. Under positive fields, the hydrogen bond is weakened, and the B3LYP dimer structure buckles. For B3LYP calculations in stronger positive fields, the monomers individually flip so that they now face downward. This leads to favorable hydrogen bond polarization (the dipole has flipped) and thus a stronger hydrogen bond. Fig. 9 shows the dependence of the hydrogen bond length on the

Table 1: The calibration is shown for the many-body expansion algortihm.

Calculation Type	Hartree-Fock Energy (Hartrees)	Correlation Energy (Hartrees)	Total Energy (Hartrees)	% Error (from full RI-MP2) for Total Energy	H-bond Length (Å)	% Error for H-Bond Length
Full RI-MP2	-300.08481	-0.62360	-300.708404		1.687	
MB2	-300.08522	-0.62288	-300.708098	0.000102	1.699	0.711
MB2-EE	-300.08512	-0.62335	-300.708470	0.0000219	1.697	0.593

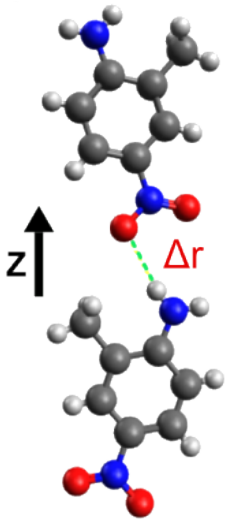

Figure 8: The system for the unconstrained dimer optimizations. Optimizations were performed for the depicted starting geometry by applying fields of varying strength along the z-axis (indicated with the vector).

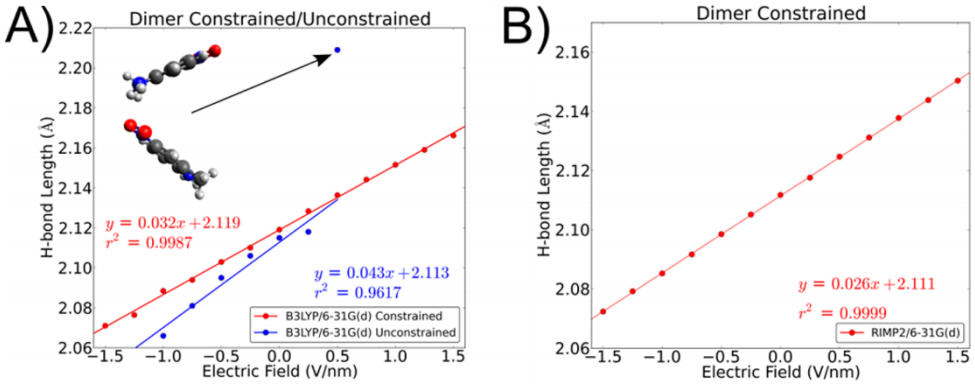

Figure 9: Dependence of the hydrogen bond length on the electric field strength is shown (A) at the B3LYP level with constraints (red) and without constraints (blue) and (B) at the RI-MP2 level with constraints.

field strength. The points for the electric field strengths of greater than 0.5V/nm are not shown, since the molecules buckled.

To alleviate the problem of buckling in these aperiodic calculations and enable comparison to the crystal geometry, constrained optimizations were performed which only allowed movement of the monomers in the z direction. Here the z-axis was chosen to lie along the hydrogen and oxygen atoms participating in the hydrogen bond of interest Fig. 10. For varying electric fields between -1.5 to 1.5 V/nm, multiple geometries were generated by changing the distance between the two monomers and single point energies were calculated. Calculations were performed at the DFT/B3LYP and the RI-MP2 levels in a 6-31G(d) basis. Hydrogen-bond distances corresponding to a minimum in energy were found by analyzing polynomial (usually of order 6) fits (Fig. 11) to the data. Results for the constrained DFT and RI-MP2 calculations are shown in Fig. 10.

Linear regressions were performed for the hydrogen bond length versus field strength data (Fig. 9). Piezoelectric coefficients can then be determined from the slopes Eq. (2.1). The slopes of the regression lines, M_{reg}, can be interpreted as the expected deformation of

$$P(pm/V) = \frac{M_{reg}(\frac{\mathring{A}\,nm}{V})}{L_0(\mathring{A})}\frac{1000\,pm}{nm} \tag{2.1}$$

the hydrogen-bond length per 1V/nm of applied electric field. The hydrogen-bond length at zero field is given by L_0 . The overall piezocoefficient, P , can then be interpreted as the fraction of deformation of the system from L_0 per unit of field. This is expressed with conversion factors for this work used in Eq. (2.1).

Due to the buckling of the dimer at a field strength of 0.5 V in the unconstrained B3LYP calculations, these points for greater than 0.5 V/nm were omitted from the regression. For the B3LYP calculations, the predicted piezoelectric coefficients for the dimer were 20.2 pm/V and 15.3 pm/V for the unconstrained and constrained geometries respectively. The piezocoefficient for the constrained RI-MP2 dimer calculations was determined to be 12.3 pm/V.

Furthermore, to investigate the impact of the basis set superposition error (BSSE)[62] and

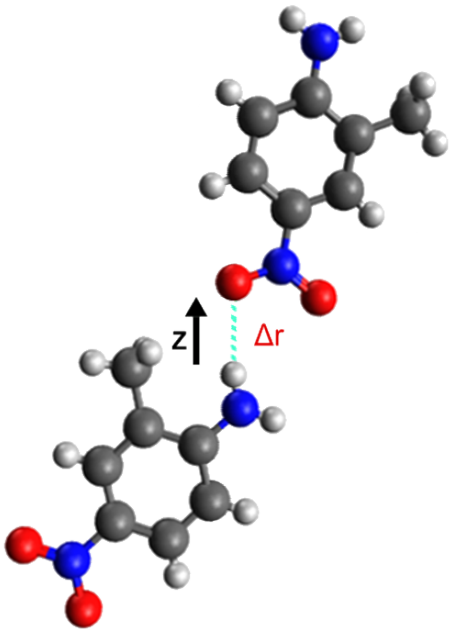

Figure 10: Here the system for the constrained dimer calculations is presented.

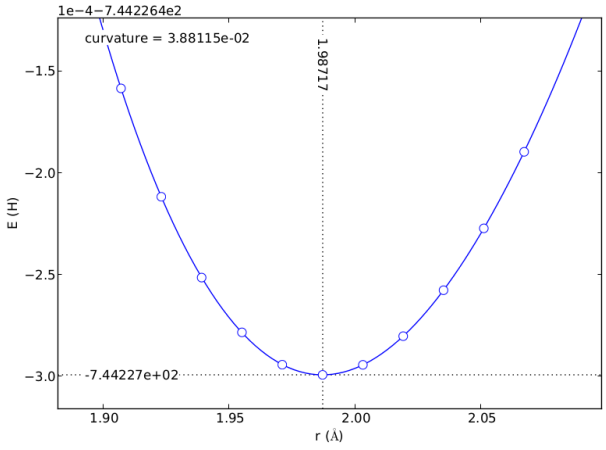

Figure 11: A sample energy "scan" along the hydrogen bond coordinate for the MNA dimer. The curve is fitted by an appropriate order polynomial.

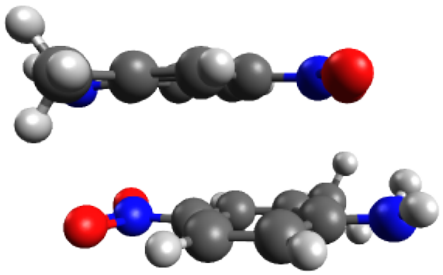

Figure 12: The unconstrained RI-MP2 optimized geometry shows the two monomers "stacked" to maximize π-πinteractions.

basis set effects, we also performed constrained calculations at the B3LYP/aug-cc-pVDZ and aug-cc-pVTZ[61,63] levels and for the RI-MP2/cc-pVTZ level. We then extrapolated the single point energies to the infinite basis set limit (A.2) for the DFT calculations. The piezo-coeffients for the double zeta, triple zeta, and complete basis set (CBS) limit are 17.1, 17.7, and 17.7 pm/V, respectively. Since the value obtained for the piezo-coefficient with the 6-31G(d) basis with this method was 15.3, (within 14% of the value obtained for the infinite basis set limit), 6-31G(d) is likely an acceptable basis for semi-quantitatively analyzing piezo-response due to hydrogen-bond deformation. The piezo-coefficient determined for the RI-MP2/cc-pVTZ level is 13.8 pm/V compared to the 12.3 pm/V for the 6-31G(d) calculation.

Dispersive interactions play a role in π- π stacking, but some popular functionals such as B3LYP are known to have shortcomings in the description of this type of interaction[59]. Simple dispersion correction schemes (like DFT-D) cannot be applied here because the empirical correction does not depend on the electric field. We therefore performed RI-MP2 calculations to assess the influence of dispersive interactions in this system. The results to the initial unconstrained geometry optimization in the absence of an electric field are shown in the Fig. 12.

Our results show that RI-MP2 predicts stronger π-π interactions than B3LYP: RI-MP2 predicts the optimized dimer structure to consist of two stacked monomers. As noted before, the π- π stacking interactions seem to be necessary for proper maintenance of the crystal

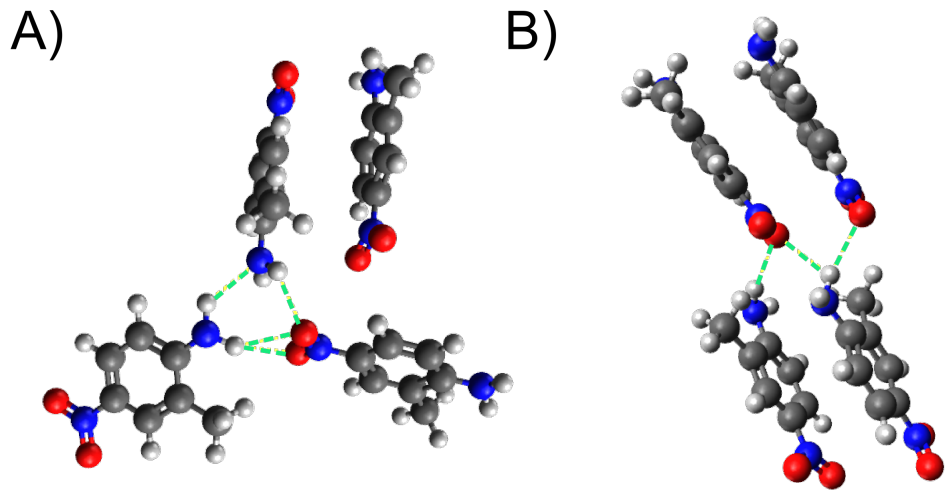

Figure 13: Unconstrained optimizations for the MNA tetramer are shown for A) B3LYP B) full RI-MP2.

structure. This means RI-MP2 optimizations should maintain the tetramer structure better than B3LYP calculations and should avoid buckling of monomers in the bigger subunit. We therefore expect MP2 to yield a more realistic description of the essential physics of this system. Unconstrained geometry optimizations were performed for the tetramers at the RI-MP2 and B3LYP levels to confirm this (Fig. 13). The B3LYP optimizations were not fully converged because it was clear that the final geometry deviates strongly from the crystal structure. The RMSD values compared to the crystal structure are 0.687 and 3.592 Å for the RI-MP2 and B3LYP calculations, respectively. The largest contribution to the RMSD for the RI-MP2 structure is likely the shifting of the aromatic planes. This effect would likely be much smaller in the crystal due to packing effects.

2.3.3 Tetramer calculations

Despite the well-behaved nature for the unconstrained RI-MP2 optimizations, there is an undesirable aspect that we addressed through a constrained optimization. In Fig. 13, three

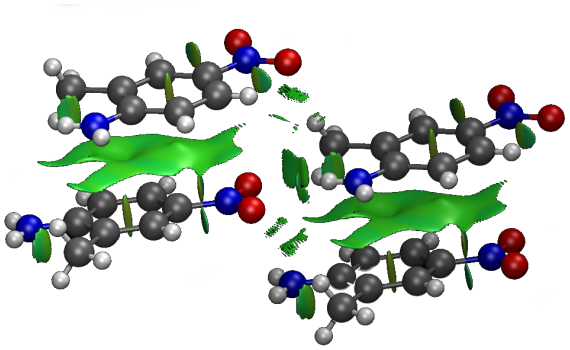

Figure 14: The noncovalent (NCI) analysis for MNA.

bifurcated hydrogen bonds can be noted between the nitro and amine groups in the tetramer. However, the crystal structure (Fig. 6) shows only one linear hydrogen bond. Because of the cluster chosen, the two outside monomers do not possess the hydrogen-bonded partners they would have in the bulk crystal. As a result, the subunit prefers a geometry where the singly hydrogen bonded monomers in the central dimer of the tetramer (Fig. 6) move out of plane with respect to one another to form two additional, but weaker hydrogen bonds with the two outside monomers. It is known that bifurcated hydrogen bonds have properties very different from linear ones in terms of binding strengths and so on,[64] so that we had to prevent this geometric distortion with respect to the crystal structure in our calculations.

We have performed noncovalent interaction (NCI) bonding analysis[65], which shows that there is no considerable hydrogen bonding between the amino groups in the crystal structure (see Fig. 14). Green surfaces in the NCI analysis represent attractive noncovalent interactions. As illustrated, there are attractive π-πinteractions, as well as interactions in-plane between NO_2–NH_2 hydrogen bonds, and between NO_2 and NH_2 groups in different planes, but a clear void path (i.e., white color in the plot) lies between NH_2 groups in adjacent molecules.

Consequently, we performed constrained optimizations for the system. The system was aligned such that the hydrogen bond in the central dimer was aligned approximately parallel to the z axis, and the π-planes of the central dimer were aligned approximately parallel to

the yz plane. The geometry for the central dimers was constrained to the yz plane, while the two outside monomers were kept unconstrained. This way, the tetramer was forced to maintain a single strong hydrogen bond, by keeping the two hydrogen-bonded monomers in the same plane. The geometry constraint is summarized in Fig. 15.

Using these constraints, optimizations were carried out using our EE-MB2 implementation. As with the dimer, different electric fields (between -1 V/nm and 1 V/nm) were applied along the z-axis, and the hydrogen bond distance was plotted versus the electric field strength (Fig. 16). From the slope of the regression line we calculate a piezoelectric coefficient of 10.7 pm/V. This is about 13% less than the value obtained for the constrained RI-MP2 dimer calculations, which illustrates that the πsystem leads to local screening of the hydrogen bond from the electric field. Tab. 2 summarizes the results for the calculated coefficients determined throughout this work.

2.4 BENCHMARKING THE EE-MB2 IMPLEMENTATION

To benchmark our EE-MB2 implementation, a single full RI-MP2 optimization was carried out under the same constraints. We find an error of 0.40 mHartree (0.006 %) in the correlation energy and a RMSD between the full and many-body expanded geometry of 0.0007 Å. These errors are likely smaller than the regular errors in geometry optimization routines due to cutoffs and convergence criteria. The hydrogen bond length differs by only about 0.002 Å. The piezoelectric hydrogen bond deformations are on the order of about 0.010 Å per 0.5 V/nm change in electric field strength, so the many body expansion likely approximates the relative changes to a sufficient degree of accuracy.

2.4.1 Monomer elongation and contraction

The work we have thus far preseneted attributes the large majority of the piezoelectric effect for the crystal due to the hydrogen bonds oriented in the direction of the net dipole for the crystal. However, each individual monomer has an individual electromechanical response

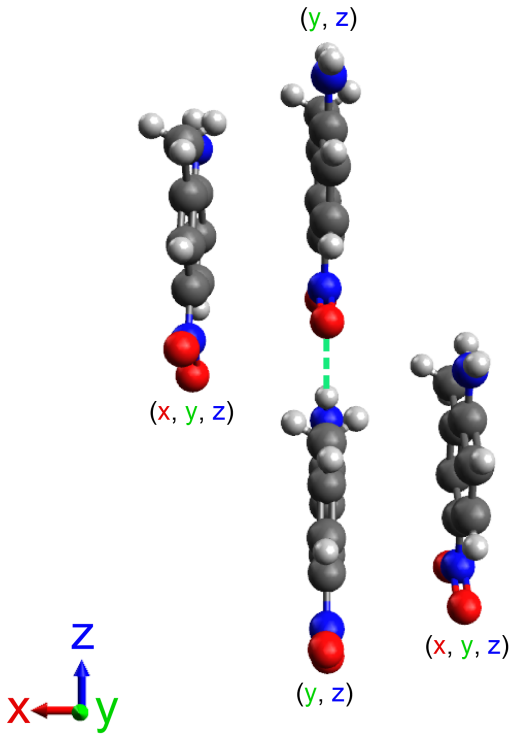

Figure 15: Orientation for the starting geometry for the constrained tetramer RI-MP2 optimization. The central dimers (the two hydrogen bonded monomers) are constrained to move in the yz plane, while the outside monomers are unconstrained.

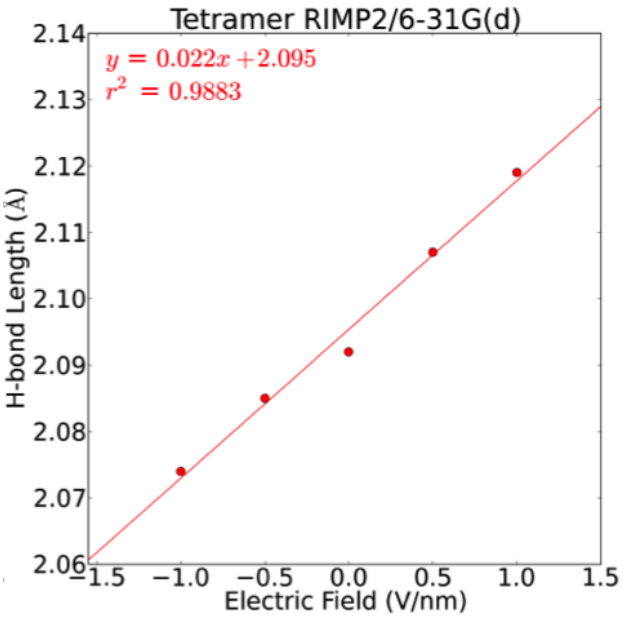

Figure 16: Dependence of the hydrogen bond length on the electric field strength for the constrained tetramer EE-MB2 optimizations is shown. Calculations were performed at the RI-MP2/6-31G* level.

Table 2: d_{33} values from constrained and unconstrained calculations are shown.

Method/Basis	Unit	piezocoefficient (pm/V)
B3LYP/6-31G(d)	dimer (UC)	20.2
	dimer (C)	15.3
B3LYP/aug-cc-pVDZ	dimer (C)	17.1
B3LYP/aug-cc-pVTZ	dimer (C)	17.7
B3LYP/CBS	dimer (C)	17.7
RI-MP2/6-31G(d)	dimer (C)	10.7
RI-MP2/cc-pVTZ	dimer (C)	13.8
	tetramer (C)	13.8
experiment[40]	crystal	13.8

due to electrostatics and polarization. First, we present the system used to analyze the individual response of a monomer subunit to an electric field. Here the monomer is aligned so that its dipole is approximately parallel with the z-axis (which is parallel with the vector shown). For this, we simply place the two nitrogen atoms on the z-axis. The system is shown in Fig. 17.

Again we apply fields of varying strength in the direction of the vector and allow the monomer to optimize. The distance between a hydrogen of the amine group and an oxygen of the nitro group is taken as the approximate length of the molecule and denoted by r. We can measure the systems piezo response in the same way as before. Fig. 18 shows r in angstroms versus the electric field in V/nm.

It is noteworthy that the slope for this system is negative, the opposite of that for the response of the hydrogen bond. The monomers elongate when the hydrogen bond contracts and contract when the hydrogen bond elongates. Intuitively this makes sense. A contraction of the hydrogen bond implies that electron density is being pushed towards the oxygens of

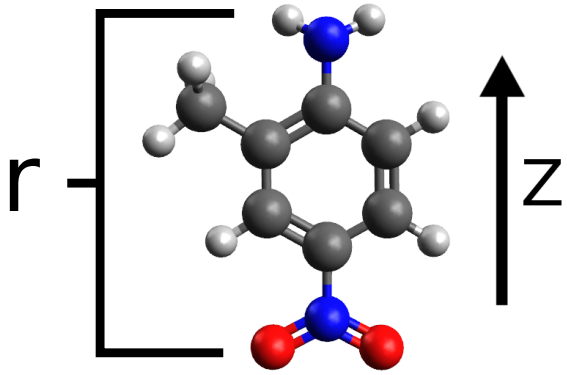

Figure 17: The monomer of MNA is shown. The hydrogen to oxygen distance of interest is denoted by r.

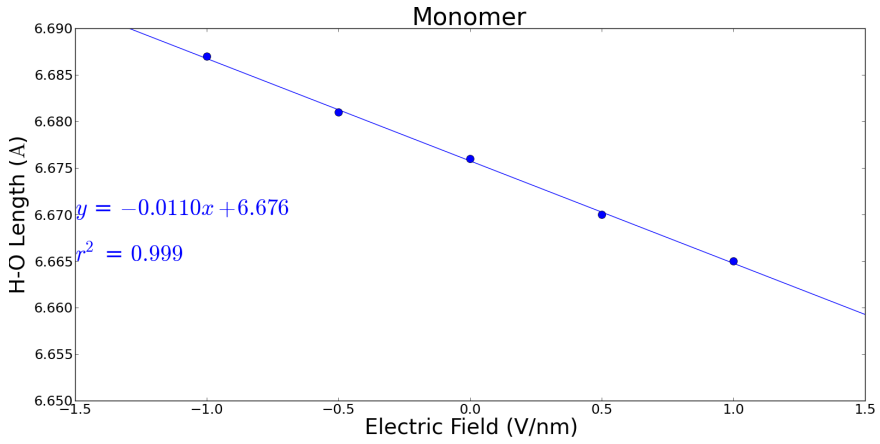

Figure 18: The linear regression for the intramolecular piezoresponse of MNA (defined in Fig. 17) vs field strength is shown.

the nitro group, and away from the hydrogens of the amine group (i.e. which leads to a stronger hydrogen-bond by electrostatic arguments). If we view the amine group as being the partially positive end of the molecules net dipole, and the nitro group as the partially negative end, then a field which polarizes the molecule for a stronger hydrogen bond (as described in the previous sentence) would likely pull on the ends of the molecule as well, elongating it. For the opposite scenario (weakened hydrogen bond via pushing of electron density away from nitro and towards amine group), the ends of the molecule are being pushed together by the field contracting the molecule.

The slope given corresponds to a piezocoefficient of about 1.65 pm/V for the monomer – an order of magnitude less than the response of the hydrogen bond. Since this effect is both small compared to and in opposition to the deformation of the hydrogen in the calculations we present, monomer elongation and contraction likely does not play a significant role in the piezoelectric properties of this compound.

2.5 PERIODIC BOUNDARY CALCULATIONS

Our approach illustrates how the crystal deforms in the presence of applied electric fields and yields results (d_{33}=10.7 pm/V) that are in good agreement with the experimental piezoelectric coefficient of 13.8 pm/V[40]. This suggests that the tetramer cluster qualitatively represents the piezoelectric nature of the crystal. Nevertheless, there are likely effects deriving from the large number of repeating subunits in the actual crystal that are not adequately captured quantitatively in the small representative cluster. These could be a combination of screening effects due to the lack of hydrogen bonding partners for the outside monomers (some of which was compensated for by the constraint). Also, extension of the cluster into the polar crystal in the x, y, and z directions induces a local electric field from the cooperative interactions (screening, induction, alignment of dipole moments) between the polarizable monomer units that could influence the piezoelectric response.

In order to assess the influence of the crystal environment, we explored several ways of estimating piezoelectric coefficients for the bulk crystal, considering extension of the cluster

along each axis. Calculations using the semi-empirical PM7 method as implemented in MOPAC[66,67] show that the piezoelectric coefficient increases with the number of monomers in the hydrogen bond chains (growing along the z axis). Using an extrapolation technique to infinite chain length, we found that the piezoelectric coefficient increases by 13% when going from the tetramer to an infinite chain in the z-direction. [1]

Using periodic boundary condition (PBC) calculations, we also evaluated the growth along the π-plane (y axis) and the influence of π-π stacking (growth in x direction as defined in Fig. 6). As expected, the π-stacking along the x-axis leads to a decrease in the piezoelectric coefficient (28%) due to screening effects. Growth along the y axis leads to an increase of 17% versus an (x,y,z)=(1,3,2) cluster. We see that the total piezoelectric coefficient depends on a fine balance of multiple factors (alignment of dipole moments, π-screening) that may have opposite effects. When we consider the overall crystal in all directions, however, these effects largely cancel and we estimate that the piezo-coefficient should increase by up to 20% when going from the tetramer to the crystal environment. Following these simple arguments, we estimate a piezo-coefficient of 11-13 pm/V when taking the crystal environment into account. Another shortcoming of the present calculations stems from the relatively limited basis set sizes used. Based on basis set extrapolation for the dimer results, we estimate that the piezo-coefficient would increase by another 15% when going to a complete basis set. This results in a piezo-coefficient for the crystal calculated at the estimated complete basis set limit of 13-15 pm/V, which is in excellent agreement with the experimental value of 13.8[40].

Finally, it is noteworthy to mention that we have only considered the hydrogen-bond interactions of the system as responsible for the piezo-response of the crystal. However, the individual monomers themselves possessing dipoles are likely to undergo similar deformation in response to applied electric fields. Monomer elongation and contraction likely oppose the piezo-response due to the hydrogen-bond (ie. monomer lengths contract when hydrogen bond lengths expand and vice versa), and is an order of magnitude (around 1.65 pm/V for RI-MP2 calculations) smaller than the piezo-coefficients determined via hydrogen-bond

[1] This extrapolation is necessary because the periodic boundary condition techniques implemented in MOPAC yielded suspicious results in this case. We suspect this is a consequence of the PBC implementation used, which requires the exchange interaction between the periodic unit cells to be small, an assumption that may not be valid for unit cells linked by hydrogen bonds.

considerations. Therefore, individual deformations of monomers likely do not contribute significantly to the piezo-properties of the crystal.

2.6 CONCLUSION

In summary, this system, because of the balance between competing non-covalent electrostatic interactions of π-π stacking and hydrogen bonding, is an interesting test case for advanced electronic structure methods. The many-body expansion discussed here is effective at treating the polarization, induction and dispersion effects important in describing the electrostatic distortions considered here within the piezoelectric deformation. The result suggests that self-assembly using hydrogen bonds can lead to meaningful piezoelectric distortion in smart materials. Considering the ubiquity of hydrogen bonding and π-stacking in biomolecules, such distortions are likely common, but subtle effects in the conformations of proteins. In materials, the synergistic alignment of dipole moments in a polar crystal, like 2-methyl-4-nitroaniline, clearly leads to an interesting piezoelectric response of the hydrogen bonds.

3.0 PIEZOELECTRIC HYDROGEN BONDS: COMPUTATIONAL SCREENING FOR A DESIGN RATIONALE

This work is published in the *Journal of Physical Chemistry A* 2014, 118, 35, 7404-7410. I am responsible for finalizing the derivation for the simple mathematical model for hydrogen bonded piezoelectric molecules and the algorithms and calculations for calculating the piezolectric coefficients. A number of calculations for this thesis were redone by myself to correct for some oversights in the calculations in the published work. Different values for d_{33} for the test bank of molecules were obtained than those reported in the the above citation, although the scientific conclusions remain unaffected.

3.1 SUMMARY

Organic piezoelectric materials are promising targets in applications such as energy harvesting or mechanical sensors and actuators. In the last chapter we have shown that hydrogen bonding gives rise to a significant piezoelectric response. In this chapter, we aim to find organic hydrogen bonded systems with increased piezo-response by investigating different hydrogen bonding motifs and by tailoring the hydrogen bond strength via functionalization. The largest piezo-coefficient of 23 pm/V is found for the nitrobenzene-aniline dimer. We develop a simple, yet surprisingly accurate rationale to predict piezo-coefficients based on the zero-field compliance matrix and dipole derivatives. This rationale increases the speed of first principles piezo-coefficient calculations by an order of magnitude. At the same time, it suggests how to understand and further increase the piezo-response. Our rationale also explains the remarkably large piezo-response of 150 pm/V and more for another class of

systems, the "molecular springs" [39].

3.2 INTRODUCTION

In this chapter we consider the underlying properties of hydrogen bonded systems that can be used to find hydrogen bonded systems with significant piezoelectricity. We use a simple model and Taylor expansion of the energy of a simple model to deduce an approximate formula for d_{33} and apply the resulting equation to a test bank of hydrogen bonded dimers. We find that the dipole derivative and curvature of the energy with respect to the bonding coordinate along with the equilibrium bond length can be used to reproduce the piezoelectric coefficient for these systems. We show that the results are consistent with piezoelectric coefficients determined from multiple energy "scans" at different field values, yet offer a significant reduction in calculation time, while reducing contamination from nonlinear effects.

3.3 A SIMPLE COMPUTATIONAL MODEL

As shown in chapter 2, the practical calculation of piezo-coefficients for molecular systems is straightforward. One calculates the equilibrium bond lengths or molecular dimensions after geometry optimization at varying applied electric fields. Within the linear regime, a plot of the length (bond or molecule) versus field strength and its linear regression yields the piezo-coefficient. In this section we address the question: What are the intrinsic molecular properties that give rise to piezoelectricity, as opposed to bulk properties, and how can one *rationalize* the different piezo-coefficients of different systems?

A cartoon of a simple system that possesses an energy surface similar to our hydrogen bonded systems is depicted in Fig. 19. From this, one can derive a compellingly simple estimate for the piezo-coefficient. Based on considerations of how much the equilibrium bond length of the piezoelectric bond changes upon application of an external field, and using a Taylor expansion of the potential energy surface along the direction under consideration,

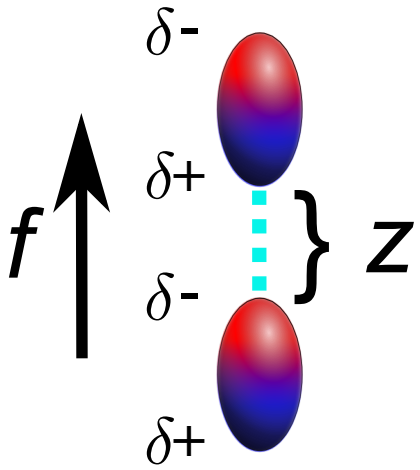

Figure 19: A cartoon illustration of two polar monomers separated by distance z and subject to electric field f along the z direction is shown. z corresponds to the hydrogen bond length in the systems we studied here.

z, and the field, f the piezo-coefficient can be estimated as in Eq. (3.1). Here, z_0 is the

$$\begin{aligned} d_{33} &\approx -\frac{1}{z_0} \cdot \left.\frac{\partial^2 E}{\partial \xi^2}\right|_{(z_0,0)} \cdot \left.\frac{\partial \mu}{\partial \xi}\right|_{(z_0,0)} \\ &\equiv -\frac{1}{z_0} \cdot h^{-1}_{0\xi\xi} \cdot \mu_{0\xi} \end{aligned} \tag{3.1}$$

equilibrium bond length, $E(\xi, f)$ the energy as a function of geometric displacement ξ (i.e. $z - z_0$) from the equilibrium, z_0 and f the electric field strength. Note that the derivatives are evaluated for the equilibrium structure at zero field (i.e. $(z, f) = (z_0, 0)$). μ is the dipole moment of the system. In our notation, we choose h to represent second derivatives of the energy of the system. The nonzero subscripts indicate the variables with respect to which we are differentiating, and the index 0 indicates that the term is evaluated at $(z, f) = (z_0, 0)$.

The notation is analogous for first derivatives. Here, we assume that the electromechanical response occurs solely along one bond direction, z, and that the electric field is applied along this direction (see Fig. 19). A more general derivation of Eq. (3.1) as well as some higher-order generalizations are presented in the following section. We note that a relation between the piezo-coefficient and dipole moment derivative has been discussed earlier[39], and subsequent to our derivation we noted that the program package GULP uses a similar expression for estimating the piezoelectric strain/stress constants[68,69].

In the second line of Eq. (3.1) we have introduced a shorthand notation to make the expression more intuitive. As Eq. (3.1) suggests, the piezo-coefficient arises, to leading order, from a balance between two factors: the inverse Hessian $h^{-1}_{0\xi\xi}$ (or compliance matrix) of the bond and the derivative of the dipole moment with respect to geometric displacements – both evaluated at the equilibrium geometry for zero field along the piezo-active coordinate. This leads to a compellingly simple rationale: To achieve a large piezo-coefficient, one needs to tune the system to have a large compliance (deformable bond) for the piezo-response and a large change in dipole moment as the bond length changes.

Is it possible to maximize the two dominating factors, compliance and dipole moment derivative, simultaneously? There are some limiting cases that suggest compliance and dipole moment are in many cases antagonists. For example, consider a pair of bare counterions such as Na^+ and Cl^-. Here, the change in dipole moment with geometric displacement is very large, but the compliance is small because of the strong ionic bond. At the other extreme, consider two helium atoms bound only by van der Waals (vdW) forces. Here the compliance is very large, but the dipole moment as well as its derivative is zero. Both extremes lead to small piezocoefficients. From this one expects that the optimization of the piezo-coefficient involves, at least for hydrogen-bonded systems, finding a delicate balance between (weak) bonding and (large) dipole moment derivatives.

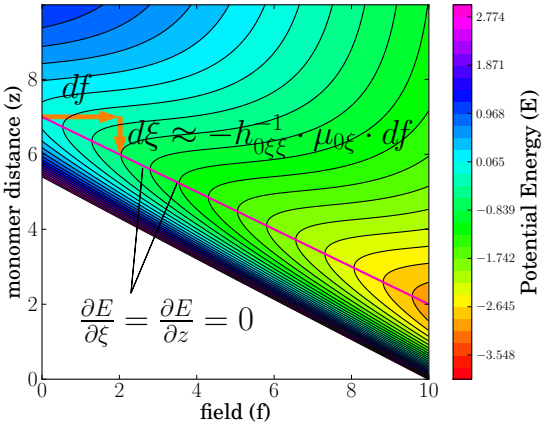

Figure 20: Schematic contour plot is shown for a potential energy surface as a function of monomer separation z and field strength f for a hydrogen bonded system (all in arbitrary units). The energy minimum for a given field is tracked with the pink line along the surface.

3.4 DERIVATION

The energy surface of our system is a function of monomer distance (z) and external field (f). An illustrative energy contour surface is depicted in Fig. 20 and will be referenced during the derivation.

Given our equilibrium geometry at zero field (denoted by $(z_0, 0)$), we can approximate the value of z that the system will adopt, when a field is applied, via a Taylor expansion. For convenience we can define a displacement variable $\xi = z - z_0$ (that is the displacement from the equilibrium geometry at zero field), and recognize that all derivatives with respect to ξ are equivalent to derivatives with respect to z. Up to second order in ξ and f the Taylor expansion is given in Eq. (3.2). For convenience we rename all first-order derivatives with g_0 and all second-order derivatives with h_0. We include indices that suggest the variables with respect to which we are differentiating. The subscript 0 implies that the derivatives are evaluated at $(z, f) = (z_0, 0)$ (Eq. (3.3)). Particularly, we are interested in solving for the displacement, ξ, at a given field strength for which the energy, E, is a minimum, i.e.

$$E(z,f) \approx E(z_0,0) + \left.\frac{\partial E}{\partial \xi}\right|_{(z_0,0)} \cdot \xi + \left.\frac{\partial E}{\partial f}\right|_{(z_0,0)} \cdot f + \frac{1}{2} \cdot \left.\frac{\partial^2 E}{\partial \xi^2}\right|_{(z_0,0)} \cdot \xi^2 + \frac{1}{2} \cdot \left.\frac{\partial^2 E}{\partial f^2}\right|_{(z_0,0)} \cdot f^2 + \left.\frac{\partial^2 E}{\partial \xi \partial f}\right|_{(z_0,0)} \cdot f \cdot \xi \tag{3.2}$$

$$E(z,f) \approx E(z_0,0) + g_{0\xi} \cdot \xi + g_{0f} \cdot f + \frac{1}{2} \cdot h_{0\xi\xi} \cdot \xi^2 + \frac{1}{2} \cdot h_{0ff} \cdot f^2 + h_{0\xi f} \cdot f \cdot \xi \tag{3.3}$$

$\frac{\partial E}{\partial \xi}(\xi, f) = 0$. This is the analytical equivalent of finding the displacement for the minimum energy geometry as a function of field strength, just as we have done via curve fitting in this work and our previous work[39,47]. Referring to Fig. 20, the equilibrium bond length as a function of the field strength is tracked via the pink line. We can take the necessary derivatives of the right hand side of Equation Eq. (3.3), set them equal to zero, and solve for ξ as a function of f (Eq. (3.4)). Here we have used $g_{0\xi} = 0$ because we start from a

$$\begin{aligned} g_{0\xi} + h_{0\xi\xi} \cdot \xi + h_{0\xi f} \cdot f \;&=\; h_{0\xi\xi} \cdot \xi + h_{0\xi f} \cdot f \;=\; 0 \\ \xi(f) &= -h_{0\xi\xi}^{-1} \cdot h_{0\xi f} \cdot f \end{aligned} \tag{3.4}$$

converged geometry.

Taking the derivative of ξ with respect to the field strength f is analogous to finding

the slope of the hydrogen-bond length versus field plots. Dividing the derivative by the equilibrium distance z_0 then yields the piezo-coefficient up to first order in f: We recognize

$$\begin{aligned} \frac{d\xi}{df} &\approx -h_{0\xi\xi}^{-1} \cdot h_{0\xi f} \\ d_{33} &\approx -\frac{1}{z_0} \cdot h_{0\xi\xi}^{-1} \cdot h_{0\xi f} \end{aligned} \tag{3.5}$$

that $h_{0\xi f} \equiv \frac{\partial^2 E}{\partial \xi \partial f}\Big|_{(z_0,0)}$ is just the derivative of the dipole of the system with respect to ξ for the optimized starting structure, $\mu_{0\xi} \equiv \frac{\partial \mu}{\partial \xi}\Big|_{(z_0,0)}$. Thus, the piezo-coefficient is approximately which concludes the derivation of Eq. (3.1).

$$d_{33} \approx -\frac{1}{z_0} \cdot h_{0\xi\xi}^{-1} \cdot \mu_{0\xi} \tag{3.6}$$

It is worthwhile at this point to note that Eq. (3.5) can also be obtained in a more concise manner. Here we consider the cyclic rule of multivariable calculus. Our variables will be g, ξ, and f, which as above, are the energy gradient, displacement from equilibrium, and field respectively. From the cyclic rule, we write Eq. (3.7). The subscripts in Eq. (3.7) indicate

$$\frac{\partial \xi}{\partial f}_g \cdot \frac{\partial g}{\partial \xi}_f \cdot \frac{\partial f}{\partial g}_\xi = -1 \tag{3.7}$$

the variable which is held constant in the corresponding partial derivative. Rearranging

$$\frac{\partial \xi}{\partial f}_{g} = -\frac{\partial g}{\partial \xi}_{f}^{-1} \cdot \frac{\partial f}{\partial g}_{\xi}^{-1} \tag{3.8}$$

the equation, we find Eq. (3.8). From the reciprocal rule of multivariable calculus we note that $\frac{\partial f}{\partial g}_{\xi}^{-1} = \frac{\partial g}{\partial f}_{\xi}$, and we also note that $g = \frac{\partial E}{\partial \xi}$. Making the appropriate substitutions and dropping our subscript notation except for the term on the left, we obtain something that looks like Eq. (3.5) in Eq. (3.9).

$$\frac{\partial \xi}{\partial f}_{g} = -\frac{\partial^2 E}{\partial \xi^2}^{-1} \cdot \frac{\partial^2 E}{\partial \xi \partial f} \tag{3.9}$$

Essentially, this is the same result as Eq. (3.5), but the fact that the term on the left is a partial derivative is somewhat odd at first glance. However, in our derivation the result holds for any point on our energy surface(ie. the result can be evaluated for any given separation, field and gradient). In our previous derivation we have chosen all of these variables to be zero. In our first derivation,we imposed the condition of constant gradient by first choosing the system to be in a state of minimum energy, $g_0 = 0$, and again solving for ξ given $\frac{\partial E(\xi, f)}{\partial \xi} = 0$. This second derivation should bolster our argument for calculating the piezo-coefficient using Eq. (3.1).

In a similar manner to the first derivation, the estimate for the piezo-coefficient can be generalized to second order in the electric field strength f (Eq. (3.10)). For brevity we drop the $\Big|_{(z_0,0)}$ notation for the derivatives and understand that they are evaluated at $(z_0, 0)$ as before. We note that this expression simplifies to Eq. (3.1) when one lets $f \to 0$. Eq. (3.10) extends the previously described estimate for the piezo-coefficient in that it includes

$$\frac{d\xi}{df} \approx -\left(\frac{\partial^3 E}{\partial \xi^2 \partial f}\cdot f + \frac{\partial^2 E}{\partial \xi^2}\right)^{-1}\cdot\left(\frac{\partial^2 E}{\partial \xi \partial f} + \frac{\partial^3 E}{\partial \xi \partial f^2}\cdot f\right) + \left(\frac{\partial^3 E}{\partial \xi^2 \partial f}\cdot f + \frac{\partial^2 E}{\partial \xi^2}\right)^{-2}\cdot\left(\frac{\partial^2 E}{\partial \xi \partial f}\cdot f + \frac{1}{2}\frac{\partial^3 E}{\partial \xi \partial f^2}\cdot f^2\right)\cdot\frac{\partial^3 E}{\partial \xi^2 \partial f} \tag{3.10}$$

deviations from the linear regime in the piezo response, which could potentially be relevant for large field strengths and/or strong piezo-responses. Recasting in terms of the gradient and Hessian with respect to nuclear displacements as well as the dipole moment and polarizability $\alpha \equiv \frac{\partial^2 E}{\partial f^2}\Big|_{(z_0,0)}$, Eq. (3.10) takes on the more handy form given in Eq. (3.11). The first line

$$\frac{d\xi}{df} \approx -\left(\frac{\partial h}{\partial f}\cdot f + h\right)^{-1}\cdot\left(\frac{\partial \mu}{\partial \xi} + \frac{\partial \alpha}{\partial \xi}\cdot f\right) + \left(\frac{\partial h}{\partial f}\cdot f + h\right)^{-2}\cdot\left(\frac{\partial \mu}{\partial \xi}\cdot f + \frac{1}{2}\frac{\partial \alpha}{\partial \xi}\cdot f^2\right)\cdot\frac{\partial h}{\partial f} \tag{3.11}$$

can be seen to be an extension of Eq. (3.1) to include the responses of the Hessian and the dipole moment derivative up to linear order in f.

3.5 RESULTS

For a systematic investigation of the correlation between hydrogen bonding and piezo-coefficients, we selected a range of organic hydrogen-bonded systems with varying bond strengths (Fig. 21). Motivated by the known[40,47,70] piezoelectricity of the $NO_2 \cdots NH_2$ bond, we initially included dimers with single and double bonds of this type. Since the

piezo-responses for double bonded systems were rather small (likely due to the expected small compliance of these hydrogen bonds), we concentrate in the following on single bonded systems.

We expect that the hydrogen bond strength and thus piezoelectricity can be controlled by varying the hydrogen donor/acceptor pair. To test this hypothesis, we include OH $\cdots$ NH_2 as well as carbonyl-amid hydrogen bonding motifs. We also expect that the hydrogen bond strength can be tuned by adding electron donating or withdrawing groups to the aromats. For this purpose we add methyl and trifluoromethyl substituents in para position for the singly-bonded systems. Finally, we include N-[2-(dimethylamino)-5-nitrophenyl]acetamide **3** and 2-methyl-4-nitroaniline **4**, due to their known field-dependent polarizability and piezoelectric properties[40,47,70–72]. We would like to note that we do not believe that piezoelectricity in the crystal arises from the hydrogen bond in **3**, but we can still investigate the piezoelectric properties of the hydrogen-bond in the dimer to gain insight.

The piezo-coefficients and hydrogen bond strengths were calculated as outlined in the 3.6, and the dependence of d_{33} on the bond energies is plotted in Fig. 22. For the series of $NH_2 \cdots N_2O$ dimers and their derivatives, we find a d_{33}-vs-bond strength plot that resembles a "volcano plot" as known from catalysis (Ref.[73]) for systems in group 2 and a relatively unchanged piezoelectric coefficient for systems in group 1. Initially we believed this could be rationalized by considering the previous discussion of Eq. (3.1), where we proposed that a hydrogen bonded system with a weaker hydrogen bond strength (expected large compliance matrix) is typically connected with a smaller dipole derivative, whereas a bond with large dipole derivative typically has a smaller compliance. Not surprisingly, we might expect this antagonism leads to a volcano plot. Our analysis was based on the assumption that low bond strength is indicative of high compliance and high bond strength is indicative of low compliance. In Fig. 23, we see the relationship between hydrogen-bond strength and curvature (inverse compliance) and dipole derivative. In general there does seem to be a net positive correlation for both, albeit a weak one. The correlation seems to be much stronger in general within groups 1 and 2 for both curvature and dipole derivative with the exception of the dipole derivative in 2a. The piezo-coefficients for all of the molecules are roughly of the same order of magnitude, indicating that it might be difficult to identify

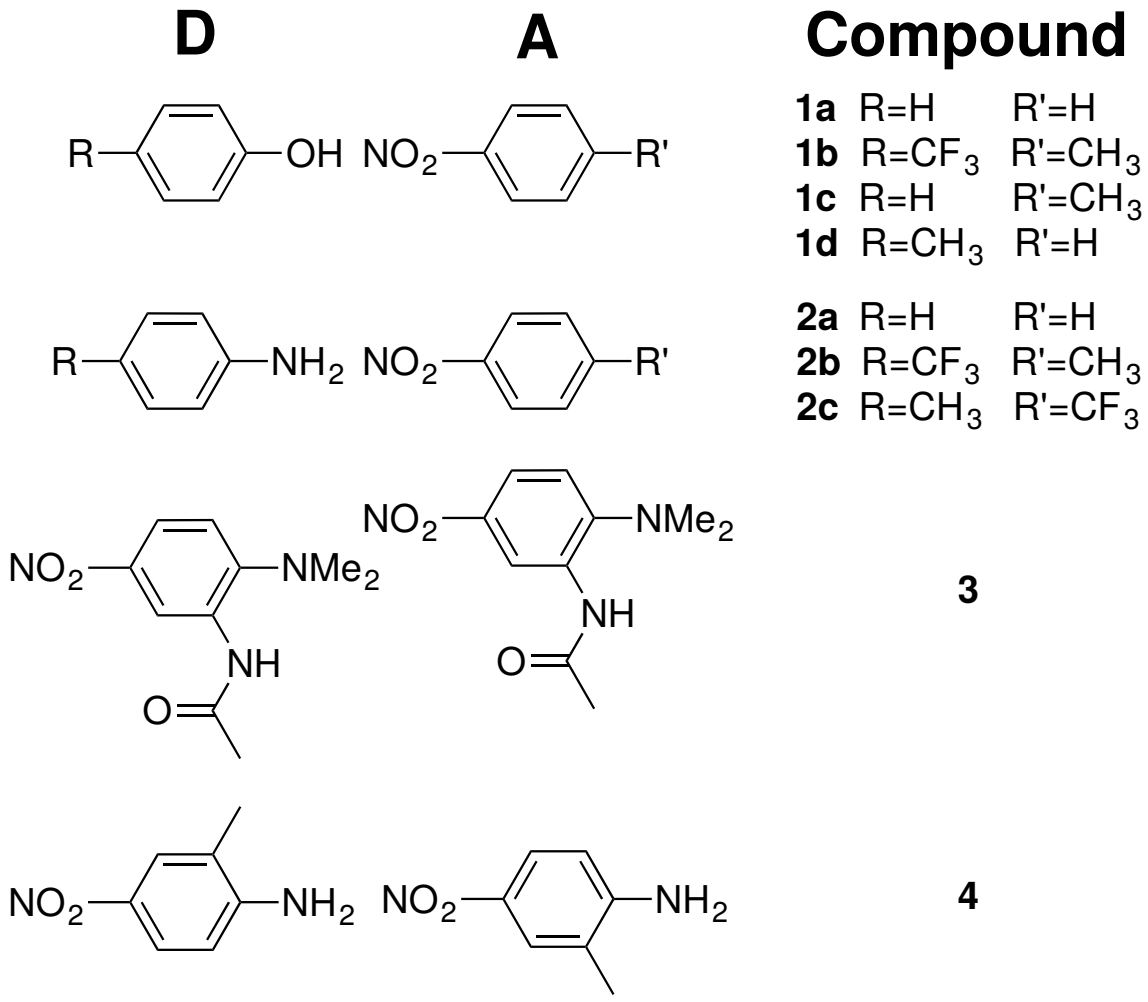

Figure 21: Molecules studied to test piezoelectric deformation of hydrogen bonds.

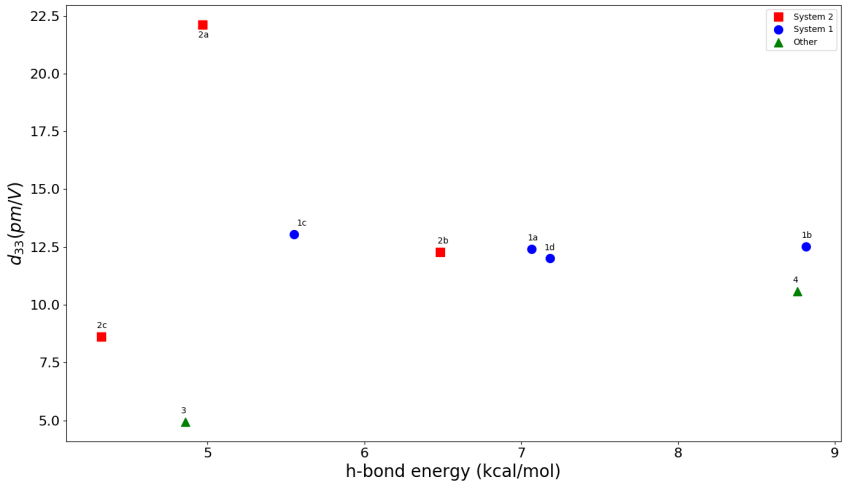

Figure 22: Plot of calculated piezo-coefficients (pm/V) versus calculated hydrogen bond strengths (kcal/mol) for different hydrogen bond types as well as different electron donating and withdrawing groups. The system labels are indicated next to the points.

organic piezoelectrics (that depend primarily on hydrogen-bonding as the primary source of deformation) that reach the 100 pm/V plus range for d_{33}. This should not be discouraging though as there are many types of interactions in the bredth of functional groups that exist in organic molecules that may lead to exceptional deformation within an applied electric field.

The largest piezo-coefficient of 22 pm/V is found for the aniline-nitrobenzene dimer **2a**. Most other systems have piezo-coefficients in the 10-13 pm/V range except for **2c** and **3** with values of about 8.6 and 4.9 pm/V respectively. Although this is a limited test bank to analyze, it is illustrative of how difficult it can be to maximize the piezocefficient for organic systems. It is interesting to note that **4** exhibits a piezo-coefficient similar to **1a**, although its hydrogen bond strength is among the largest in the test. For the slightly exotic hydrogen bonded system N-[2-(dimethylamino)-5-nitrophenyl]acetamide **3**, the piezo-coefficient of 5 pm/V is relatively small. Interestingly, the hydrogen bond strength is very similar to that of **1a**, but d_{33} is smaller by a factor of three. Our analysis indicates that

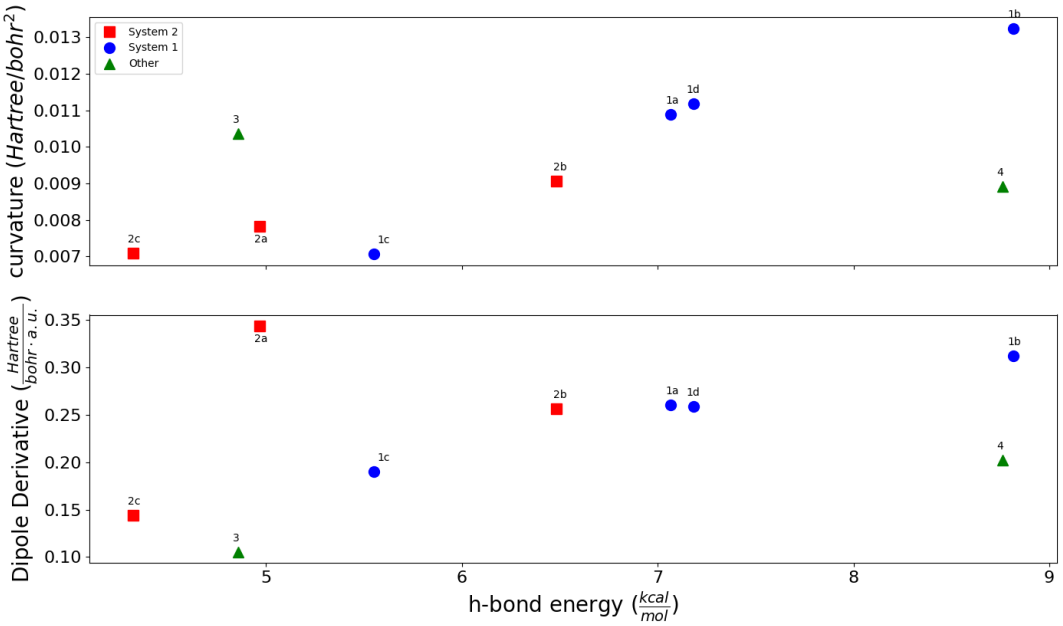

Figure 23: Dipole derivative and curvature vs. hydrogen bond energy for test systems (see Fig. 21) is shown.

bond-strength is not really a good indicator of piezocoefficients for these types of systems. Furthermore, we also found that dipole-derivative and compliance for these compounds do not necessarily show a clear antagonistic relationship. There are clearly many factors at work that influence the piezoeffect in these compounds, but their relationships with one another are not necessarily straightforward. Regardless, below we demonstrate that we can accurately calculate piezocoefficients (as compared to our earlier approximate methods) via Eq. (3.1).

In the previous discussion, we have noted that the piezoelectric behavior of our dimer systems is not straightforward when looking at hydrogen bond strength. Furthermore, in complicated systems, the relationship between bond strength and curvature or even dipole derivative and curvature is not straightforward. Eq. (3.1), however, gives us a compellingly simple rationale with which to estimate the piezo-coefficient. But how accurate is it? In Fig. 24 we show the correlation between the estimate and the fully calculated piezo-coefficient. Although Eq. (3.1) holds only to second order in ξ and mixed first order in ξ/f, fitting all data using linear regression yields a nearly perfect correlation ($R^2 = 0.997$ and Slope $= 1.02$) between estimated and calculated piezo-response.

We remark that for **1a** we have omitted data points for stronger field strengths in the linear regression analysis where the deviation from a linear behavior becomes significant. For stronger piezosystems or for larger field strengths, higher-order terms in the piezo-rationale likely need to be taken into account for an accurate estimate, but here we have only considered the piezocoefficient around zero field. Currently, we utilize numerical derivatives for the $\mu_{0\xi}$ term, as outlined in the Computational Details section. For a more accurate determination of stronger piezosystems, caution must be taken to ensure an adequate approximation of this term. Nevertheless, the performance of the rationale in its current implementation is excellent for the systems considered here, which is impressive considering the simplicity of the rationale.

We conclude that Eq. (3.1) is quite helpful at guiding the development of stronger hydrogen-bonded piezo-systems, and likely also those of other piezo-systems such as molecular springs[39]. Eq. (3.1) is much cheaper to calculate than our previous methods, since all necessary quantities are calculated at $f = 0$, whereas a full calculation requires calcula-

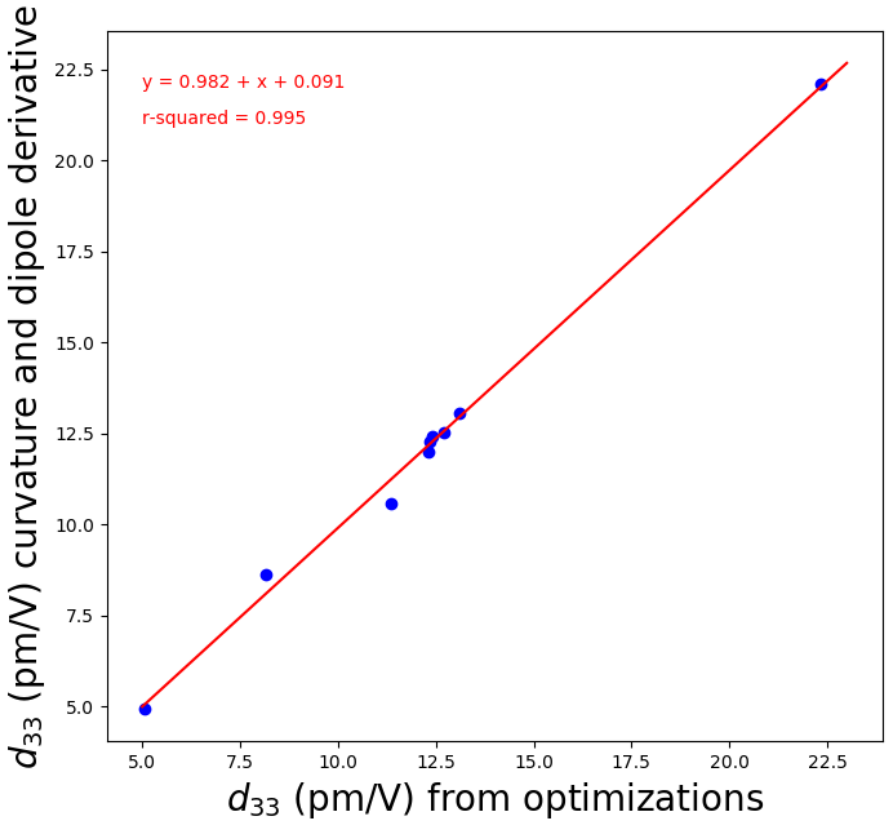

Figure 24: Plot of our estimated piezo-coefficient (Eq. (3.1)) versus the calculated piezo-coefficients (from optimizations) for the full data set is shown.

tions at five to ten different field strengths (see Computational Details). The Hessian and dipole moment derivative can be calculated from a curve fit requiring about ten single point calculations at most, as compared to about 100 calculations for our previous approach.

There is still room for improvement in both efficiency and accuracy of piezo-coefficient prediction in general. In this study we exploited a system type (ie. hydrogen-bonded organic molecules) which in general can be approximated as two rigid bodies (the individual molecules in each dimer pair) connected by a weak potential. We have shown previously that in this type of system the individual relaxation of intramolecular atoms is typically negligible compared to the change in length of the hydrogen-bond[47]. The system thus allows us to reduce the geometric dimensionality of our system to one variable (hydrogen-bond distance) in order to, at least to good approximation, predict the piezo-coefficients for these types of systems. This is also why it is cheaper to compute the derivatives (hessian and dipole) via single point energy calculations. Analytical methods used in program packages typically involve evaluations for all the degrees of freedom in the system, which is time consuming and not necessary for our purpose here.

However, a more accurate method applicable to many types of systems is desirable and would likely require the coordinated response of the energy to all degrees of freedom. This is indeed the subject of the next chapter and gives us the ability to deal with more general systems for better screening methods to predict good piezo compound candidates.

3.6 COMPUTATIONAL DETAILS

We now review the process of calculating the piezo-coefficient, which is similar to our earlier approach outlined in the previous chapter[47]. We first generated the dimer molecules from our database in Avogadro[50]. For all calculations we used the B3LYP density functional[52–55] in combination with the 6-31G* basis[57,58], which we found to qualitatively reproduce higher-level results[47]. A development version of the Q-Chem program package was used throughout[74]. After the dimer geometries were optimized at zero field, the hydrogen bonds were aligned along the z-axis, so the piezo-response could be investigated by potential energy sur-

face scans along the z-axis. We then performed subsequent calculations on the dimer pairs at varying field strengths applied along the z-axis (cf. Fig. 19). The field strengths typically ranged between -1.0 and 1.0 V/nm, incremented in steps of 0.25 V/nm.

For each field strength, we scanned the potential energy surface by varying the dimer distances, z, in steps of about 0.02 Å and calculated single point energies at each point. We plotted the energy versus hydrogen bond distance and performed a polynomial fit (usually of order 6) of the data. The equilibrium (minimum energy) hydrogen bond length for each field was found from the fit and was used to determine the piezo-coefficient. It is worthwhile to mention that the miminimum energy hydrogen bond length could also be found via geometry optimizations of the dimers subjected to external fields, but as shown previously[47], this involves complications in hydrogen bond maintenance and can be time consuming. Furthermore the constraints implicit to the scanning method were shown to not yield very different results from the optimization method.[47] To this end, we plotted the equilibrium bond lengths versus the field strength for each dimer pair. The slope of a linear regression performed for the data of one of these plots can then be used to calculate the piezo-coefficient (Eq. (3.12)). It should be noted that for one dimer (molecule **2a**), the equilibrium distance vs. field

$$d_{33} \approx \frac{1}{z_0} \cdot \text{Slope} \tag{3.12}$$

strength plot showed strong non-linearity above 0.5V/nm field strength. For this compound, these three points were deleted and the linear regression was performed as usual. This is a potential problem in this method of piezo-coefficient analysis but is avoided in the new method of piezocoefficient determination which utilizes Eq. (3.1). Looking more closely at Eq. (3.11), the degree of non-linearity will likely depend on the displacement derivative of the polarizability for the molecule.

An intuitive interpretation for Eq. (3.12) is that the slope is related to $\frac{dz_{min}}{df}$, where z_{min} is the hydrogen bond length for the two monomers of our system that minimizes the energy and f is the field strength. The piezo-coefficient can be defined as $\frac{dS_z}{df}$, where S_z is the

strain in the z direction for the system. The strain can be viewed as the fraction or percent deformation in the z direction, which one can approximate as $\frac{dz_{min}}{z_0}$, and dividing this term by *df* yields Eq. (3.12).

The method just described for piezo-coefficent calculation typically requires many single point energy calculations in addition to an initial geometry optimization. For example, in this study, after the initial geometry optimization was performed, typically around 99 single point energy calculations were carried out (for each of the 9 field strengths, typically 11 single point energies were calculated to scan the potential energy surface). Given Eq. (3.1), we can in practice reduce the number of single point energy calculations by an order of magnitude.

We now outline how we estimate the piezo-coefficient for our systems based on Eq. (3.1). z_0 was determined in the initial geometry optimization. Furthermore, the Hessian $h_{0\xi\xi} \equiv \left.\frac{\partial^2 E}{\partial \xi^2}\right|_{(z_0,0)}$ was obtained from scanning the potential energy surface at zero field, which requires only on the order of 11 single point calculations, and performing a polynomial fit of the data as described above. From the fit equation and the equilibrium hydrogen bond length, it is then straightforward to determine $h_{0\xi\xi}$.

No additional calculations are typically necessary to determine $\mu_{0\xi} \equiv \left.\frac{\partial^2 E}{\partial f \partial \xi}\right|_{(z_0,0)}$, since the potential energy surface has already been scanned and the dipole moments can be collected from the previous calculations. This last derivative was simply evaluated numerically, from the z-component of the dipole moment for the system given as output for the two single point energy calculations closest to the equilibrium hydrogen bond length (Eq. (3.13)). Here, z_1 and z_2 are the hydrogen bond lengths nearest to the equilibrium bond length.

$$\mu_{0\xi} \approx \frac{\mu(z_2) - \mu(z_1)}{z_2 - z_1} \tag{3.13}$$

The inverse Hessian and dipole moment derivatives were then combined to estimate the piezo-coefficient according to Eq. (3.1). The results for the estimate and the conventionally calculated coefficient are compared in Fig. 24, which shows a remarkable agreement as discussed earlier.

At this point, it should be noted that the dipole derivatives calculated here introduce some unknown error into our approximation of the piezo-coefficient. It is therefore advisable to use small displacements in the separation coordinate z in order to evaluate the piezo-coefficient more accurately. There are also well known methods for efficiently and accurately calculating diopole derivatives which invole the numerical calculation of the derivative of the gradient for the system with respect to the field[75]. Euler's relation, which is actually also used in the Derivation Section, allows us to write $\frac{\partial^2 E}{\partial \xi \partial f} \equiv \frac{\partial^2 E}{\partial f \partial \xi}$ or $\frac{\partial \mu}{\partial \xi} \equiv \frac{\partial g}{\partial f}$, where g is of course the gradient.

For the determination of hydrogen bond energies within our system database, we simply used the difference in energy between the optimized isolated monomers and the dimers. We are aware that the energies are only very approximate without counterpoise correction or dispersion correction, but here we aim only at the investigation of qualitative trends.

3.7 CONCLUSION

To find systems with a large piezo-response, one needs to find a bond or vibrational mode with a large compliance (i.e., low force constant) and a large change in dipole moment as the bond length changes. For hydrogen-bonded systems at least, this requires systems that are neither too weakly bound (i.e., low force constant but also small change in dipole moment) nor too strongly bound (i.e., large change in dipole moment, but large force constant). Our computational screening in this work suggests such systems are rare, but one $NH_2 \cdots O_2N$ candidate, the simple aniline-nitrobenzene dimer **1a**, has a larger predicted piezo-response (23 pm/V) than 2-methyl-4-nitroaniline **4** (14 pm/V), the organic crystal with the largest known piezoelectric response, and similar to PVDF, the most widely used piezoelectric polymer.

The accuracy of the estimated piezo-coefficient derived here and the high correlation with explicitly-calculated geometric deformations suggest a rapid method to screen a wide range of hydrogen-bond motifs and molecular materials. While few piezoelectric organic crystals are known, many more likely exist and can be found by high-throughput computational

techniques. We anticipate that by subtle tailoring of the substituents with the the aniline-nitrobenzene and phenol-nitrobenzene dimers and similar hydrogen-bonded families, we may find larger electromechanical deformations than previously experimentally reported.

Another promising application of the estimate is that it provides a simple rationale for the piezo-response that makes it fairly simple to understand how to obtain increased piezo-coefficients. For example, it can be understood why molecular springs with polar end groups[76] exhibit large piezo-coefficients in excess of 100 pm/V and more: the restoring force of the spring counteracts the attractive force between the polar end groups, which effectively increases the compliance along the piezo-active coordinate. Thus, a large compliance plus a large dipole moment derivative can be achieved simultaneously, leading to a large piezo-coefficient. Molecules of the molecular spring type thus seem particularly attractive to explore for improved piezo-materials.

In short, electromechanical hydrogen bonds and molecular systems are likely to be ubiquitous and can be rapidly screened using accurate first principles electronic structure calculations. Based on the trade-off between hydrogen-bond strength and change in dipole moment in intermolecular interactions, we believe that electric-field driven molecular conformational changes will bring more substantial piezoelectric response, and deformable hydrogen bonds can be used to produce polar, self-assembled piezoelectric materials designed through computational approaches.

4.0 METHOD FOR CALCULATING ELECTROMECHANICAL RESPONSE FOR MOLECULES AND NANOSTRUCTURES

This work is in the process of being submitted for publication and a preliminary version can be found on arXiv (https://arxiv.org/abs/1707.07464). My contribution includes all derivations and discussion save the 4d piezoelectric tensor and the linear regressions in the Results section.

4.1 SUMMARY

Devoloping a method for the calculation of electromechanical response of aperiodic materials is a prerequisite for understanding the piezoelectric properties of systems such as nanoparticles or biomolecule agglomerates. The focus of this chapter is to establish a formalism for describing *molecular* piezoelectric responses. We define the piezoelectric matrix, $\mathbf{P}$, to describe the electromechanical deformation properties between bodies of interest in (small) finite systems (though the ideas may be extended to periodic systems). To this end, we develop a computational procedure for practical calculations of piezoelectric matrices for molecular systems. Our studies demonstrate that the new procedure yields results that are consistent with fully numerical computations from geometry optimizations and in fact are more stable with respect to numerical convergence and field strength. It is expected that the present work will aid in developing design strategies for aperiodic piezoelectric systems by revealing connections between molecular structure and piezoelectric response.

4.2 INTRODUCTION

There is no established formalism, let alone an established language, to describe *molecular* piezoelectricity. In contrast, notions from continuum mechanics (bulk scale), to define quantities such as strain and stress, typically derived for crystalline (periodic) systems based on unit cells and their deformations. This approach is not able to describe the piezoelectric response of individual molecules and (small) finite systems. Developing a molecular understanding of piezoelectric response is, however, important to describe (noncrystalline) polymers, as well as responses of small (e.g. nano) systems that are inhomogeneous, anisotropic, and aperiodic, so that the bulk description is not yet applicable. Examples of the latter include the electromechanical response of biomolecules, coiled or strained organic molecules, clusters from organic crystals as well as nano-scale machines. In this chapter, we aim to establish a method for calculating *molecular* piezoelectric responses.

In the previous chapters, we developed a computational approach to predict piezoelectric responses based on the definition of the converse piezoelectric effect, ie. the deformation of a system in response to an applied field. This approach is most natural in aperiodic calculations, where it is straightforward to apply an electric field perturbation to the Hamiltonian. We established a simple computational procedure where the piezo-coefficient d_{33} is estimated by calculating the geometric response while applying a finite electric field. We then improved on this approach by developing an analytical expression that calculates d_{33} from the zero-field geometric Hessian and dipole moment derivative. This approach has several advantages over our first procedure–for example by avoiding the finite-field calculations (which can be problematic because of electronic instability of molecules in finite electric fields)[77–80] and by cutting down on the computational cost via requiring only zero-field calculations (as opposed to calculations at several finite field strengths). We demonstrated that both approaches yield comparable results for molecular systems and used these approaches to explore piezoelectric responses in hydrogen-bonded systems. In fact, we showed that hydrogen bonding in 2-methyl-4-nitroaniline (MNA) gives rise to significant piezoelectricity[47]. We then explored several examples of hydrogen donor-acceptor systems to help establish a general rationale for the construction of systems with large d_{33}. We found that our analytical expression is

also useful in explaining piezoelectric responses by showing that a large d_{33} requires both a sufficiently large inverse Hessian (large compliance of the bond) and large dipole moment derivative.

This previous approach is limited to dimer systems with deformation properties dominated by intermolecular as opposed to intramolecular piezoelectric response along a single axis. In this work, we extend our previous approach by taking the full response of the nuclear coordinates into account. By doing this, we can predict the piezoelectric response properties of any finite system (single molecule, bio-molecule/s, nano-particles, etc.) and forgo the need to apriori predict a single, dominating direction of largest piezoelectric response. In fact, in a sense molecules give rise to the most anisotropic cases imaginable compared to the unit cell parameters of crystals. Therefore, extending the dimensionality of our previous equations would reveal the full anisotropy. We will show that the axis and magnitude of the largest piezoelectric response for a given pair of coordinates in a system can be obtained by diagonalizing a matrix derived from the yet to be presented molecular piezoelectric matrix. Furthermore, we derive a useful formula to calculate the piezoelectric matrix and discuss its connection to our previous work. Our approach shares features with previous methods to calculate (electro)mechanical responses in periodic systems from first principles,[81–88] but our formulation provides a convenient formalism for describing electromechanical responses specific to aperiodic molecular- and nano-scale systems. The method we present for calculating the piezoelectric matrix can be used to understand the deformation properties between any two bodies in a system and has applicability to the rational design of organic piezoelectric materials. Another advantage is that this generalized approach can be automated and only requires that the user specify an orientation relative to which the response is predicted and interpreted. We discuss this and other aspects which users might find useful to understand and predict the response of molecular deformation in the presence of fields.

4.3 TOPICS FROM CONTINUUM MECHANICS AND STRAIN THEORY

The theory of piezoelectric response is well-established for crystalline (bulk) systems. For more information on piezoelectricity we refer the reader to Ref.[27–29]. Recall from the constituitive equations presented in 1.1.2, that the piezoelectric tensor **d** is a third rank tensor and has the following definitions for the direct and converse piezoelectric effect. For the direct effect, the piezoelectric tensor is given by Eq. (4.1). Here **D** is the polarization vector, **T** is

$$d_{ijk} = \left(\frac{\partial D_i}{\partial T_{jk}}\right)_{\mathbf{f}} \tag{4.1}$$

the stress tensor and **f** is the electric field. For the converse effect, the piezoelectric tensor is then given by Eq. (4.2). Here **E** is the strain tensor (here we will use the Green strain

$$d_{ijk} = \left(\frac{\partial E_{ij}}{\partial f_k}\right)_{\mathbf{T}} \tag{4.2}$$

tensor (see B.1), and the other variables are the same as defined above. We will restrict the discussion of the piezoelectric tensor to the definition for the converse effect. We note that the indices pertaining to strain, ij, depend on the coordinate system used as a reference frame for measuring strain (which can be e.g. unit cell parameters or cartesian coordinates, etc.), whereas the index contracted with the field, k, depends on the external (laboratory) reference frame of the applied field.

To understand how to calculate d_{ijk} in practice and to provide some context for the following sections, we introduce here selected concepts of strain theory within the framework of continuum mechanics. In continuum mechanics, the material is treated as a continuum of infinitesimally small particles (ie. any division of the material, no matter how small, will

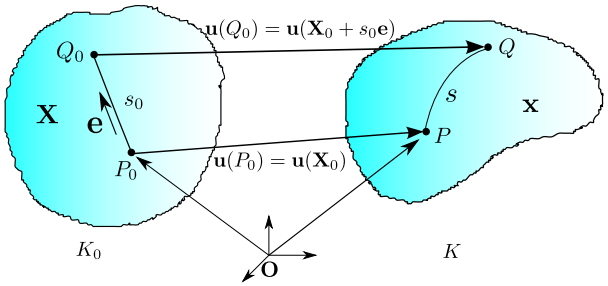

Figure 25: A general deformation of a continuum body is shown (adapted from[1]). The position vectors for the undeformed body, K_0, and the deformed body, K are given by $\mathbf{X}$ and $\mathbf{x}$ respectively. The displacement vector, $\mathbf{u}$, maps the position in the undeformed coordinates to a position in the deformed coordinates and indicates the direction and magnitude in the "shift" of an infinitetesimal particle (point) in space as the body deforms.

contain matter). Obviously, this is not an appropriate description for a molecular system, but starting from these definitions, we will therefore develop a theory for molecular (i.e., discrete, anisotropic and inhomogeneous) systems.

Generally, strain analysis is concerned with concepts such as longitudinal strain, shear strain, and volumetric strain. We will be mostly concerned with longitudinal strain for the discussion that follows. To this end, consider a body undergoing mechanical deformation (Fig. 25). Configurations K_0 and K correspond to the undeformed and deformed bodies, respectively. Particle positions before and after deformation are denoted by $\mathbf{X}$ and $\mathbf{x}$, respectively, where we note that these positions are specified within the same (external) coordinate frame. The vector field $\mathbf{u}(\mathbf{X}, t)$ gives the displacement vector from a point in the undeformed body to a corresponding point in the deformed body. The displacement vector field will become important later when we define the Green strain tensor. For molecular systems a discrete displacement vector field exists for each atom in a molecule or a system as said body deforms. A central question is how a given material line deforms as the body is deformed from the initial (K_0) to the final (K) shape. For our purposes, the material line can be seen as any line drawn through some arbitrary but continuous path of particles in

the body. For convenience, we show the undeformed material line as a straight line segment P_0Q_0 with length s_0 and the deformed material line as the curve along PQ with length s. The unit vector along the line segment P_0Q_0 is called $\mathbf{e}$. Based on this picture, one defines the longitudinal strain ϵ, i.e. the strain along the direction of $\mathbf{e}$, as the relative change in the length of the material line upon deformation in the limit of infinitesimal line length (Eq. (B.1)). We note that we used a very similar, though less rigorous definition in our previous

$$\epsilon = \lim_{s_0 \to 0} \frac{s - s_0}{s_0} = \frac{ds - ds_0}{ds_0} = \frac{ds}{ds_0} - 1 \tag{4.3}$$

work[47,89] where we used the percent deformation in bond lengths to approximate the piezoelectric deformation. As noted, we are not concerned with volumetric or shear strain here, although appendix section B.1 presents more details about the Green strain tensor which can be used to completely specify the linear deformation around a point within a continuum body.

4.4 PIEZOELECTRIC MATRIX

In the previous chapter 3, we found d_{33} for a simple system of hydrogen-bonded dimers (Eq. (4.4)). Here z_0 is the equilibrium hydrogen-bond distance for the two dimers, H_{zz}^{-1}

$$d_{33} \approx -\frac{1}{z_0} H_{zz}^{-1} \cdot H_{zf} \tag{4.4}$$

is the inverse curvature of the electronic energy as the two dimers are separated along the hydrogen bond coordinate z, and H_{zf} is the derivative of the dipole moment with respect to

the hydrogen-bond coordinate. The simple model utilizes the fact that for many hydrogen-bonded dimers, the intramolecular piezoelectric response is substantially (at least an order of magnitude) smaller than the deformation of the hydrogen bond. Hence, we can approximate d_{33} using Eq. (4.4), by assuming only a one-dimensional hydrogen bond length parameter (z) that relaxes in a one-dimensional field f that is applied in the direction of the bond. The derivative of the hydrogen bond distance with respect to field (under the conditions of geometric equilibrium and zero field) is given by Eq. (4.5). The multidimensional version of

$$\left.\frac{dz}{df}\right|_{\frac{dE}{dz}=0,f=0} = H_{zz}^{-1} \cdot H_{zf} \tag{4.5}$$

Eq. (4.5) is given by Eq. (B.36). where $\mathbf{u}$ is the displacement vector for all nuclear positions

$$\left(\frac{\partial \mathbf{u}}{\partial \mathbf{f}}\right)_{\mathbf{f}=\mathbf{0},\nabla_{\mathbf{u}}E=\mathbf{0}} = -\mathbf{H}_{\mathbf{uu}}^{-1} \cdot \mathbf{H}_{\mathbf{uf}} \tag{4.6}$$

of a small system, and $\mathbf{f}$ is the full three-dimensional field vector. This result is known from Ref.[81] but can easily be derived from a Taylor expansion of the energy of the system in displacement and field coordinates (see appendix, section B.4). $\mathbf{H_{uu}}$ and $\mathbf{H_{uf}}$ are the full nuclear Hessian and dipole derivative (with respect to nuclear displacement) matrix.

From Eq. (B.36), we introduce the Piezoelectric matrix, $\mathbf{P}$ for a pair of coordinates (Eq. (B.42)). Here the superscripts 1 and 2 correspond to two bodies in the system. The bodies could be two atoms or perhaps the geometric center or center of mass for two sets of atoms in the system for example. The vector $\mathbf{u}$ then has indices over the x,y, and z components for the positions of these bodies (or other length variables in a different basis). In practice, it is simple to find the derivatives for variables which are linear combinations of atom positions like the geometric center, owing to the linearity of the derivative operator. but in principle

$$\mathbf{P} = \frac{1}{r_0}\left(\frac{\partial \mathbf{u}^2}{\partial \mathbf{f}} - \frac{\partial \mathbf{u}^1}{\partial \mathbf{f}}\right) \tag{4.7}$$

nonlinear coordinates can also be employed. For variables which are linear combinations of position variables, we have Eq. (4.8). For nonlinear variables, we have Eq. (4.9). The sums

$$\begin{aligned} \mathbf{u}^a &= \sum_i c_i \mathbf{u}_i \\ \frac{\partial \mathbf{u}^a}{\partial \mathbf{f}} &= \sum_i c_i \frac{\partial \mathbf{u}_i}{\partial \mathbf{f}} \end{aligned} \tag{4.8}$$

$$\begin{aligned} \mathbf{u}^a &= \mathbf{g}(\{\mathbf{u}_i\}) \\ \frac{\partial \mathbf{u}^a}{\partial \mathbf{f}} &= \sum_i \frac{\partial \mathbf{g}}{\partial \mathbf{u}_i} \cdot \frac{\partial \mathbf{u}_i}{\partial \mathbf{f}} \end{aligned} \tag{4.9}$$

over i are over the sets of nuclei in the system which are used to construct the variables $\mathbf{u}^a$. The vector function $\mathbf{g}$ has a set of variables $\{\mathbf{u}_i\}$, and the matrix product under the summation in the second line for Eq. (4.9) is just the result of the chain rule for multivariable functions for a vector valued function.

Similar to our second publication[89], we avoid having to perform multiple geometry optimizations in a number of fields to measure the linear piezoelectric response of systems. (Finite field approaches are problematic in that, strictly speaking, static electronic structure calculations in finite fields are not well-defined due to the instability of the molecule in the field.) Moreover, it is difficult to control the numerical accuracy of finite-field calculations because of small mechanical deformations. Finally, geometry optimizations in finite fields can lead to deformations containing unwanted motions (ie. rotations) due to the inevitable coupling of rotational and vibrational degrees of freedom for all but infinitesimal motions. This will be expounded later, but this coupling can lead to wildly erroneous answers. Unlike our previous methods for calculating d_{33}, we take into account the full geometric relaxation of the nuclei in an applied field and measure the deformation of the nuclei in all three dimensions. This new approach extends our abilities to calculate piezoelectric responses to arbitrary classes of molecules and without need to define a preferred coordinate of deformation a priori. After the calculation of $\frac{\partial \mathbf{u}}{\partial \mathbf{f}}$, instead we may calculate the deformation properties for any coordinate we choose and store the information as the piezoelectric matrix. This feature reduces the need for user input in the calculation and thus reduces the possibility of human error, increases objectivity and reproducibility, and overall is essential for computational screening.

One important aspect of Eq. (B.36), is that a naive inversion of the Hessian will produce abnormally large results for the displacement derivatives of the nuclei. This is due to the Hessian containing rotations and translations which have zero (near-zero in practice) eigenvalues for systems. It is known from[90] how to project out these unwanted modes, and B.6 gives detailed information on how to construct rotational and translational modes and how to ensure that they are adequately separated from the vibrational basis for the molecule. The remaining orthonormalized modes that live in the space of the vibrational modes can then be organized in the columns of the matrix $\mathbf{V}$ and the following transformations to and from the new basis can be performed to calculate $\frac{\partial \mathbf{u}}{\partial \mathbf{f}}$ (Eq. (B.38). Transforming back to the original coordinate system is then straightforward and leads to Eq. (B.41). We introduce the subscript vib to signify that these displacements correspond only to intramolecular deformations in the space of vibrations. It should be mentioned that one can also choose to project

$$\left(\mathbf{V}^T \cdot \frac{\partial \mathbf{u}}{\partial \mathbf{f}}\right)_{\mathbf{f=0}} = -\left(\mathbf{V}^T \cdot \mathbf{H_{uu}} \cdot \mathbf{V}\right)^{-1} \cdot \mathbf{V}^T \cdot \mathbf{H_{uf}}$$
$$\left(\frac{\partial \mathbf{v}}{\partial \mathbf{f}}\right)_{\mathbf{f=0}} = -\mathbf{H_{vv}^{-1}} \cdot \mathbf{V}^T \cdot \mathbf{H_{vf}} \tag{4.10}$$

$$\left(\frac{\partial \mathbf{u}_{\text{vib}}}{\partial \mathbf{f}}\right)_{\mathbf{f=0}} = -\mathbf{V} \cdot \mathbf{H_{vv}^{-1}} \cdot \mathbf{H_{vf}} \tag{4.11}$$

out other "motions" from the Hessian if they wish to constrain the movement in some way. For example, we can disallow the relative twisting of molecules out of plane or side to side movement etc. This might be useful to impose certain symmetries, such as those present in periodic systems, at the cost of aperiodic calculations. In such cases, however, it might also be necessary to project out such movements during the zero field geometry optimization to minimize the molecule's energy only along allowed modes. In this case these motions should also be projected out of the gradient because otherwise the optimization might not reach its convergence tolerance for the gradient.

4.4.1 Optimal piezoelectric response

d_{33} can be be approximated in a manner similar to our previous paper by Eq. (4.12). We contract the $\mathbf{P}$ matrix over the indices for the displacement vector with the unit vector (to ensure consistency of our units) $\mathbf{e} = \frac{\mathbf{r}_2 - \mathbf{r}_1}{r_0}$. Furthermore, we would also contract over the field indices, multiplying by a unit vector also in the direction of $\mathbf{e}$, (the basis chosen for the field

$$\begin{aligned} d_{33} &= \mathbf{e}_u^T \cdot \mathbf{P} \cdot \mathbf{e}_f \\ &= \frac{\partial^2 u_{r_0}}{\partial r_0 \partial f_{r_0}} \end{aligned} \tag{4.12}$$

must coincide with the basis for the nuclear coordinates if the contracted vector is actually **e**). The subscripts attached to the **e** vector are to indicate both indices of contraction (ie. the vector **u** or **f**) and to indicate that although the vector **e** is in the direction of the material line it might have two different representations depending on the nuclear coordinate and field bases. The only difference between calculating d_{33} in this way vs. our previous paper[89] is that we take the full geometric relaxation of the nuclei (only in the basis of vibrations) into account.

The piezoelectric matrix can also be used to find the largest piezoelectric response between two coordinates and the direction of applied field which yields the highest response. This is an important application given the convoluted deformation of aperiodic systems such as molecules. The procedure results in an eigenvalue problem for a new matrix $\mathbf{P}^T \cdot \mathbf{P}$ (Eq. (4.13)). This result follows from optimizing Eq. (4.14) under the constraint given in Eq.

$$\mathbf{P}^T \cdot \mathbf{P} \cdot \mathbf{f} = \lambda \mathbf{f} \tag{4.13}$$

(4.15) where k is some constant. The value of k is unimportant as it scales the result of multiplying $\mathbf{P}^T \cdot \mathbf{P}$ by **f** but not relative proportions between different directions of **f**. The approximation of Eq. (4.14) is justified because we are only interested in the strain derivative with respect to the field and not the deformation at finite field values. The resulting lagrange equation yields Eq. (4.13). Appendix B discusses in full the derivation of the piezo-

$$\left|\frac{du}{dr_0}\right|^2 \approx \mathbf{f}^T \cdot \mathbf{P}^T \cdot \mathbf{P} \cdot \mathbf{f} \tag{4.14}$$

$$\mathbf{f}^T \cdot \mathbf{f} = k \tag{4.15}$$

electric matrix from strain theory and how the matrix may be interpreted in a molecular or nanosystem context.

4.4.2 Full molecular piezoelectric response as a rank 4 tensor

After the calculation of $\frac{\partial \mathbf{u}}{\partial \mathbf{f}}$ for the system we can organize the piezoelectric matrices for every pair of atoms in the system into a single supermatrix $\mathbf{D}$ (or rank-4 tensor D_{ijkl}). Here N is

$$\mathbf{D} \equiv \begin{pmatrix} \mathbf{P}_{1,1} & \mathbf{P}_{1,2} & \cdots & \mathbf{P}_{1,N-1} & \mathbf{P}_{1,N} \\ \mathbf{P}_{2,1} & \mathbf{P}_{2,2} & \cdots & \mathbf{P}_{2,N-1} & \mathbf{P}_{2,N} \\ \vdots & \vdots & \ddots & \vdots & \vdots \\ \mathbf{P}_{N-1,1} & \mathbf{P}_{N-1,2} & \cdots & \mathbf{P}_{N-1,N-1} & \mathbf{P}_{N-1,N} \\ \mathbf{P}_{N,1} & \mathbf{P}_{N,2} & \cdots & \mathbf{P}_{N,N-1} & \mathbf{P}_{N,N} \end{pmatrix} \tag{4.16}$$

the total number of atoms. An entry $\mathbf{P}_{ij}$ in the supermatrix is given by Eq. (4.17). Here $\frac{\partial \mathbf{u}}{\partial \mathbf{f}}_i$ is the portion of the field derivative of the displacement vectors for the system corresponding to atom i (as discussed in the previous sections), and r_{ij} is the distance between atom i and j in the equilibrium geometry.

$$\mathbf{P}_{ij} = \frac{\frac{\partial \mathbf{u}}{\partial \mathbf{f}}_j - \frac{\partial \mathbf{u}}{\partial \mathbf{f}}_i}{r_{ij}} \tag{4.17}$$

By definition of $\mathbf{P}_{ij}$ the matrices along the diagonal of the supermatrix are undefined $r_{ii} = 0$, and the supermatrix is antisymmetric (Eq. (4.18)).

$$\mathbf{D} \equiv \begin{pmatrix} \mathbf{P}_{1,1} & \mathbf{P}_{1,2} & \cdots & \mathbf{P}_{1,N-1} & \mathbf{P}_{1,N} \\ -\mathbf{P}_{1,2} & \mathbf{P}_{2,2} & \cdots & \mathbf{P}_{2,N-1} & \mathbf{P}_{2,N} \\ \vdots & \vdots & \ddots & \vdots & \vdots \\ -\mathbf{P}_{1,N-1} & -\mathbf{P}_{2,N-1} & \cdots & \mathbf{P}_{N-1,N-1} & \mathbf{P}_{N-1,N} \\ -\mathbf{P}_{1,N} & -\mathbf{P}_{2,N} & \cdots & -\mathbf{P}_{N-1,N} & \mathbf{P}_{N,N} \end{pmatrix} \tag{4.18}$$

4.5 PROCEDURE FOR DETERMINING THE PIEZOELECTIC MATRIX

The procedure for calculating the piezoelectric matrix is outlined in Fig. 26. For all numerical test calculations, we used the B3LYP[52–55] functional. We found that using a finer grid for the numerical quadrature of the exchange-correlation part of the energy functional had a profound impact on the numerical accuracy in the derivatives of the electronic energy. We found using 128 radial grid points per atom and 302 Lebedev angular points satisfactory for the test systems[51].

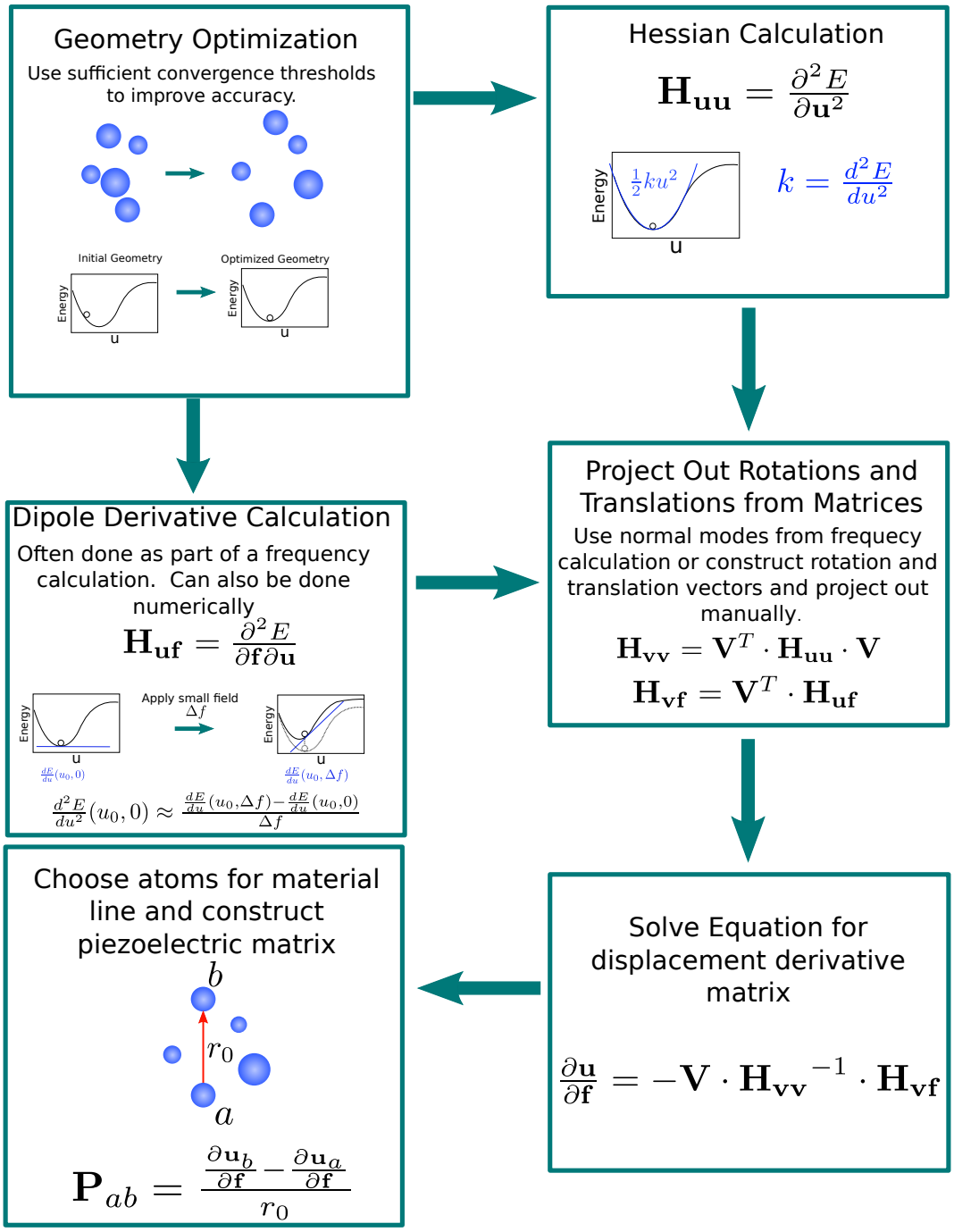

Figure 26: Flowchart depicting the computational procedure for calculating piezoelectric matrices.

4.5.1 Geometry optimization

The first step is to optimize the geometry of the system. Highly piezoelectric molecules typically have an electronic energy with low curvature along one or several vibrational modes; it is therefore required to use strict convergence thresholds for the geometry optimization. For the calculations presented in section 4.6, we used an energy change of 1×10^{-7} hartree from the previous optimization cycle , a maximum absolute value for a component of the gradient of 1×10^{-5} hartree/bohr, and a maximum absolute value for a component of the displacent of the nuclei from the previous step of 5×10^{-5} bohr. In Q-chem only two of these criteria have to be met for convergence to be "achieved."

If one wishes to constrain the system during optimization in some way (eg. to impose restrictions on motion that might be caused by the local environment not represented in the system), lagrange multiplier or projection techniques might be employed[91–93]. When finding the piezoelectric matrix, it is then possible to project such motions out of the vibrational basis and perform the aforementioned transformations with a further reduced $\mathbf{V}$ matrix. See sections B.4 and B.6 for details.

4.5.2 Hessian calculation

Analytical methods to calculate the Hessian might be too slow if the program package used does not have parallel implementations. For the molecules given in the results section we used parallelelized numerical Hessian calculations available in Q-Chem over several cores[51] in vibrational analysis calculations. Results for the numerical Hessians did not differ significantly from the analytical calculations.

4.5.3 Dipole derivative calculation

The dipole derivative, $\frac{\partial^2 E}{\partial \mathbf{u} \partial \mathbf{f}}$, calculation may be performed in combination with the Hessian calculation. Alternatively, if one is performing a vibrational analysis for the Hessian calculation, the dipole derivatives are usually calculated analytically as well since they have a well established relationship with the intensity of infrared active vibrational modes[94]. In

Q-Chem, the dipole derivative matrix is calculated analytically as the geometric derivative of the expectation value of the dipole operator on the wavefunction. In this case, one can merely retrieve the dipole derivatives together with the Hessian at the end of a frequency calculation. Dipole derivatives can also be calculated numerically as discussed in Ref[94].

4.5.4 Project out rotations and translations

To construct the transformation matrix $\mathbf{V}$ from Eq. (B.38), we first determine the eigenvectors of the Hessian matrix. We then construct rotation and translation vectors from the nuclear positions in the optimized geometry. (See B.6 for details). We proceed to project out the rotation and translation vectors from each vector in the eigenvector basis. The vectors are then renormalized if their maximum absolute value of a component exceeds a certain threshold (here taken to be 10^{-5}). This leads to $3N-5$ or $3N-6$ (for linear or nonlinear molecules respectively) nonzero vectors, which can then be internally reorthonormalized via the Gram-Schmidt algorithm (though other algorithms can also be used)[91,95,96].

4.5.5 Solve for displacement derivative matrix

Now that we have the transformed Hessian and dipole derivative matrix ($\mathbf{H_{vv}}$ and $\mathbf{H_{vf}}$ respectively), we may solve for the displacement derivative matrix $\frac{\partial \mathbf{u}_{\text{vib}}}{\partial \mathbf{f}}$. This matrix contains the derivatives of all the nuclear displacement vectors $\mathbf{u}$ with respect to the field vector $\mathbf{f}$ under the condition that the energy remain minimized and only deformations in the space of the vibrational motion of the molecule is allowed. The matrix dimensions are inherently $3N \times 3$ once transformed back into cartesian coordinates. We generally solve in the vibrational mode space, but subsequently transform back to the cartesian coordinates. The equation given by Eq. (B.41) is also included in Fig. 26. Even though the inverse of the $\mathbf{H_{vv}}$ is written in Eq. (B.41), it is not necessary to invert this matrix; it is generally more efficient to just solve $\mathbf{H_{vv}} \cdot \frac{\partial \mathbf{v}}{\partial \mathbf{f}} = -\mathbf{H_{vf}}$ for $\frac{\partial \mathbf{v}}{\partial \mathbf{f}}$ via known algorithms[97–99]. Subsequently, one transform $\frac{\partial \mathbf{v}}{\partial \mathbf{f}}$ back to cartesian coordinates via $\mathbf{V} \cdot \frac{\partial \mathbf{v}}{\partial \mathbf{f}}$.

4.5.6 Construct piezoelectric matrix

The piezoelectric matrix for a pair of nuclei is constructed by first obtaining the necessary 3×3 matrices $\frac{\partial \mathbf{u}_i}{\partial \mathbf{f}}$ for the ith atoms. Then after finding the distance, r_0, between the two atoms in the minimized geometry, the Piezoelectric matrix is constructed via Eq. (B.42). Due to linearity of derivative operators, if instead we choose to use two coordinates, formed from linear combinations of the nuclear positions, like the center of mass or geometric center of some set of atoms in the system (for example two benzene rings), the $\frac{\partial \mathbf{u}_i}{\partial \mathbf{f}}$ matrices are formed from linear combinations of the individual matrices for the nuclei in the sets with the same coefficients (Eq. (4.8)).

4.6 RESULTS

Three molecules were used to test the method developed to calculate a piezoelectric matrix **P**. Fig. 27 shows the three molecules and the pairs of atoms in each which were used to calculate a piezoelectric matrix (a). The Piezoelectric matrix based on the atom pairs is also reported from our calculations outlined in the Procedure section (b). We also report an estimated piezoelectric matrix from finite-field optimizations (c). All energy calculations were performed at the B3LYP/6-31G(d) level with Q-chem[51]. The plots shown in (c) correspond to geometry optimizations performed with fields applied in the x, y, and z direction (columns). The rows of the matrix correspond to differences in the displacement vectors from zero field between the two highlighted atoms–ie. u_x, u_y, and u_z. A single plot shows the change in displacement ($u_{bi} - u_{ai}$ (atoms a and b and component of displacement vector, u_i)) from equilibrium between the two highlighted atoms for the corresponding coordinate u_i (given by row) for varying values of the corresponding field direction f_j (given by column). All other field components are held at zero for a given plot. The number reported in each plot is the slope of the plot divided by the equilibrium distance (r_0) for the two atoms; the numbers should be close to the corresponding entry in the reported **P** matrix. The molecules chosen are helicene-like because they offer us the ability to test our new method

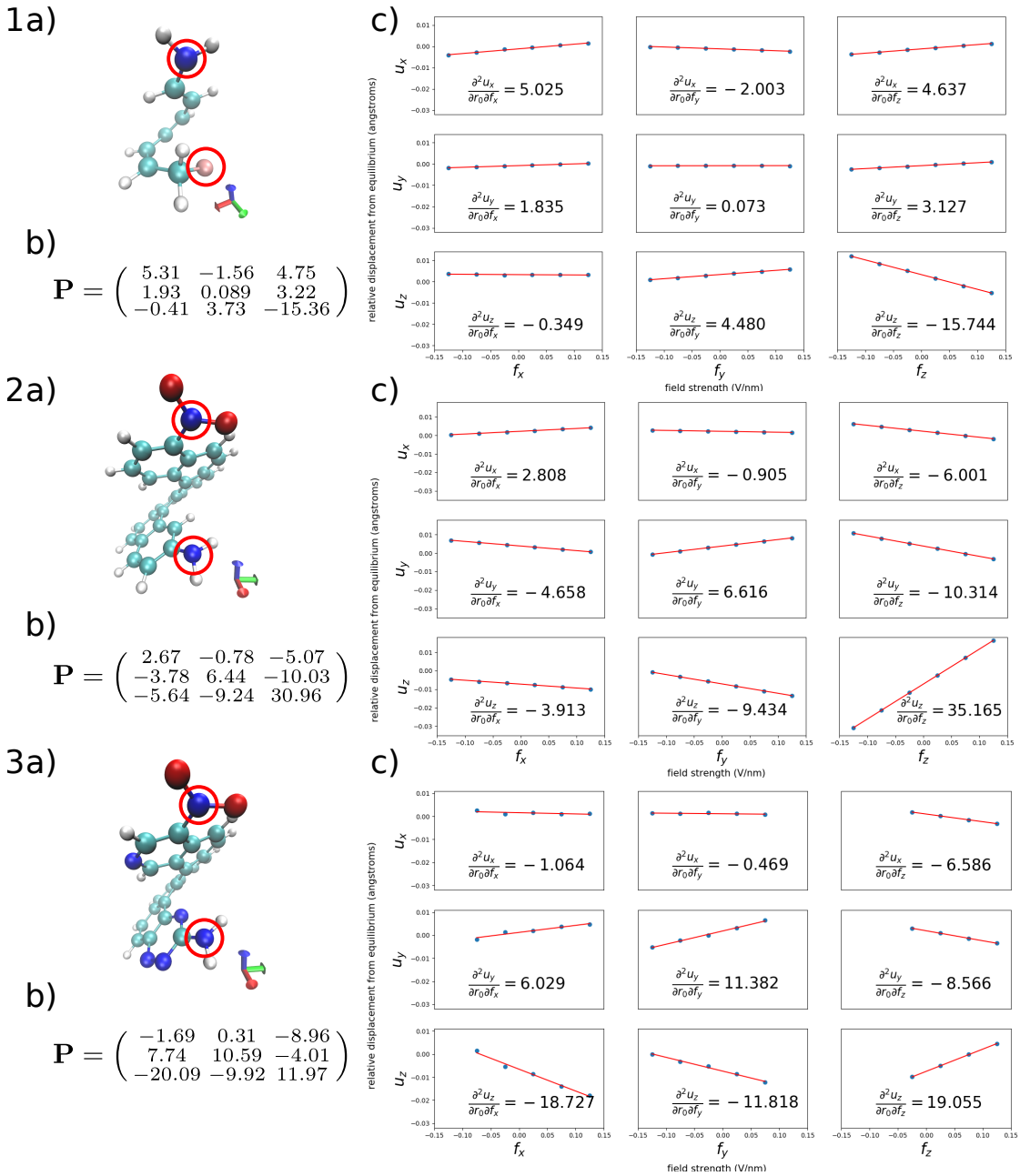

Figure 27: Numerical benchmarks on: 1a) a small conjugated helical molecule (the terminating halogen is fluorine), 2a) a typical helicene molecule, and 3a) a nitrogen-rich helicene molecule. The atoms chosen for the Piezoelectric matrix are highlighted with red circles. We compare results from the calculated piezoelectric matrix (b) with those for an estimated matrix obtained from geometry optimizations within applied fields (c). Molecules are rendered with Tachyon in VMD[100,101].

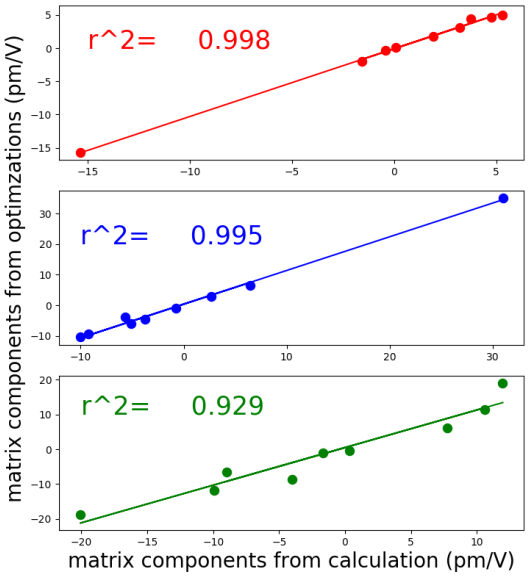

Figure 28: Linear regressions were performed between the matrix values shown in Fig. 27 between the matrices calculated with Eq. (B.42) and the approximated values from the geometry optimizations. The r^2 values are given. The red, blue and green plots correspond to the first, second and third molecules respectively as shown in Fig. 27.

on single molecule systems which were outside the abilities of our previous methods. The reason helicene molecules are interesting is because the attractive interactions of the polar ends of the molecules are balanced by repulsion between the coils. Previous work by Hutchison et al.[102] shows that these molecules exhibit considerable piezoelectric response for single organic molecules.

The equilibrium (zero field) structure for each molecule was aligned with the z-axis such that the two atoms of interest lie on the z-axis. The atoms highlighted for construction of the piezoelectric matrices were chosen to be part of the polar functional groups. We generally expected the response to be greatest for the displacment in the z direction with an applied z field ($\mathbf{P}_{33}$) which was the case for the first two molecules. The last molecule, however, showed a large $\mathbf{P}_{31}$ component (3rd row and 1st column), or in other words a substantial change in displacement in the z direction between the two atoms when a field was applied in the x direction. Fig. 28 shows the correlation between the calculated piezoelectric components and the components predicted by geometry optimizations. The r^2 values are very high for the first two molecules (0.99), but not quite as high for the last molecule (0.93) (Fig. 28). The last molecule was particularly problematic for measuring piezoelectric response via finite-field optimizations. The results for the optimziations shown in 3c for Fig. 28 are highly dependent on numerical parameters and hard to numerically converge. When performed with a max allowed step size of 0.1 bohr per step in the geometry optimization. If the default of 0.3 bohr is instead used, the r^2 valued for the 3rd molecule in Fig. 28 drops to about 0.7 with errors as high as a hundred percent for some components of the matrix. The r^2 values for the other molecules, however, remain above 0.95. In contrast, our new method for calculating the piezoelectric matrices detailed in the previous section is much more numerically stable and are only limited by the accuracy of the Hessian, dipole derivative matrix, and zero field equilibrium geometry calculated for the molecule. In practice the calculation of these contributions are more robust and avoid difficulties with measuring the small geometric response of a molecule within a field. The main problem in numerical finite-field calculations stems from the inevitable coupling of rotations and vibrations in finite optimizations in applied fields and the fact that non-charged molecules with a net dipole do not have a rotationally invariant energy within applied fields. The method proposed in the

procedure section alleviates these difficulties.

4.7 CONCLUSION AND OUTLOOK

Up to this point, we have sought to explore the piezoelectric properties of organic piezoelectrics – which have promising applications in material science. In two previous chapters we have shown that we can predict the piezoelectric properties of organic crystals like MNA to high accuracy via methods that involve finite field optimizations and/or simple energy "scans" along a coordinate of interest (eg. hydrogen bonds). While these methods are useful for monomeric systems in which one can use chemical intuition to select a coordinate of interest for which to measure the field dependent deformation properties, for single molecules and slightly larger systems, it may be difficult to identify and exploit such properties in more complex systems where different types of intra- and inter-molecular deformations give rise to a non-trivial geometric response.

In this work we have extended the mathematical model and equations from our previous work to the full nuclear dimensionality of small systems. In this way, with just one geometry optimization and one frequency calculation (sometimes gradient calculations as well), we can acquire all of the necessary information to describe how the molecule or system will deform in a small field and hence obtain the full piezoelectric properties for the system around zero field. To this extent we do not need to use any apriori knowledge or intuition for a system and do not need to treat the system in a reduced-dimensional fashion. To this end we show that we can approximate a piezoelectric matrix which acts like a contraction of the piezoelectric tensor with a unit vector in the direction of the vector between two atoms in the system. We have also demonstrated that due to the discrete nature of the system, a full piezoelectric tensor field cannot be calculated (without ascribing three basic vectors to the system in some systematic albeit hand-waving manner), but instead we can calculate a piezoelectric matrix for each pair of atoms or any linear combination of atom positions. In a sense, the piezoelectric properties of a molecule or small system show extreme anisotropy and discontinuity.

However, we have shown here that this method can be used to select for "good" organic piezoelectric candidates by screening similar families of molecules for specific deformation properties of one or many different pairs of atoms (or linear combinations of atoms). To this extent we hope that this work serves as a staging point for further investigation into other areas of molecular or finite system piezoelectrics – like controlling oscilations in a field or optimizing the work done by actuators, etc. Also we hope that the connections we have made to continuum strain theory will raise and may have already answered philosophical questions such as at what length scale something can be called piezoelectric and how do and can we quantify properties like the piezoelectric tensor for finite systems.

5.0 CALCULATIONS FOR PERIODIC SYSTEMS

5.1 INTRODUCTION

In this chapter we discuss the extrapolation of many of the techniques we have thus far covered in previous chapters to periodic boundary calculations for crystals of organic molecules. In this chapter we will discuss how to measure volumetric and longitudinal strain for a piezoelectric material and how we can use relative deformations between different bodies in a periodic boundary system to identify traits in organic crystals that convey strong piezoelectricity to a species. Thus far calculations have only been performed in MOPAC[66] on a large database of organic piezoelectric crystals, and the results in general show large inaccuracies mostly due to the inability of semiempirical methods like PM7[67] to adequately reproduce the electronic potential energy surfaces for exotic hydrogen-bonds.

5.2 THE PIEZOELECTRIC TENSOR FOR PERIODIC SYSTEMS

All of the concepts from previous chapters can be used to evaluate the full piezoelectric tensor, $\mathbf{d}$, for a crystalline system. In the previous chapter (4), we used the displacement of positions of the nuclei themselves $\mathbf{u}_a$ for a system to determine the deformation properties of different bodies in the system. For periodic boundary systems, the coordinates of interest are more straightforward. The deformation of the cell parameters is all that is needed to calculate $\mathbf{d}$ (with the caveat that nuclear relaxation is taken into consideration). If we see the unit cell vectors as being positioned at the origin and denote them as $\mathbf{x}_a$, $\mathbf{x}_b$ and $\mathbf{x}_c$ (in the cartesian basis), we may then measure their displacements $\mathbf{u}_i$ (in the cartesian basis

as well) under the application of a small field df_j. We do this for the three field directions x, y, and z as we have done in the previous chapter. After a geometry optimization, we record $\mathbf{u}_a$, $\mathbf{u}_b$ and $\mathbf{u}_c$ for the three vectors and we have the three matrices given by Eq. (5.1). Coincidentally, these matrices divided by 1 are equivalent to the approximations for $\frac{\partial^2 \mathbf{u}_i}{\partial \mathbf{f} \partial i}$,

$$\frac{\partial \mathbf{u}_i}{\partial \mathbf{f}} \approx \frac{\mathbf{u}_i}{d\mathbf{f}} \tag{5.1}$$

where i denotes the approximations for the length parameters we name a, b, and c, for the basis consisting of the three triclinic cell vectors (Eq. (5.2)). This is because the origin of

$$\frac{\partial^2 \mathbf{u}_i}{\partial \mathbf{f} \partial i} \approx \frac{\mathbf{u}_i}{d\mathbf{f}} \tag{5.2}$$

the cell vectors is always fixed, so the partial derivative of the origin of the vectors is a zero matrix with respect to the field vector, and as we move from the origin to the tip of the cell vectors to measure their displacement we have only covered exactly 1 unit in this basis. The transformation from the coordinates a, b ,c to x, y, z (which we will denote as $\mathbf{a}$ and $\mathbf{X}$ respectively) is then given by Eq. (5.3). Here we have used Einstein notation over the

$$\mathbf{X} = i\mathbf{x}_i \tag{5.3}$$

coordinates for a, b , and c. If we organize the vectors $\mathbf{x}_i$ as column vectors into the matrix $\mathbf{V}$, we have Eq. (5.4). The transformation of $\frac{\partial^2 \mathbf{u}_i}{\partial \mathbf{f} \partial \mathbf{a}}$ to $\frac{\partial^2 \mathbf{u}_i}{\partial \mathbf{f} \partial \mathbf{X}}$ then follows Eq. (5.5). In Eq. (5.5) we use Eq. (5.6).

$$\begin{aligned} \mathbf{X} &= \mathbf{V}\mathbf{a} \\ \mathbf{V}^{-1}\mathbf{X} &= \mathbf{a} \end{aligned} \tag{5.4}$$

$$\frac{\partial^2 \mathbf{u}_i}{\partial \mathbf{f} \partial X_j} = \frac{\partial^2 \mathbf{u}_i}{\partial \mathbf{f} \partial i} V_{ij}^{-1} \tag{5.5}$$

$$\frac{\partial}{\partial X_j} = V_{ij}^{-1} \frac{\partial}{\partial i} \tag{5.6}$$

$$\mathbf{E} = \frac{1}{2}\left(\mathbf{A} + \mathbf{A}^T + \mathbf{A}^T \cdot \mathbf{A}\right) \tag{5.7}$$

The Green strain tensor (derived in B.1) is given by Eq. (5.7). Here the matrix $\mathbf{A}$ is known as the displacement gradient and is given by $A_{ij} = \frac{\partial u_i}{\partial X_j}$, where $\mathbf{u}$ is the displacement vector field described in Fig. 25. As describe in the Appendix (B.2), the zero field piezoelectric tensor simplifies to Eq. (5.8). Here $\frac{\partial \mathbf{A}(\mathbf{0})}{\partial \mathbf{f}}$ in component form is just $\frac{\partial^2 \mathbf{u}_i}{\partial \mathbf{f} \partial X_j}$, and hence we have calculated the zero field piezoelectric tensor for periodic systems.

$$\mathbf{d} = \frac{1}{2}\left(\frac{\partial \mathbf{A}^T(\mathbf{0})}{\partial \mathbf{f}} + \frac{\partial \mathbf{A}(\mathbf{0})}{\partial \mathbf{f}}\right) \tag{5.8}$$

5.3 OPTIMIZING STRAIN

Once we have $\mathbf{d}$ for a given periodic system, there are a few possible interesting questions which we may ask. Some examples we outline here: What direction of applied field leads to optimal longitudinal strain? volumetric strain? Recall the definition for longitudinal strain presented in the previous chapter (Eq. (B.1)). We may present similar equations for

$$\epsilon = \lim_{s_0 \to 0} \frac{s - s_0}{s_0} = \frac{ds - ds_0}{ds_0} = \frac{ds}{ds_0} - 1 \tag{5.9}$$

volumetric and shear strain. Volumetric strain is given by Eq. (C.1). Here V_0 is the volume

$$\nu = lim_{V_0 \to 0} \frac{(V - V_0)}{V_0} = \frac{dV}{dV_0} - 1, \tag{5.10}$$

of a region in the undeformed body and V is the volume of said region after deformation.)

Because we are only concerned with infinitesimal deformations under infinitesimal applied fields, ν and ϵ for a system under an infinitesimally small field must be zero. However, we can approximate changes in these values for an applied field via Taylor expansions truncated at linear order (Eq. (5.11)). In principle we can constrain $\mathbf{f}$ to be some vector of unit length and optimize (minimize or maximize) the functions above. In the Appendix (B.2), we simplify

$$\begin{aligned} \epsilon &\approx \frac{\partial \epsilon}{\partial \mathbf{f}}(\mathbf{0})\mathbf{f} \\ \nu &\approx \frac{\partial \nu}{\partial \mathbf{f}}(\mathbf{0})\mathbf{f} \end{aligned} \tag{5.11}$$

$$\frac{\partial \epsilon(\mathbf{0})}{\partial \mathbf{f}} = \mathbf{e}^T \frac{\partial \mathbf{A}(\mathbf{0})}{\partial \mathbf{f}} \mathbf{e}. \tag{5.12}$$

$\frac{\partial \epsilon}{\partial \mathbf{f}}(\mathbf{0})$ to Eq. (5.12). Substituting into the first equation in Eq. (5.11), we have Eq. (5.13). We clearly need to optimize here for the material line direction, $\mathbf{e}$, and the field direction,

$$\epsilon \approx \mathbf{e}^T \frac{\partial \mathbf{A}(\mathbf{0})}{\partial \mathbf{f}} \mathbf{e}\mathbf{f} \tag{5.13}$$

$\mathbf{f}$. Optimization can then tell us which direction of applied field and along which material line we can expect the largest or smallest longitudinal strain in the small field limit. The derivative with respect to the components of $\mathbf{e}$ yields Eq. (5.14). For a given set of vectors,

$$\frac{\partial \epsilon}{\partial \mathbf{e}} = \left(\frac{\partial \mathbf{A}^T(\mathbf{0})}{\partial \mathbf{f}} + \frac{\partial \mathbf{A}(\mathbf{0})}{\partial \mathbf{f}} \right) \mathbf{e}\mathbf{f}. \tag{5.14}$$

we may use typical algorithms and these gradients to find minima and maxima. When $\mathbf{e}$

and $\mathbf{f}$ are updated, they may then be rescaled to unity in magnitude and the algorithms continued. In the sections to come we find the field direction to apply to the system in order to calculate the optimal longitudinal strain response for organic piezoelectric tensors obtained from semiempirical calculations for organic piezoelectric crystals.

Also in the Appendix (C.1), we derived the working equations for volumetric strain (Eq. (5.15)) using the displacement gradient $\mathbf{A}$. The gradient of ν with respect to field may be

$$\nu = det(\mathbf{I} + \mathbf{A}) - 1 \tag{5.15}$$

calculated numerically. The direction of the gradient then specifies the direction in which to apply the field so as to have the largest increase in volume. Applying the field in any direction orthogonal to this should yield no change in the volumetric strain in the limit of infinitesimal field.

5.4 METHODS FOR CALCULATING THE PIEZOELECTRIC TENSOR

The methods for calculating the tensor for periodic systems strongly resemble how we have thus far calculated $d_{33}$and the piezoelectric matrices of past chapters. The degrees of freedom of interest to us for periodic systems include the nuclear positions of atoms within one unit cell and the unit cell vectors themselves (a total of 3N + 9). All other positions of nuclei can be calculated from these vectors. We can calculate the dipole derivative matrix and the hessian matrix for all of the $3N + 9$ coordinates, and in a manner akin to Eq. (B.36), Eq. (B.38), and Eq. (B.41) then form $\frac{\partial^2 \mathbf{u}}{\partial \mathbf{f} \partial \mathbf{X}}$ and the piezoelectric tensor. C.2 in the Appendix shows how to calculate rotation and translation vectors for periodic systems. projecting out the vectors is essentially the same as presented in the previous chapter except now the Hessian and dipole derivative matrices have 9 more dimensions. Alternatively geometry optimizations (of both the nuclear coordinates for the unit cell and the cell parameters) may

be performed under varying field strengths and direction to perform 9 linear regressions in order to determine the nine values of $\frac{\partial^2 \mathbf{u}}{\partial \mathbf{f} \partial \mathbf{X}}$.

5.5 INITIAL MOPAC CALCULATIONS

We have performed piezoelectric tensor calculations for around 200 candidates organic piezoelectric crystals identified from the crystallagraphic database. As a general order of magnitude calculation, we performed geometry optimizations (of both unit cell nuclear positions and unit cell parameters) using the semiempirical method PM7 in MOPAC[66,67], and then performed 3 more geometry optimizations under fields applied in the x,y and z directions. We then formed and transformed to cartesian coordinates (as explained in the previous section) $\frac{\partial \mathbf{A}^T(\mathbf{0})}{\partial \mathbf{f}}$ for each system and compared predicted longitudinal strain values for an applied field of 1 V/pm (we are only interested in direction so the size of field appplied to the linear equations does not matter) and ranked piezoelectric systems. Some values were noticeably in the thousands and inspection of these led us to believe many of these were outliers, and many of the values in the piezoelectric tensors themselves were similarly high. Fig. 29 shows the results for optimizing the longitudinal strain for one of the systems. The eigenvalues of the strain tensor produced from contracting the piezoelectric tensor with the field direction are shown as surfaces for different theta and phi values for the field direction.

Like the hydrogen bond of MNA in the first chapter (2), there is usually some type of intermolecular interaction between monomers of the system which we can ascribe as the major contributing factor to the deformation properties of the system. It is likely that the PM7 Hamiltonian cannot adequately describe the intermolecular forces between a lot of the intermolecular interactions for many of the systems. This can lead to an underbinding along the axis of interaction between the two monomers (ie. lower compliance) and artificially higher piezoelectric coefficients.

We were able to extract interacting dimers from the MOPAC calculations by identifying monomers in the super cells via clustering algorithm and then looking for the smallest "bond" between pairs of monomers. Such a "bonding" pair was then extracted into an xyz file for all

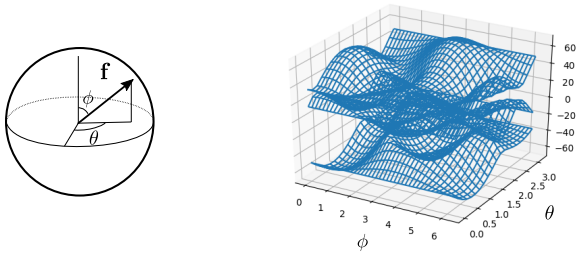

Figure 29: A sample of the eigenvalue surfaces for the strain tensor produced for different field directions of an organic piezoelectric material. The piezoelectric tensor was calculated from MOPAC optimizations using PM7.

of the calculations. We are then able to perform one-dimensional piezoelectric calculations of the bonds using ab initio methods (as was done in the first and second chapters) to compare to the longitudinal strains calculated via the piezoelectric tensors obtained from the PM7 calculations.

Preliminary calculations show that many of the pair interactions have piezoelectric coefficients on the order of 10 pm/V, like the other organic systems of previous chapters, supporting that PM7 does not adequately describe many of the interactions that hold the molecular crystals together and are likely what is largely responsible for the piezoelectric effect in these systems. As a result we move to using ab initio calculations to predict piezoelectric tensors for these piezoelectric systems. It should be noted that it is not guarenteed that the "bonding interaction" between the pairs of monomers found with this algorithm is the main contributor to the piezoelectricity for these systems. It can be difficult to determine by algorithm what the main contribution is but is generally fairly simple by human inspection of a reasonable super cell of the system. That being said we have also created an algorithm which can calculate the piezoelectric matrices (as done in the third chapter) between all monomers in a given supercell for the system, and correlating the matrices with the piezoelectric tensors is a good way to identify which interactions have the largest effect on the piezoelectric response for these systems.

6.0 CONCLUSION AND FUTURE WORK

With the work presented, we have shown that modern ab initio quantum chemistry can be used to qualitatively and quantitatively predict the piezoelectric response of organic piezoelectric molecules. We have shown that the bulk piezoelectric response of organic crystals such as MNA can be explained by considering the piezoelectricity of specific intermolecular bonds, such as hydrogen bonds. Through the use of a simple model we were able to show that the zero field piezoelectric properties of a system are directly related to the inverse curvature of the electronic potential and the geometric dipole derivative of the system of interest. Through the language and principles of strain theory, we have extended the simple model to take into account the full dimensional relaxation of small or finite systems to predict deformation properties which might find use in a multitude of new flexible piezoelectric materials. The methods introduced reduce the computation time and increase accuracy of the linear deformation properties of these systems by avoiding numerically tricky finite-field calculations.

We have futhermore extended these methods to be able to identify interactions in periodic systems which may yield strong piezoelectric response. In the work to come we hope that these methods may be used to screen for functional groups and molecules that offer high mechanical deformations and provide insight into what kinds of piezoelectric materials are possible to create with organic systems.

APPENDIX A

SUPPORTING INFORMATION REGARDING CHAPTER 2

A.1 MANY-BODY EXPANSION

The many-body theory used in 2 is similar to the approach described by Dahlke and Truhlar[60]. As in a typical RI-MP2 calculation, the total energy for the system (E_T) can be represented as the Hartree-Fock energy (E_{hf}) for the system plus the RI-MP2 approximation for the energy due to electron correlation (E_{corr}) for the system, or just Eq. (A.1). Here

$$E_T = E_{hf} + E_{corr} \tag{A.1}$$

the RI-MP2 energy is approximated using the many-body expansion due to poor scaling with system size. In general, for an N monomer system, we have Eq. (A.2). E_{corr} represents

$$E_{corr} = E_{corr1} + E_{corr2} + E_{corr3} + ... + E_N \tag{A.2}$$

the total correlation energy of the system. Here E_{corrn}, represents the additional correlation energy due to the interactions of n monomers of the system. For $n = 1$, this is just the sum of the correlation energies over all monomers Eq. (A.3).

$$E_{corr1} = \sum_i e_i \tag{A.3}$$

Here the *corr* subscript has been dropped and instead e_i represents the correlation energy for the ith monomer of the system. For $n = 2$, this correlation energy can be seen as the sum of the correlation energies for all possible dimer pairs of the system minus the contributions from the individual monomers to each pair, or just Eq. (A.4). Here e_{ij} is the total correlation

$$E_{corr2} = \sum_{j>i} e_{ij} - e_i - e_j \tag{A.4}$$

energy for the ijth dimer pair. Note that for an N monomer system, each monomer can be part of a dimer pair $(N-1)$ times (matched with one of the other $N-1$ molecules once), so each monomer correlation energy is subtracted this many times in the summation. Hence, Eq. (A.4) can also be written as Eq. (A.5).

$$E_{corr2} = \sum_{j>i} e_{ij} - (N-1)\sum_i e_i \tag{A.5}$$

The formula for E_{corr3} is not presented here, but can be seen as the sum of the total correlation energies for all possible 3 monomer combinations minus the comprising monomer correlation energies and dimer energies. For a many-body expansion of order 2 (MB2), E_{corr} is approximated by truncating after the second term – ie. contributions from trimer and

$$E_{corr} \approx E_{corr1} + E_{corr2} \tag{A.6}$$

larger subunits of the system are negligible (Eq. (A.6)). If we write Eq. (A.6) explicitly in terms of monomer and dimer energies, we obtain Eq. (A.7). The overall energy of the system

$$\begin{aligned} E_{corr} &\approx \sum_i e_i + \sum_{j>i} e_{ij} - (N-1)\sum_i e_i \\ E_{corr} &\approx \sum_{j>i} e_{ij} - (N-2)\sum_i e_i \end{aligned} \tag{A.7}$$

is then just Eq. (A.8). This approximation lends itself nicely to geometry optimizations since

$$E_{corr} \approx E_{hf} + \sum_{j>i} e_{ij} - (N-2)\sum_i e_i \tag{A.8}$$

the gradient is a linear operator. The gradient can then be written as Eq. (A.9).

$$\nabla E_T \approx \nabla E_{hf} + \sum_{j>i} \nabla e_{ij} - (N-2)\sum_i \nabla e_i \tag{A.9}$$

The MB2 expansion can also be made more accurate, and maintain most of the cost benefits by using electrostatic embedding. Normally monomer and dimer energy and gradient

calculations are performed in the absence of any other parts of the larger system for a many body expansionhence the faster computation times. However, the other molecules of the system can be crudely represented as point charges fixed at the nuclei with corresponding Mulliken[103] or CHELPG[104] charges for the different atoms. The charges just need to be calculated (usually at the end of a single point energy calculation) before calculating energies for the monomers and dimers of the system.

A.2 COMPLETE BASIS SET EXTRAPOLATION

To analyze the BSSE error the simple formula in Eq. (A.10) was utilized. Here x and y refer to the largest orbital angular momentum quantum number for the basis set to which E_x and E_y correspond. Since we used augmented correlation consistent Dunning basis sets, x and y correspond to $l = 2$ and 3 respectively. By generating E_{CBS} for multiple geometries, hydrogen-bonding distances corresponding to minima in the energy are then determined, as in Fig. 11, for multiple fields. The slope of the regression line for this data can then be used to approximate the piezocoefficient in the CBS limit as given in the Tab. 2.[105]

$$E_{CBS} = \frac{x^5 E_x - y^5 E_y}{x^5 - y^5} \tag{A.10}$$

APPENDIX B

SUPPORTING INFORMATION REGARDING CHAPTER 4

B.1 RELEVANT STRAIN THEORY

For convenience we again include Fig. 30. Recall that configurations K_0 and K correspond to the undeformed and deformed bodies, respectively. Particle positions before deformation are given by $\mathbf{X}$ and after deformation are given by $\mathbf{x}$ and are represented in the same external basis. The displacement vector field $\mathbf{u}(\mathbf{X}, t)$, also in the same basis, maps the transition in space from points in the undeformed to deformed body. A material line is given by segments P_0Q_0 and PQ in the undeformed and deformed bodies. The longitudinal strain is then if s_0 and s are the undeformed and deformed length parameters.

The goal now is to find working equations for calculating the longitudinal strain ϵ from

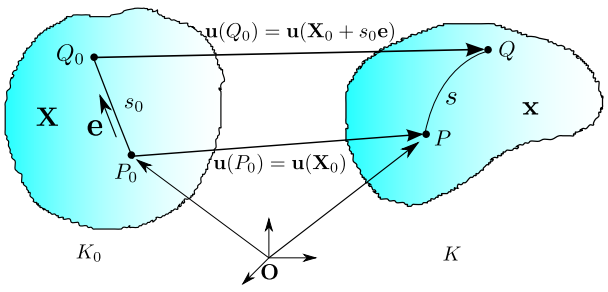

Figure 30: General deformation of a body.[1]

$$\epsilon = \lim_{s_0 \to 0} \frac{s - s_0}{s_0} = \frac{ds - ds_0}{ds_0} = \frac{ds}{ds_0} - 1 \tag{B.1}$$

Eq. (B.1). To this end, one needs to determine the arc length s of the deformed material line. Treating s_0 as a variable parameter, any point along the undeformed material line P_0K_0 can be written as $\mathbf{X}_0 + s_0\mathbf{e}$, where $\mathbf{X}_0$ is the starting point of the undeformed material line. The positions of particles in the deformed body can then be defined as functions of the undeformed point positions as well as a time coordinate t that determines the progress of the deformation: $\mathbf{x} = \mathbf{x}(\mathbf{X}_0 + s_0\mathbf{e}, t)$. The arc length of s as a function of s_0 (which we treat as a curve parameter) is then given by Eq. (B.2). The arc length derivative with respect

$$s(s_0) = \int_0^{s_0} \sqrt{\frac{dx_i}{d\bar{s}_0}\frac{dx_i}{d\bar{s}_0}}\, d\bar{s}_0, \tag{B.2}$$

to s_0 and it's square are then given by Eq. (B.3). To evaluate $\frac{ds(s_0)}{ds_0}$, we can examine how

$$\frac{ds(s_0)}{ds_0} = \sqrt{\frac{dx_i}{ds_0}\frac{dx_i}{ds_0}} \tag{B.3}$$

the components of a vector along P_0Q_0 change as we vary s_0, the length parameter of our undeformed material line. If we write this vector as $\mathbf{r}_0 = X_k\mathbf{e}_k$, where $\mathbf{e}_k$ are the unit vectors which make up the basis (therefore $\mathbf{e} = e_k\mathbf{e_k}$), we have for a small change in the vector Eq. (B.4). We will use Eq. (B.4) later.

$$
\begin{aligned}
d\mathbf{r}_0 &= \mathbf{e}\, ds_0 = dX_k\, \mathbf{e}_k \\
\Rightarrow \quad dX_k &= e_k\, ds_0 \\
\Leftrightarrow \quad e_k &= \frac{dX_k}{ds_0}
\end{aligned}
\tag{B.4}
$$

If we consider the vector differential along s, tangent to the curve, which we call $d\mathbf{r}$ and has components dx_i, we may write Eq. (B.5). Now we would like to relate the line elements

$$
d\mathbf{r} = \frac{d\mathbf{r}}{ds_0} ds_0 \quad \Rightarrow \quad dx_i = \frac{dx_i}{ds_0} ds_0 \tag{B.5}
$$

$d\mathbf{r}_0$ from K_0 with $d\mathbf{r}$ in K (Eq. (B.6)).

$$
d\mathbf{r} = \frac{\partial \mathbf{r}}{\partial \mathbf{r}_0} \cdot d\mathbf{r}_0 \quad \Leftrightarrow \quad dx_i = \frac{\partial x_i}{\partial X_k} dX_k \tag{B.6}
$$

We thus have the deformation gradient $\mathbf{F}$ (Eq. (B.7)).

$$
\mathbf{F} = \bigtriangledown (\mathbf{r}) = \frac{\partial \mathbf{r}}{\partial \mathbf{r}_0} \quad \Leftrightarrow \quad F_{ik} = \frac{\partial x_i}{\partial X_k} \tag{B.7}
$$

We would like to calculate $\left(\frac{ds}{ds_0}\right)^2$ from before, noting that $\frac{\partial x_i}{\partial s_0} = \frac{\partial x_i(\mathbf{X},t)}{\partial X_k} \frac{dX_k}{ds_0}$ leads to Eq. (B.8). In the last step we have used our result from Eq. (B.4). This is analogous to a

$$\frac{\partial x_i}{s_0} = \frac{\partial x_i}{\partial X_k}\frac{dX_k}{ds_0} = F_{ik}e_k \tag{B.8}$$

directional derivative, but instead of using the gradient of a scalar quantity, we instead use the the gradient of a vector quantity, which is inherently a matrix–the deformation gradient.

We can now write Eq. (B.9), where $\mathbf{C}$ is known as the Green deformation tensor. Recall

$$\begin{aligned}\left(\frac{ds}{ds_0}\right)^2 &= \frac{dx_i}{ds_0}\frac{dx_i}{ds_0} \\ &= \left(F_{ik}e_k\right)\left(F_{il}e_l\right) \\ &= \mathbf{e}^T \cdot \left(\mathbf{F}^T \cdot \mathbf{F}\right) \cdot \mathbf{e} \\ &= \mathbf{e}^T \cdot \mathbf{C} \cdot \mathbf{e},\end{aligned} \tag{B.9}$$

that the displacement of a particle during deformation is given by $\mathbf{u}\left(\mathbf{r_0}, \mathbf{t}\right)$. We would like to recast the deformation tensor in terms of the displacement gradient, which we call $\mathbf{A}$ (Eq. (B.10)). Recall Eq. (B.11). From this, we may infer Eq. (B.12) or Eq. (B.13). We recast

$$\mathbf{A} = \frac{\partial \mathbf{u}}{\partial \mathbf{r}_0} \quad \Leftrightarrow \quad A_{ik} = \frac{\partial u_i}{\partial X_k} \tag{B.10}$$

the Green deformation tensor in Eq. (B.14). The Green strain tensor, $\mathbf{E}$ is defined in Eq. (B.15), which we can represent by elements as in Eq. (B.16). We have cast the Green strain tensor in terms of displacement derivatives.

$$x_i\left(\mathbf{X},t\right)=X_i+u_i\left(\mathbf{X},t\right) \tag{B.11}$$

$$\frac{\partial x_i}{\partial X_k}=\frac{\partial X_i}{\partial X_k}+\frac{\partial u_i}{\partial X_k} \tag{B.12}$$

$$F_{ik}=\delta_{ik}+A_{ik} \quad \Leftrightarrow \quad \mathbf{F}=\mathbf{1}+\mathbf{A} \tag{B.13}$$

$$\mathbf{C}=\mathbf{F}^T\cdot\mathbf{F}=\left(\mathbf{1}+\mathbf{A}^T\right)\left(\mathbf{1}+\mathbf{A}\right)=\mathbf{1}+\mathbf{A}+\mathbf{A}^T+\mathbf{A}^T\cdot\mathbf{A} \tag{B.14}$$

$$\mathbf{E}=\frac{1}{2}\left(\mathbf{A}+\mathbf{A}^T+\mathbf{A}^T\cdot\mathbf{A}\right) \tag{B.15}$$

Hence we can rewrite the Green deformation tensor, $\mathbf{C}$ (Eq. (B.17)). Looking back at Eq. (B.9), we can rewrite the equation as Eq. (B.18). Hence, recalling Eq. (B.1), we can also rewrite our longitudinal strain from before in terms of the Green strain tensor Eq. (B.19). For the purposes of this thesis, this is all that we need to understand in terms of

$$E_{kl} = \frac{1}{2}\left(\frac{\partial u_k}{\partial X_l} + \frac{\partial u_l}{\partial X_k} + \frac{\partial u_i}{\partial X_k}\frac{\partial u_i}{\partial X_l}\right) \tag{B.16}$$

$$\mathbf{C} = \mathbf{1} + 2\mathbf{E} \tag{B.17}$$

$$\left(\frac{ds}{ds_0}\right)^2 = \mathbf{e}\cdot\mathbf{C}\cdot\mathbf{e} = \mathbf{e}\cdot(\mathbf{1}+2\mathbf{E})\cdot\mathbf{e} = 1 + 2\mathbf{e}\cdot\mathbf{E}\cdot\mathbf{e} \tag{B.18}$$

$$\epsilon = \frac{ds}{ds_0} - 1 = \sqrt{1 + 2\mathbf{e}\cdot\mathbf{E}\cdot\mathbf{e}} - 1 \tag{B.19}$$

strain theory. We will build off these ideas to derive a molecular approach for zero field piezoelectricity.

We now wish to show how we can approximate d_{33} in a manner equivalent to our previous papers[47,89]. For our situation, we take the undeformed body, K_0 to be the optimized geometry at zero field. The only source of deformation for our system will be the applied electric field $\mathbf{f}$, which implies that the Green strain tensor is also a function of $\mathbf{f}$, i.e. $\mathbf{E} = \mathbf{E}(\mathbf{f})$. We can therefore rewrite Eq. (B.1). If we take the derivative with respect to $\mathbf{f}$, we obtain the following. Because we choose K_0 as our system at zero field, $\mathbf{E}\,(\mathbf{f} = \mathbf{0}) = \mathbf{0}$ ($\mathbf{0}$ on the

$$\epsilon = \sqrt{1 + 2\,\mathbf{e}^T \cdot \mathbf{E}\,(\mathbf{f}) \cdot \mathbf{e}} - 1 \approx \mathbf{e} \cdot \mathbf{E}\,(\mathbf{f}) \cdot \mathbf{e} \tag{B.20}$$

$$\frac{\partial \epsilon\,(\mathbf{f})}{\partial \mathbf{f}} = \frac{\mathbf{e}^T \cdot \frac{\partial \mathbf{E}(\mathbf{f})}{\partial \mathbf{f}} \cdot \mathbf{e}}{\sqrt{1 + 2\mathbf{e}^T \cdot \mathbf{E}\,(\mathbf{f}) \cdot \mathbf{e}}} \tag{B.21}$$

right hand side is a matrix, not a vector)–ie. the displacement derivatives contained in $\mathbf{A}$ are all zero since the $\mathbf{u} = \mathbf{0}$ everywhere. If we evaluate Eq. (B.21) at $\mathbf{f} = \mathbf{0}$ the derivative reduces to the following equation. Eq. (B.22) not surprisingly, matches the field derivative

$$\frac{\partial \epsilon\,(\mathbf{0})}{\partial \mathbf{f}} = \mathbf{e}^T \cdot \frac{\partial \mathbf{E}\,(\mathbf{0})}{\partial \mathbf{f}} \cdot \mathbf{e} \tag{B.22}$$

of the longitudinal strain at small defomations (Eq. (B.20)). The derivative of the Green strain tensor $\mathbf{E}$ with respect to the field, $\mathbf{f}$ is just the piezoelectric tensor, $\mathbf{d}$ (Eq. (4.2)). Thus the derivative of the longitudinal strain at zero field reduces to the following: In the

$$\frac{\partial \epsilon\,(\mathbf{0})}{\partial \mathbf{f}} = \mathbf{e}^T \cdot \mathbf{d}\,(\mathbf{0}) \cdot \mathbf{e} \tag{B.23}$$

sections to come, we will reduce Eq. (B.23) to a simpler form, devise a method for calculating piezoelectric coefficients for molecules, and introduce the piezoelectric matrix, $\mathbf{P}$. Eq.

(B.23) can be used to approximate d_{33} in the same manner as our previous papers[47,89], but is a generalization, which we will find useful later. Furthermore, it connects the work we have done thus far to strain theory, which we hope serves as a tool for future work in this area.

B.2 SIMPLIFYING THE EQUATION FOR THE PIEZOELECTRIC COEFFICIENT

Recall Eq. (B.23). We have claimed that this equation is equivalent to our previous methods for estimating d_{33} for molecules[89]. Before we can make this connection, we will find it useful to first simplify Eq. (B.23). We can reduce Eq. (B.22) further by using the definition for the Green strain tensor $\mathbf{E}$ (Eq. (B.15)). We first rewrite Eq. (B.22) elementwise (Eq. (B.24)) (the derivative is a vector quantity with components of field) using the definition of $\mathbf{A}$ (Eq. (B.10)). The last two terms in Eq. (B.24) result from the product rule for $\mathbf{A}^T\mathbf{A}$ from Eq.

$$\begin{aligned}\frac{\partial \epsilon(\mathbf{0})}{\partial f_l} = \frac{1}{2} e_i \Bigg(& \frac{\partial^2 u_i(\mathbf{0})}{\partial X_k \partial f_l} + \frac{\partial^2 u_k(\mathbf{0})}{\partial X_i \partial f_l} + \\ & \frac{\partial^2 u_j(\mathbf{0})}{\partial X_i \partial f_l} \frac{\partial u_j(\mathbf{0})}{\partial X_k} + \frac{\partial u_j(\mathbf{0})}{\partial X_i} \frac{\partial^2 u_j(\mathbf{0})}{\partial X_k \partial f_l} \Bigg) e_k\end{aligned} \tag{B.24}$$

(B.15). Both terms vanish when evaluated at zero field. This is because $\frac{\partial u_j(\mathbf{0})}{\partial X_i} = A_{ji}(\mathbf{0}) = 0$ (every element is zero) if we take the zero field body as K_0 and K (which is equivalent to evaluating $\mathbf{A}$ at zero field). If this is the case, the displacement vector for every point in the body is constant (and actually $\mathbf{0}$), and hence the derivative in any direction (X_i) vanishes. We can therefore rewrite Eq. (B.24), ignoring the last two terms as Eq. (B.25). We can rewrite Eq. (B.25) in terms of matrix derivatives for simplicity (Eq. (B.26)). Because both matrices are contracted by $\mathbf{e}$ on both sides, and one is the transpose of the other, both terms in the first line are equivalent and reduce to twice the value of one term, which

$$\frac{\partial \epsilon(\mathbf{0})}{\partial f_l} = \frac{1}{2} e_i \left(\frac{\partial^2 u_i(\mathbf{0})}{\partial X_k \partial f_l} + \frac{\partial^2 u_k(\mathbf{0})}{\partial X_i \partial f_l} \right) e_k \tag{B.25}$$

$$\begin{aligned} \frac{\partial \epsilon(\mathbf{0})}{\partial \mathbf{f}} &= \frac{1}{2} \mathbf{e}^T \left(\frac{\partial \mathbf{A}^T(\mathbf{0})}{\partial \mathbf{f}} + \frac{\partial \mathbf{A}(\mathbf{0})}{\partial \mathbf{f}} \right) \mathbf{e} \\ \frac{\partial \epsilon(\mathbf{0})}{\partial \mathbf{f}} &= \mathbf{e}^T \frac{\partial \mathbf{A}(\mathbf{0})}{\partial \mathbf{f}} \mathbf{e} \end{aligned} \tag{B.26}$$

cancels the prefactor of $\frac{1}{2}$ in the final line. $\frac{\partial \mathbf{A}(\mathbf{0})}{\partial \mathbf{f}}$ is a rank 3 tensor. Although it is not equivalent to the field derivative of the Green strain tensor evaluated at zero field (ie. the piezoelectric tensor evaluated at zero field), when contracted with the same unit vectors it produces the same value for the field derivative of longitudinal strain in the direction of the two vectors. It is important to note however that if one obtains $\frac{\partial \mathbf{A}(\mathbf{0})}{\partial \mathbf{f}}$ that one can immediately calculate the zero field piezoelectric tensor by adding $\frac{\partial \mathbf{A}^T(\mathbf{0})}{\partial \mathbf{f}}$ and taking half of the result (Eq. (B.27)). In the sections to come we will show why the calculation of a true

$$\mathbf{d} = \frac{1}{2} \left(\frac{\partial \mathbf{A}^T(\mathbf{0})}{\partial \mathbf{f}} + \frac{\partial \mathbf{A}(\mathbf{0})}{\partial \mathbf{f}} \right) \tag{B.27}$$

piezoelectric tensor is untenable for molecules and finite systems, but we will show instead how to calculate piezoelectric matrices for pairs of atoms (or points) within a molecule and construct a rank 4 piezoelectric tensor for a given system, which contains the unique field deformation properties of the system. We will work with Eq. (B.26) in the sections to come.

B.3 MOLECULAR CONNECTIONS TO STRAIN THEORY AND THE PIEZOELECTRIC MATRIX

Thus far, we have claimed that the derivative of the longitudinal strain Eq. (B.23) with respect to the applied electric field is related to our calculations of d_{33} in our previous work[47,89]. In this section we will attempt to explain geometrically the connection of strain theory to our work, and apply our equations to molecular systems. Furthermore, we will demonstrate why, for molecules, the full piezoelectric tensor is untenable for calculation and introduce the piezoelectric matrix ($\mathbf{P}$), which will take the place of the piezoelectric tensor for molecules.

In the sections above we presented a working equation (Eq. (B.23)) with dependence on the piezoelectric tensor ($\mathbf{d}$), and we further reduced this equation to Eq. (B.26) for the zero field evaluation of d_{33}. We have yet, however, to explain the direct connection of Eq. (B.26) to our previous work. To interpret Eq. (B.26) geometrically, we need to look back to Fig. 25. As we recall, longitudinal strain deals with how material lines in continuum bodies deform. The direction of the material line in the undeformed body was given by $\mathbf{e}$. In Eq. (B.26), two of the indexes of $\frac{\partial \mathbf{A}(\mathbf{0})}{\partial \mathbf{f}}$ are contracted with $\mathbf{e}$–namely the indexes of the undeformed coordinates X_i and displacement vector coordinates u_i. If we ask what the contractions with $\mathbf{e}$ mean, we can gain insight into how to understand d_{33} and furthermore connect strain theory to molecular piezoelectricity and point out differences. First we define a vector $\mathbf{X}$ in the direction of $\mathbf{e}$ with a length parameter of s_0 (equivalent to that shown in the undeformed body in Fig. 25) (Eq. (B.28)). Taking the derivative with respect to s_0 tells

$$\mathbf{X} = s_0 \mathbf{e} \tag{B.28}$$

us how the vector changes per unit change in the length of s_0 (Eq. (B.29)) Here we have a useful definition of $\mathbf{e}$. The change in coordinates in the undeformed system per unit of s_0 corresponds to the vector $\mathbf{e}$, which gives the direction of our material line in the undeformed

$$\frac{d\mathbf{X}}{ds_0} = \mathbf{e} \equiv \frac{dX_i}{ds_0} = e_i \tag{B.29}$$

body. With this definition we may further simplify Eq. (B.26) into Eq. (B.30). We will again use the definition of $\mathbf{A}$. We have substituted in for e_k our definition in Eq. (B.29)

$$\begin{aligned}
\frac{\partial \epsilon(\mathbf{0})}{\partial f_l} &= e_i \frac{\partial^2 u_i(\mathbf{0})}{\partial f_l \partial X_k} e_k = e_i \frac{\partial^2 u_i(\mathbf{0})}{\partial f_l \partial X_k} \frac{dX_k}{d_{s_0}} \\
\frac{\partial \epsilon(\mathbf{0})}{\partial f_l} &= e_i \frac{\partial^2 u_i(\mathbf{0})}{\partial f_l \partial s_0} \\
\frac{\partial \epsilon(\mathbf{0})}{\partial f_l} &= e_i P_{il}(\mathbf{0}) \\
\frac{\partial \epsilon(\mathbf{0})}{\partial \mathbf{f}} &= \mathbf{e}^T \cdot \mathbf{P}(\mathbf{0})
\end{aligned} \tag{B.30}$$

and contracted over the index k in $\mathbf{A}$, corresponding to the undeformed coordinates X_k. We have renamed the resulting matrix from this contraction $\mathbf{P} = \frac{\partial^2 \mathbf{u}}{\partial s_0 \partial \mathbf{f}}$. We will call $\mathbf{P}$, in the sections to come, the piezoelectric matrix. Here we focus on the matrix in the context of a continuum body; later we will apply the ideas to discrete and finite molecular systems. As we move along the material line in the undeformed coordinates, s_0 is the curve parameter for the displacement vectors to the deformed coordinates (see Fig. 25). We may evaluate the vector derivatives of the the displacement vector $\mathbf{u}$ as we move infinitesimally along s_0. This gives us $\frac{\partial \mathbf{u}}{\partial s_0}$ evaluated at our point of interest in the body. We may then evaluate the derivative of $\frac{\partial \mathbf{u}}{\partial s_0}$ with respect to the field vector at a given field magnitude (which in our case is 0). We then obtain the matrix $\mathbf{P}$. Of course it is equally valid to view the matrix by looking at $\frac{\partial \mathbf{u}}{\partial \mathbf{f}}$ at a given point in our body first and then asking how this matrix changes by moving infinitesimally along our material line. The order we take the derivatives of $\mathbf{u}$

should not matter because we assume $\mathbf{u}(\mathbf{f}, s_0)$ to be smooth and obey Euler's rule for mixed derivatives.

In the sections to come $\mathbf{P}$ will become very important for us. First, however, we must finish explaining the connection between Eq. (B.26), which we have just rewritten as Eq. (B.30). We need to explain the other contraction with $\mathbf{e}$, which contracts the index for the displacement vector field, $\mathbf{u}$. Since $\mathbf{e}$ is a unit vector, if we project $\mathbf{u}$ onto $\mathbf{e}$ the resulting vector will have the length $\mathbf{u}\cdot\mathbf{e}$. We can name this length variable v, we recognize it is merely a linear combination of the individual components of $\mathbf{u}$. v describes the portion of $\mathbf{u}$ which is along $\mathbf{e}$, which is the direction of our undeformed material line (Eq. (B.31)). Hence, any

$$v = \mathbf{u} \cdot \mathbf{e} = u_i e_i \tag{B.31}$$

derivatives of $\mathbf{u}$ will carry through in the typical manner for linear equations (Eq. (B.32)). If we evaluate these derivatives at a particular point in the undeformed body and at zero

$$\frac{\partial^2 v}{\partial s_0 \partial f_l} = e_i \frac{\partial^2 u_i}{\partial s_0 \partial f_l} \tag{B.32}$$

field, we obtain a result identical to Eq. (B.30). Hence, Eq. (B.30) describes field derivative of the change in the displacement vector along $\mathbf{e}$ per unit of change along the material line in the undeformed body. In simpler terms, as we move along the undeformed material line, the piezoelectric matrix measures how the strain changes per unit of field in each direction.

From Eq. (B.32), which is equivalent to Eq. (B.23), we can easily see how evaluating the field derivative of longitudinal strain is similar to our previous work[47,89]. In our previous work we estimated the deformation of organic dimer systems in the direction of an applied field. In this work we separated the dimers by aligning two atoms (usually hydrogen-bonded) along a particular axis and estimated how applying a field in this direction would change the

distance between these two atoms. We accomplished this through a potential energy "scan" along this separation coordinate. However, we only approximated the deformation in the direction of the original bond direction. For example, if the hydrogen-bond was along the z-axis, we would only approximate the deformation of the bond-along the z-axis–even though there are three possible dimensions in which the bond may deform. Eq. (B.32) is similar in that the contraction the components of $\mathbf{u}$ with $\mathbf{e}$, projects the deformation onto the original material line direction $\mathbf{e}$. The only difference is that the result of Eq. (B.23) is a vector with field components because the derivative was taken with respect to each field component. If we wanted to recover a similar approximation to d_{33}, which mirrors our previous work, we would either take the derivative of the longitudinal strain with respect to just one component of the field along the direction of the original bond, or of course we may project the result of Eq. (B.32) onto $\mathbf{e}$ to find the field derivative of the strain along $\mathbf{e}$ with accompanying field length parameter, in a manner akin to projecting the derivative of the displacent with respect to the undeformed coordinates, $\mathbf{X}$, onto $\mathbf{e}$ with accompanying length parameter s_0.

All of the work described so far has been done in the spirit of continuum mechanics. Meaning that on any length scale the system will always contain matter. For our molecular considerations in this work, the continuum hypothesis clearly does not hold. We are mostly interested in calculating something similar to piezoelectric coefficients for single or several molecular systems that are in general aperiodic. In a periodic system like a crystal, we can talk about the deformation of unit cells in which case the cell vectors are the basis for the displacement derivatives discussed above. In this case, the continuum derivatives involved in strain are easily translated into the molecular realm. However, when we have single molecules or small systems which show marked anisotropy in form, we lack the unit cells or raw choice of basis vectors to describe the deformation of the system. It is for this reason that it is impossible to calculate the full third rank piezoelectric tensor for a molecule. If we were to ask how the molecule or system deforms as we move in the X, Y, or Z direction in the undeformed body, we would be at a loss for how to adequately describe the response. We can instead ask how two nuclei (or points formed from linear combinations of nuclear positions) deform relatively in response to a field. But this only describes the response in one direction (described by the Piezoelectric matrix $\mathbf{P}$discussed above).

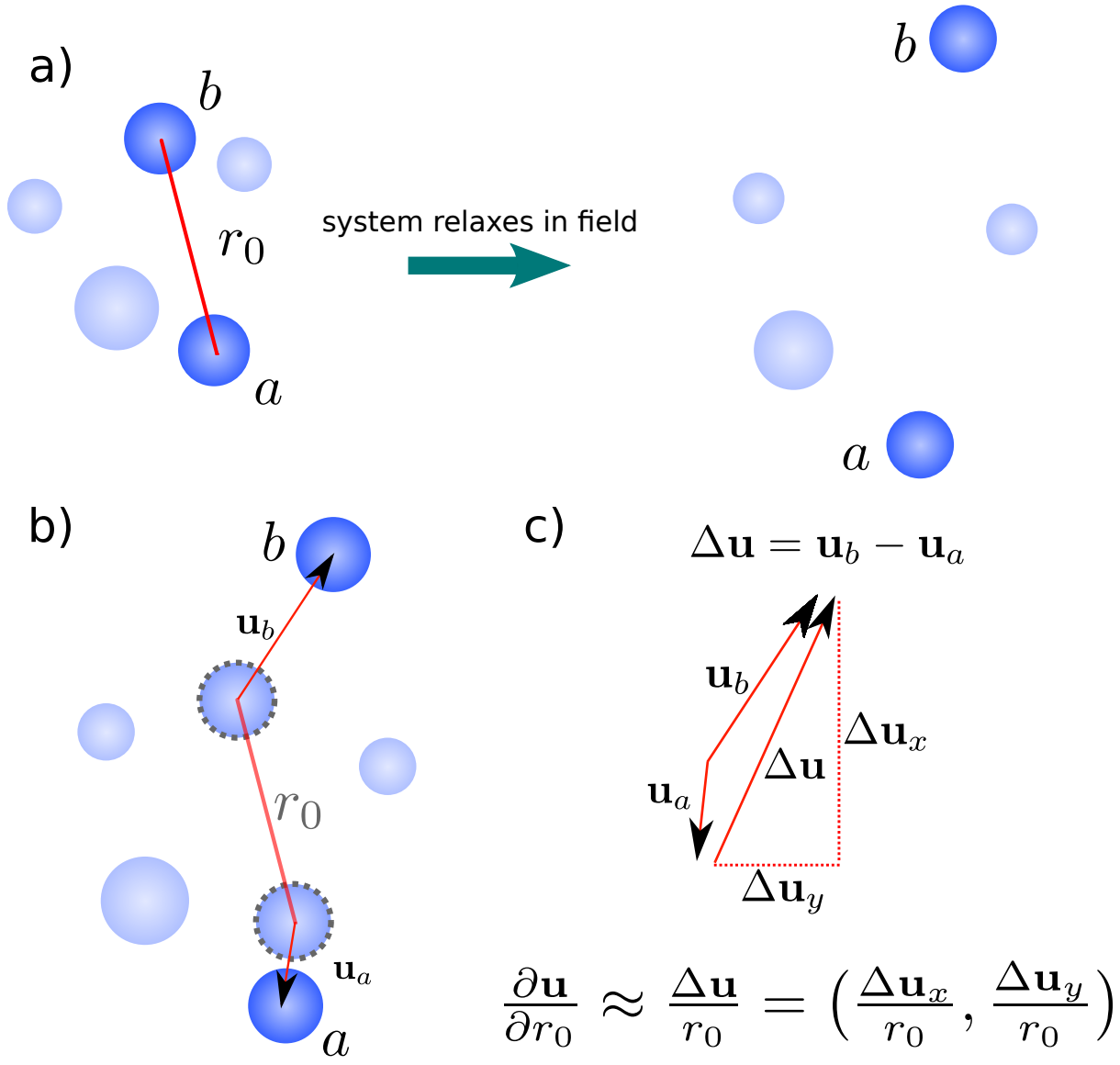

Figure 31: We draw a material line between nuclei a and b in a hypothetical small system. A) If we were to apply a field, the nuclei would be allowed to "relax" within the field to find a minimum in energy. B)We calculate the displacement vectors for each nuclei from their previous to current positions. C) Subtracting the displacement vectors and dividing by the equilibrium "bond" distance yields what would be an approximation to $\frac{\partial \mathbf{u}}{\partial r_0}$ if we could draw the material line between a continuous set of points between the nuclei.

Fig. 31 describes how we can measure the response of two nuclei in a system in an applied field. Just as we chose a material line along which to measure the longitudinal deformation in the continnum body in Fig. 25, we choose a material line in our hypothetical system of nuclei in Fig. 31 (a). We imagine that the system relaxes in an applied electrostatic field or deforms in a manner akin to how the undeformed body K_0 deforms to the body K in Fig. 25 (a). We can draw the displacement vectors $\mathbf{u}$ between the original positions of the nuclei and their final positions (c). In the continuum body (Fig. 25), this akin to the displacement vectors from the points P_0 and Q_0 (undeformed body) to P and Q (deformed body) respectively . In a continuum body if we wished to calculate $\frac{\partial \mathbf{u}}{\partial r_0}$ at the starting point of our material line (P_0 in the continnum body in Fig. 25), we would take the limit of $\frac{\mathbf{u}_{Q_0}-\mathbf{u}_{P_0}}{s_0}$ as $s_0 \to 0$. For a molecule we cannot have $r_0 \to 0$ since the line segment only consists of two points and not a continuous set of points. So instead we "approximate" $\frac{\partial \mathbf{u}}{\partial r_0}$ with the finite difference formula–$\frac{\mathbf{u}_b-\mathbf{u}_a}{r_0}$. We say "approximate" because without quotations we imply the derivative actually exists, when in reality this is not the case. Taking the field derivative of $\frac{\partial \mathbf{u}}{\partial r_0}$ then results in the piezoelectric matrix as presented in Eq. (B.30) but for a discrete system of nuclei instead of a continuum body.

From this perspective, it is clear that for a finite molecular system it is impossible to calculate the full zero field piezoelectric tensor ($\mathbf{d}$) for a given point. Instead we project a molecular version of $\frac{\partial \mathbf{A}(\mathbf{0})}{\partial \mathbf{f}}$ onto a single coordinate along our "material line" in the undeformed system to recover the piezoelectric matrix. One might wonder if we choose two other material lines stemming from the same atom, if we could then solve for the components of $\frac{\mathbf{A}(\mathbf{0})}{\partial \mathbf{f}}$ and then calculate $\mathbf{d}$ from Eq. (B.27). In this framework this is impossible without a "good" choice for material lines. As stated before, unit cell vectors are a natural basis to work in for periodic crystal systems, and we can recover the full piezoelectric tensor for these cases. This is because the distortion of the unit cell is also periodic and reflects the distortion of the whole body. Single molecules and small systems present a unique anisotropy in this framework. Consider the following example. If we draw two material lines stemming from the same nuclei in our system in Fig. 31, it is possible that the two lines lie in the same direction. If we then allow the system to deform in the applied field and draw the displacement vectors again, we can calculate two matrices for $\frac{\partial \mathbf{u}}{\partial r_0}$, but r_0 is in the same direction in

the undeformed body for both material lines. Yet, the resulting matrices for $\frac{\partial \mathbf{u}}{\partial r_0}$ could be very different – ie. two different nuclei oriented in space in line with a third nuclei (P_0) can move in very different directions in a field. To recover the same matrix, the two nuclei would have to remain in a line and move an amount in proportion to their starting distance from the third nuclei. This is incredibly unlikely. Therefore, if we wished to recover $\frac{\partial \mathbf{A}(\mathbf{0})}{\partial \mathbf{f}}$ for a given nuclei from three different "material lines" stemming from that nuclei. we would likely recover a different tensor for any three lines. To get around this, we may in fact try to create a unit cell around the molecule or small system. It would likely have little to no meaning in terms of periodicity like a traditional unit cell, but could be a way of measuring the "space" a molecule or small system occupies. Then issues arise for how to actually choose a box – perhaps the smallest rectangular prism which contains all nuclear centers, but this would likely have little practical meaning. In summary, without a systematic way of creating three distinct basis vectors to resolve $\frac{\partial \mathbf{A}(\mathbf{0})}{\partial \mathbf{f}}$, it is impossible to calculate the full piezoelectric tensor $\mathbf{d}$ for a finite molecular system.

One might wonder why we bother with strain theory at all if this were the case. We could afterall develop this theory from simple geometric arguments and nothing would change–we would merely dispense with the connections to continuum body mechanics. The reason we approach this problem from the view point of continuum mechanics is so that we can use this formalism for any further development of this theory (time depenence, nonequilibrium and finite field calculations) and so that we may compare single molecule deformation to the full piezoelectric response of a crystal, which we have done previously.

B.4 THE MOLECULAR DISPLACEMENT DERIVATIVE WITH RESPECT TO FIELD

We now wish to derive a practical way to calculate piezoelectric matrices for molecular systems. As mentioned in the above section, when constructing the piezoelectric matrix $(P) = \frac{\partial^2 \mathbf{u}}{\partial s_0 \partial \mathbf{f}}$, we may choose either to take the field derivative of $\frac{\partial \mathbf{u}}{\partial s_0}$ or the derivative of $\frac{\partial \mathbf{u}}{\partial \mathbf{f}}$ with respect to the material line length parameter s_0. We will find the latter of the two

methods advantageous because it requires no actual finite field calculations. In a continuum body we would calculate $\frac{\partial \mathbf{u}}{\partial \mathbf{f}}$ at some point of interest or as a tensor field for the whole body. The molecular equivalent is to calculate $\frac{\partial \mathbf{u}}{\partial \mathbf{f}}$ for all of the nuclei of the system–ie. here we take the vector $\mathbf{u}$ to be the displacement for every nuclear coordinate as a molecule or small system relaxes in a field. Therefore, the matrix $\frac{\partial \mathbf{u}}{\partial \mathbf{f}}$ will have dimensions of $3N \times 3$.

In our previous paper we calculate the derivative of the hydrogen-bond length parameter with respect to the field magnitude in the z direction $\frac{dz}{df}$ [47,89]. The derivation will proceed via a similar path for $\frac{\partial \mathbf{u}}{\partial \mathbf{f}}$ but adds the complication of multiple variables, and as we shall see, rotation and translation contamination. To this end, we use a Taylor series of the molecular energy in terms of atomic displacements $\mathbf{u}$ for an arbitrary molecular system and electric field vector $\mathbf{f}$ (Eq. (B.33)). We truncate after the quadratic (bilinear) terms. Here, we use

$$\begin{aligned} E(\mathbf{u},\mathbf{f}) = E(\mathbf{0},\mathbf{0}) + \mathbf{g}_{\mathbf{u}}^T \cdot \mathbf{u} + \mathbf{g}_{\mathbf{f}}^T \cdot \mathbf{f} + \frac{1}{2}\,\mathbf{u}^T \cdot \mathbf{H}_{\mathbf{uu}} \cdot \mathbf{u} \\ + \frac{1}{2}\,\mathbf{f}^T \cdot \mathbf{H}_{\mathbf{ff}} \cdot \mathbf{f} + \mathbf{u}^T \cdot \mathbf{H}_{\mathbf{uf}} \cdot \mathbf{f} \end{aligned} \tag{B.33}$$

$\mathbf{g}_x$ to denote the gradient with respect to the full cartesian nuclear coordinates (denoted by $\mathbf{u}$), and $\mathbf{H}_{\mathbf{uu}}$ for the full nuclear cartesian Hessian (denoted by $\mathbf{u}$). We aim to predict the new equilibrium geometry in response to an applied electric field (Eq. (B.34)). Assuming

$$\nabla_{\mathbf{u}} E(\mathbf{u},\mathbf{f}) = \mathbf{0} = \mathbf{g}_{\mathbf{u}} + \mathbf{H}_{\mathbf{uu}} \cdot \mathbf{u} + \mathbf{H}_{\mathbf{uf}} \cdot \mathbf{f} \tag{B.34}$$

that the initial geometry has been optimized, the gradient $\mathbf{g}_{\mathbf{u}}$ is the zero vector and thus we can solve easily for the displacement (Eq. (B.35)). This equation for $\mathbf{u}$ is quite useful, because differentiation with respect to $\mathbf{f}$ and s_0 (the length of the material line) under the constraints of zero field and strain (which is consistent with the assumption that the energy is minimized) will yield the piezoelectric matrix, as desired.

$$\mathbf{u} = -\mathbf{H_{uu}}^{-1} \cdot \mathbf{H_{uf}} \cdot \mathbf{f} \tag{B.35}$$

Following through and taking the derivative with respect to $\mathbf{f}$ yields the matrix $\frac{\partial \mathbf{u}}{\partial \mathbf{f}}$ (Eq. (B.36)). This equation can be seen as a generalization of eq. (6) from our previous publi-

$$\left(\frac{\partial \mathbf{u}}{\partial \mathbf{f}}\right)_{\mathbf{f=0,T=0}} = -\mathbf{H_{uu}^{-1}} \cdot \mathbf{H_{uf}} \tag{B.36}$$

cation[89] to the full dimensionality of the potential energy surface. We note that even if the gradient were not ignored in Eq. (B.35), it would disappear upon differentiation with respect to $\mathbf{f}$ anyways. Furthermore, this equation, if evaluated at zero field is exact and follows from the multivariable cyclic rule of calculus (the three vectors of interest are the gradient, the displacement, and the field), and this can be seen by keeping higher order terms and setting $\mathbf{u} = \mathbf{0}$ and $\mathbf{f} = \mathbf{0}$ in the result.

Although Eq. (B.36) is formally correct, calculating $\frac{\partial \mathbf{u}}{\partial \mathbf{f}}$ in practice requires us to remove translations and rotations from the coordinate system. Taking this step ensures (a) the physicality of the result, since a molecular rotation or translation is typically made impossible by external mechanical constraints of the system, and (b) that there is no problem due to singularity of the geometric Hessian $\mathbf{H_{uu}}$.

At this point, it is useful to illustrate the physical picture underlying the derivation presented thus far. By rearranging Eq. (B.35), we obtain Eq. (B.37). The Hessian matrix contains the second derivatives of the energy with respect to nuclear positions, and hence, the term on the left is the change in force (or gradient) generated by moving the nuclei by the vector $\mathbf{u}$ from equilibrium (within the harmonic approximation). The term on the right is the approximate change in force generated by the field vector $\mathbf{f}$ on the nuclei. At equilibrium

$$\mathbf{H_{uu}} \cdot \mathbf{u} = -\mathbf{H_{uf}} \cdot \mathbf{f} \tag{B.37}$$

(minimum energy), these forces must be equal. Since the geometric Hessian is a symmetric matrix, it has orthogonal eigenvectors, and one can represent the displacement vector $\mathbf{u}$ as a linear combination of these eigenvectors. Since translations and rotations correspond to zero or near-zero eigenvalues, respectively, one can construct infinitely many displacement vectors that solve Eq. (B.37) and only differ by the weight of the translation and rotation eigenvectors. We also note that strain should not depend on translations and rotations (if Coriolis forces are neglected). Aside from avoiding numerical problems in the inversion, it is therefore useful to remove translations and rotations to obtain unique solutions for the displacement vectors. Since we are merely interested in describing strain, ony relative (intramolecular) deformation of the constituents of the system is important.

We will now give a general outline of how to remove rotation and translation vectors from the Hessian. Projecting out these vectors is easily accomplished by first constructing translation vectors and rotation vectors for the system. Appendix B gives a detailed account of how to construct rotation and translation vectors for the system in the nuclear cartesian space. We use a tensor similar to the moment of inertia tensor (but instead mass independent). The eigenvectors of this matrix are used to construct the rotation vectors plus three translation vectors (altogether 5 vectors for linear and 6 vectors for non-linear systems). We may then choose a basis from which we project out these rotations and translations. The eigenvectors of the Hessian are suitable although any basis which spans the full nuclear space will do. Appendix B outlines how we then create a basis of either $3N-5$ (linear) or $3N-6$ (nonlinear) vectors which are orthogonal to our rotation and translation vectors. For convenience we choose this basis to be orthonormal. We then organize this basis into the column vectors of a $n \times m$ matrix $\mathbf{V}$ ($n = 3N$ and $m = 3N-5$ or $m = 3N-6$) . It is important to note that this basis only lives in the vibrational space of the molecular system.

Because the basis is orthonormal we have $\mathbf{v} = \mathbf{V}^T \cdot \mathbf{u}$. We then transform Eq. (B.36) into the new coordinate system which occupies a subspace of the original system (Eq. (B.38)). The geometric Hessian on the left-hand side is now of reduced dimensionality $m \times m$, and

$$\begin{aligned} \mathbf{V}^T \cdot \mathbf{H_{uu}} \cdot \mathbf{V} \cdot \mathbf{V}^T \cdot \mathbf{u} &= -\mathbf{V}^T \cdot \mathbf{H_{uf}} \cdot \mathbf{f} \\ \mathbf{H_{vv}} \cdot \mathbf{v} &= -\mathbf{H_{vf}} \cdot \mathbf{f} \end{aligned} \tag{B.38}$$

$\mathbf{H_{vf}}$ is of dimension $m \times 3$. We leave the coordinates for the field unchanged because $\mathbf{H_{vf}}$ is a two-point tensor, and we can choose the basis of $\mathbf{f}$ to be whatever we like. We usually choose them to be Cartesian coordinates which are in the same direction as the Cartesian coordinates of the nuclei for analysis purposes (ease of interpretation).

Now that $\mathbf{H_{vv}}$ is, in general, no longer singular, we can safely calculate the inverse (although this is not necessary the most efficient approach for solving this type of problem), to solve for the displacements in our new coordinates (Eq. (B.39)). There can be cases where

$$\mathbf{v} = -\mathbf{H}_{\mathbf{vv}}^{-1} \cdot \mathbf{H_{vf}} \cdot \mathbf{f} \tag{B.39}$$

the initial geometry optimization finds a saddle point instead of a minimum in the energy. In this case there may be additional modes which correspond to negative eigenvalues which may be projected out in addition to rotations or translations.

To convert the displacements back to Cartesian nuclear coordinates, one simply needs to multiply by $\mathbf{V}$ from the left to yield Eq. (B.40). Here we introduce the subscript vib to signify that these displacements correspond only to intramolecular deformations. Again, we differentiate with respect to the field under the constraint in the zero-field and zero-strain limit to obtain Eq. (B.41). Eq. (B.41) is our final result, and we now have only to concern ourselves with retrieving the final formulas for the piezoelectric matrix for small systems.

$$\mathbf{u}_{\text{vib}} = \mathbf{V} \cdot \mathbf{v} = -\mathbf{V} \cdot \mathbf{H}_{\mathbf{vv}}^{-1} \cdot \mathbf{H}_{\mathbf{vf}} \cdot \mathbf{f}, \tag{B.40}$$

$$\left(\frac{\partial \mathbf{u}_{\text{vib}}}{\partial \mathbf{f}}\right)_{\mathbf{f}=\mathbf{0},\mathbf{T}=\mathbf{0}} = -\mathbf{V} \cdot \mathbf{H}_{\mathbf{vv}}^{-1} \cdot \mathbf{H}_{\mathbf{vf}} \tag{B.41}$$

B.5 THE P MATRIX FOR MOLECULAR SYSTEMS

We have thus far discussed the derivation of the Piezoelectric matrix $\mathbf{P}$ from a discussion of continuum mechanics, and how it encapsulates the deformation properties along a material line at a given point in a continuum body. We have calculated $\frac{\partial \mathbf{u}_{\text{vib}}}{\partial \mathbf{f}}$ for a molecular system as a replacement to calculating the tensor field (can be specified for every point in a continuum body) $\frac{\partial \mathbf{u}}{\partial \mathbf{f}}$ for a continuum body. We have also discussed calculating the piezoelectric coefficient as the derivative of the longitudinal strain of a material line with respect to field, which we then evaluate at zero field. Now that we have $\frac{\partial \mathbf{u}_{\text{vib}}}{\partial \mathbf{f}}$, we can present how to calculate a molecular version of $\mathbf{P} = \frac{\partial^2 \mathbf{u}}{\partial s_0 \partial \mathbf{f}}$ to describe the field deformation characteristics around the molecular equivalent of a material line.

To calculate a $\mathbf{P}$ matrix, we start by picking a material line in our system. This part can be (somewhat) tricky and has an incredible impact on the piezocoefficient. In a crystal it makes sense to study the deformation of a unit cell due to the periodic nature of the crystal, since we expect that within a uniform field the deformation of all of the images of the unit cell should be identical. There is no such natural kernel in the finite system realm. We have had much success in previous work in approximating the piezocoefficient by studying the deformation of the attribute of our system we expect to have the most deformation within

a field. One should take care however, in the assumption that the deformation properties of a small system extend to a bulk material. However, if we are to compare similar molecular systems for their deformation properties, it is reasonable to assume that picking a similar attribute in a group, such as the hydrogen-bond in our previous systems, would *a priori*, be a good way to establish which members of the group are the best piezoelectrics.

For our purposes here, we need only be concerned with a general method by which we choose a material line. We shall, then with our freedom, choose our material line to be a line segment between two atoms. We choose the two atoms via chemical intuition and the deformation we expect (ie. hydrogen-bonded atoms and the like). One of the atoms will act as the point P_0 in Fig. 25 in the undeformed system and will thus serve as the point of origin for our material line. We could also form linear combinations of points. For instance, consider a line segment between the centers of mass for two monomers in our system, but we need not discuss this at this point. Now that we have our line segment, we recall the knowledge we have accumulated about deformation analysis to aid in our efforts. We wish to approximate $\mathbf{P} = \frac{\partial^2 \mathbf{u}}{\partial s_0 \partial \mathbf{f}}$ around the point P_0 of our material line. We have the $3N \times 3$ matrix $\frac{\partial \mathbf{u}_{\text{vib}}}{\partial \mathbf{f}}$ wich holds the 3×3 matrix $\frac{\partial \mathbf{u}}{\partial \mathbf{f}}_i$, indicating the displacement field derivative for the 3 nuclear coordinates with respect to the field coordinates, for the ith atom of the molecule or system. We have dropped the "vib" subscript for convenience, though it is understood. The molecular version of the $\mathbf{P}$ for this material line in the vicinity of these two atoms is then given by Eq. (B.42), where r_0 is the distance between these two atoms in the equilibrium

$$\mathbf{P} = \frac{\frac{\partial \mathbf{u}}{\partial \mathbf{f}}_2 - \frac{\partial \mathbf{u}}{\partial \mathbf{f}}_1}{r_0} \tag{B.42}$$

geometry. This is equivalent to a numerical derivative, though we can not arbitrarily choose how small to make r_0, but are handcuffed by the distance in the equilibrium geometry (a consequence of the discrete nature of the system). It should be pointed out that the difference of any linear combination of matrices $\frac{\partial \mathbf{u}}{\partial \mathbf{f}}_i$ can be used to calculate a piezoelectric matrix. The matrix would then coincide with the deformation properties of a material line connecting

the two points given by the same linear combinations of $\mathbf{u}_i$ for the molecular system. For example the geometric center or the center of mass of two regions of a bigger molecular system can be used and the deformation properties for the material line between these two points can be determined.

As discussed in the previous sections, if we wished to calculate d_{33} in a method similar to our other papers, we must contract the $\mathbf{P}$ matrix over the indices for the displacement vector with unit vector $\mathbf{e} = \frac{\mathbf{r}_2 - \mathbf{r}_1}{r_0}$. Furthermore, we would also need to contract over the field indices, multiplying by a unit vector also in the direction of the $\mathbf{e}$, (the basis chosen for the field must coincide with the basis for the nuclear coordinates if the contracted vector is actually $\mathbf{e}$). We would thus obtain Eq. (B.43). The subscripts attached to the $\mathbf{e}$ vector are

$$\begin{aligned} d_{33} &= \mathbf{e}_u^T \cdot \mathbf{P} \cdot \mathbf{e}_f \\ &= \frac{\partial^2 u_{r_0}}{\partial r_0 \partial f_{r_0}} \end{aligned} \tag{B.43}$$

to indicate both indices of contraction (ie. the vector $\mathbf{u}$ or $\mathbf{f}$) and to indicate that although the vector $\mathbf{e}$ is in the direction of the material line it might have two different representations depending on the nuclear coordinate and field bases. As an example, if the 3×3 piezoelectric matrix were calculated for two atoms along the z-axis, and the field basis was chosen to correspond with the x, y, and z direction, then $\mathbf{e}_f$ and $\mathbf{e}_u$ both have the representation of $(0, 0, 1)$, and the matrix component P_{33} would be equal to d_{33} as in our previous papers. At this point we should again mention that two piezoelectric matrices for two material lines (line segments between atoms) for a molecule can be very different even if the material lines occupy a similar region of space and are in similar directions. It is for this reason that there is no way to logically approximate the full third rank piezoelectric tensor for an arbitrary molecule. In a sense, the derivation for the piezoelectric matrix and the connection to our calculated piezoelectric matrix is somewhat tenuous, but from a philosophical point of view and a practical point of view the authors of this paper believe that the connections should

be made.

To this end the piezoelectric matrix also has significant utility beyond approximations of d_{33}. We can ask questions like, what direction of applied field is necessary to get the largest possible deformation betweent two atoms of a molecular system? If we apply a small field $\mathbf{f}$ to our molecule, $\mathbf{P} \cdot \mathbf{f}$ will tell us the relative direction of the displacemement vectors of the two nuclei which make up our material line per unit of the distance separating the two nuclei. If we were to diagonalize $\mathbf{P}$, we would obtain eigenvectors which indicate in what direction to apply a field to have our strain vector $\frac{\partial \mathbf{u}}{\partial r_0}$ to be in the same direction as the field. This is of course not the same as optimizing the deformation response for an applied field. To do so we can optimize $|\frac{\partial \mathbf{u}}{\partial r_0}|^2$ under the constraint of a small finite field–namely, $\mathbf{f}^T \cdot \mathbf{f} = k$, where k is some arbitrary small square of the magnitude of the field. We construct the equation to optimize with the appropriate lagrange equation and set the gradient with respect to the field coordinates equal to zero. The result is the typical eigenvalue problem for the matrix $\mathbf{P}^T \cdot \mathbf{P}$ (Eq. (B.44)). The constraint equations is given by $g(\mathbf{f})$ along with the equation we

$$\begin{aligned} \left|\frac{\partial \mathbf{u}}{\partial r_0}\right|^2 &= \mathbf{f}^T \cdot \mathbf{P}^T \cdot \mathbf{P} \cdot \mathbf{f} \\ g(\mathbf{f}) &= \mathbf{f}^T \cdot \mathbf{f} - k = 0 \end{aligned} \tag{B.44}$$

wish to optimize. We combine the two by multiplying $g(\mathbf{f})$ by λ (lagrange multiplier) and subtracting the two equations to obtain our lagrange equation. We then differentiate with respect to the field and set the result equal to zero (Eq. (B.45)).

The matrix, $\mathbf{P}^T \cdot \mathbf{P}$, is symmetric and real, and therefore has orthogonal eigenvectors and real eigenvalues. The largest eigenvalue gives the maximum value of $|\frac{\partial \mathbf{u}}{\partial r_0}|^2$ for an applied field of magnitude one unit and the eigenvector indicates the direction in which to apply the field to get the optimum deformation. Since we construct $\mathbf{P}$ for two atoms in the molecule or small system, it is possible to find the optimum field direction to apply to the system to get the best deformation for any pair of atoms. The direction of the relative change in the

$$
\begin{aligned}
L(\mathbf{f}) &= \mathbf{f}^T \cdot \mathbf{P}^T \cdot \mathbf{P} \cdot \mathbf{f} - \lambda(\mathbf{f}^T \cdot \mathbf{f} - k) \\
\frac{\partial g(\mathbf{f})}{\partial \mathbf{f}} = 0 &\implies \mathbf{P}^T \cdot \mathbf{P} \cdot \mathbf{f} = \lambda \mathbf{f}
\end{aligned}
\tag{B.45}
$$

displacement vector between the two atoms will have the direction given by $\mathbf{P} \cdot \mathbf{f}$ which is not necessarily in the direction of the distance vector between the two atoms.

B.6 CONSTRUCTION OF ROTATION AND TRANSLATION VECTORS

In an earlier section of this work we mentioned that in order to solve for $\frac{\partial \mathbf{u}_{\text{vib}}}{\partial \mathbf{f}}$ (Eq. (B.41)) it is useful to construct a set of vectors which span the $3N - 6$ (or $3N - 5$ for linear molecules) dimensional vibrational space of the molecule or system to exclude rotations and translations from the generated displacement vectors in Eq. (B.39). To understand why this is necessary we must consider the interpretation of the Hessian matrix acting on an infinitesimal displacement vector. The Hessian matrix is given by the second derivatives of the energy with respect to the nuclear coordinates, $\frac{\partial^2 E}{\partial u_i \partial u_j}$, or the first derivative of the gradient, $\frac{\partial \nabla E}{\partial u_j}$. When the Hessian matrix acts on a displacement vector it gives the change in force generated by moving the nuclei along the electronic potential energy surface, in the way described by the vector, if the potential was harmonic (Eq. (B.46)). At equlibrium, the

$$
\mathbf{H}_{\mathbf{uu}} \cdot d\mathbf{u} = \frac{\partial \nabla \mathbf{E}}{\partial u_j} du_j \approx \partial \nabla \mathbf{E} \tag{B.46}
$$

gradient for the system is at (or approximately at) $\mathbf{0}$, meaning there is no net force acting

on the nuclei. Therefore a change in the force following displacement of nuclei around the equilibrium is equal but opposite to the force needed to displace the nuclei. If we imagine the effect of moving the nuclei in a manner that mimics a rotation or translation, we should not find that any net force now acts on the nuclei (granted that there is no external field or stress acting on the molecule). This is equivalent to saying that the energy of a molecule or system should only depend on the relative position of its nuclei and not its orientation in space if there is no external force acting on the system. This is obvious for translations but only true for infinitesimal vectors corresponding to rotation. As a result, if the equilibrium Hessian acts on these vectors, we expect to receive a zero vector as an output. This implies that rotational and translational vectors are eigenvectors of the Hessian with zero eigenvalues. This is the reason the equilibrium Hessian should be singular and why inverting it poses a problem in Eq. (B.35).

The particular reason the Hessian's singularity poses a problem for neutral molecules or systems is due to rotations. A neutral molecule with a dipole has no net translational movement in an electric field, but it will rotate to align the dipole in the direction of the field. From Eq. (B.35) we see that the change in force on the nuclei caused by the electric field is approximated by the matrix product of the field with the dipole derivative matrix $\mathbf{H_{uf}}$. If the resulting vector from this operation were to "contain" (which it inevitably does since the dipole interacts with the field) some force generated by rotation, the predicted displacement vector in the direction of rotation would become infinite, making our calculations no longer useful. For this reason we imagine that the molecule does not have any rotational freedom (as it would likely not in a piezoelectric bulk material), and we instead project Eq. (B.35) into the space of the remaining vibrational degrees of freedom.

In many cases, it is acceptable to diagonalize the Hessian and omit the 5 or 6 vectors (linear or nonlinear) which correspond to the lowest eigenvalues (usually very close to zero). The remaining vectors usually correspond to the relative deformation of atoms of the molecule. The remaining vectors organized as columns can thus make up the transformation matrix, $\mathbf{V}$, and Eq. (B.41) may thus be used to calculate $\frac{\partial \mathbf{u}_{\text{vib}}}{\partial \mathbf{f}}$. In practice, however, for numerical calculations of the Hessian or for systems with negative eigenvalues (which might be desirable for reasons of representing a smaller subunit of a bulk material), it is safer to construct

rotation and translation vectors and remove them manually from the full basis (which could be the eigenvectors of the Hesssian or any basis which spans the full $3N$ space.

As discussed earlier, we can view the vectors the Hessian acts on as displacement vectors for the nuclei. In this sense the relative velocities of the nuclei under rotational or translational motion can be reflected in the displacements. To build the translation vectors, it must be true that all of the nuclei must "move" or be displaced by the same vector if the energy of the system is not to change. The molecule also has three dimensions in which it can move. To make the vectors orthogonal, we just pick the x, y, and z directions and construct the unit vectors. We will assume that the vectors are ordered so that the x,y, and z components of displacement are given for an atom before moving on to the next atom in the vector. To illustrate this we will assume u_{ix} is the x component of displacement for the ith atom in the system, and the full displacement vector for an N atom system has the form shown in Eq. (B.47). Thus the 3 normalized translation vectors for the x, y, and z directions ($\mathbf{u}^{tx}$,$\mathbf{u}^{ty}$, and

$$\mathbf{u} = (u_{1x}, u_{1y}, u_{1z}, u_{2x}, u_{2y}, u_{2z}, ..., u_{Nx}, u_{Ny}, u_{Nz}) \tag{B.47}$$

$\mathbf{u}^{tz}$ respectively) have the form given in Eq. (B.48).

$$\begin{aligned}
\mathbf{u}^{tx} &= \left(\frac{1}{\sqrt{N}}, 0, 0, \frac{1}{\sqrt{N}}, 0, 0, ..., \frac{1}{\sqrt{N}}, 0, 0\right) \\
\mathbf{u}^{ty} &= \left(0, \frac{1}{\sqrt{N}}, 0, 0, \frac{1}{\sqrt{N}}, 0, ..., 0, \frac{1}{\sqrt{N}}, 0\right) \\
\mathbf{u}^{tz} &= \left(0, 0, \frac{1}{\sqrt{N}}, 0, 0, \frac{1}{\sqrt{N}}, ..., 0, 0, \frac{1}{\sqrt{N}}\right)
\end{aligned} \tag{B.48}$$

The rotation vectors are a little trickier to write. We first need to calculate the geometric center vector for the system and then the position vectors for the nuclei relative to the

$$\mathbf{r}_{gc} = \frac{\sum_i^N \mathbf{x}_i}{N} \tag{B.49}$$

geometric center (Eq. (B.49)). Here $\mathbf{x_i}$, N, and $\mathbf{r}_{gc}$ are the positions of the nuclei, total number of nuclei, and the geometric center vector for the molecule respectively. The position vector relative to the geometric center for the ith atom is given by Eq. (B.50). It is important

$$\mathbf{r}_i = \mathbf{x}_i - \mathbf{r}_{gc} \tag{B.50}$$

to note here that for our purposes we will rotate the molecule about the geometric center and not the center of mass in free rotation. We will show later that rotating about the geometric center creates vectors orthogonal to the translational vectors. For a given angular velocity vector ω for a molecule, the velocity vector for an atom in the molecule ($\mathbf{v}_i$) is given by Eq. (B.51). Thus the displacement vectors we wish to construct have the form given in

$$\mathbf{v}_i = \mathbf{r}_i \times \boldsymbol{\omega} \tag{B.51}$$

Eq. (B.52) before normalization.

For a linear or nonlinear molecule, we should be able to construct 2 or 3 rotation vectors respectively that span our space of interest. To do so efficiently we will try to construct orthogonal vectors. We proceed by first realizing that a dot product of two rotation vectors is equivalent to the sum of individual dot products of the displacement vectors for atoms with the same index. There are two different angular velocity vectors ($\boldsymbol{\omega}_j$ and $\boldsymbol{\omega}_k$) associated with

$$\mathbf{u}^{r\omega} = (\mathbf{r}_1 \times \boldsymbol{\omega}, \mathbf{r}_2 \times \boldsymbol{\omega}, \mathbf{r}_3 \times \boldsymbol{\omega}, ..., \mathbf{r}_N \times \boldsymbol{\omega}) \tag{B.52}$$

$$\mathbf{u}^{r\omega_j} \cdot \mathbf{u}^{r\omega_k} = \sum_i^N ((\mathbf{r}_i \times \boldsymbol{\omega}_j) \cdot (\mathbf{r}_i \times \boldsymbol{\omega}_k)) \tag{B.53}$$

two different rotation vectors (Eq. (B.53)). At this point it is helpful to rewrite the cross products as matrix products with the angular velocity vectors. The cross product matrix has the form given in Eq. (B.54). Here r_{ij} is the jth (x,y, or z) component of the vector $\mathbf{r}_i$.

$$\mathbf{R}_i \equiv \begin{pmatrix} 0 & -r_{iz} & r_{iy} \\ r_{iz} & 0 & -r_{ix} \\ -r_{iy} & r_{ix} & 0 \end{pmatrix} \tag{B.54}$$

We then replace the cross products with matrix products to obtain Eq. (B.55). Then

$$\mathbf{u}^{r\omega_j} \cdot \mathbf{u}^{r\omega_k} = \sum_i^N ((\mathbf{R}_i \cdot \boldsymbol{\omega}_j) \cdot (\mathbf{R}_i \cdot \boldsymbol{\omega}_k)) \tag{B.55}$$

recognizing that the dot product is equivalent to a matrix product of a row and column vector, we may take the transform of the matrix product on the left and multiply it by the

$$\mathbf{u}^{r\omega_j} \cdot \mathbf{u}^{r\omega_k} = \sum_i^N \left(\left(\boldsymbol{\omega}_j^T \cdot \mathbf{R}_i^T \right) \cdot \left(\mathbf{R}_i \cdot \boldsymbol{\omega}_k \right) \right) = \boldsymbol{\omega}_j^T \cdot \left(\sum_i^N \left(\mathbf{R}_i^T \cdot \mathbf{R}_i \right) \right) \cdot \boldsymbol{\omega}_k \tag{B.56}$$

matrix product on the right (Eq. (B.56)). In the last step we have moved the summation over atoms to inside the multiplications with the angular velocity vectors. From this we obtain a new matrix $\mathbf{S}$ (Eq. (B.57)). This is a sum over the matrix product shown and is

$$\mathbf{S} = \sum_i^N \left(\mathbf{R}_i^T \cdot \mathbf{R}_i \right) \tag{B.57}$$

necessarily symmetric. Our original goal was to choose angular velocity vectors such that we construct orthogonal rotation vectors. Thus we impose the requirement that this dot product yields zero (Eq. (B.58)). Since our matrix $\mathbf{S}$ is symmetric, it has orthogonal eigenvectors.

$$\mathbf{u}^{r\omega_j} \cdot \mathbf{u}^{r\omega_k} = \boldsymbol{\omega}_j^T \cdot \mathbf{S} \cdot \boldsymbol{\omega}_k = 0 \tag{B.58}$$

Therefore our choice for the set of vectors $\boldsymbol{\omega}_i$ is obvious. If we choose the eigenvectors of $\mathbf{S}$ to be our angular velocity vectors we have met the conditions (Eq. (B.59)). Here λ_k is the eigenvalue for the eigenvector ω_k. As we stated before, we chose the geometric center as our rotation point for the system because it also yields rotation vectors orthogonal to the translation vectors. This is not hard to show. As a matter of fact, we only need the sum of the rotation vectors for each atom per full rotation vector to yield the zero vector (Eq. (B.60)). To show that this is the case we substitute Eq. (B.50) into Eq. (B.60) to yield Eq.

$$\mathbf{u}^{r\omega_j} \cdot \mathbf{u}^{r\omega_k} = \boldsymbol{\omega}_j^T \cdot \mathbf{S} \cdot \boldsymbol{\omega}_k = \lambda_k \boldsymbol{\omega}_j^T \cdot \boldsymbol{\omega}_k = 0 \tag{B.59}$$

$$\sum_i^N \mathbf{u}_i^{r\omega_j} = \sum_i^N (\mathbf{r}_i \times \boldsymbol{\omega}_j) = \mathbf{0} \tag{B.60}$$

$$\begin{aligned}
\sum_i \mathbf{u}_i^{r\omega_j} &= \sum_i^N (\mathbf{r}_i \times \boldsymbol{\omega}_j) = \left(\sum_i^N (\mathbf{x}_i - \mathbf{r}_{gc}) \right) \times \boldsymbol{\omega}_j \\
&= \left(\sum_i^N \left(\mathbf{x}_i - \frac{\sum_k^N \mathbf{x}_k}{N} \right) \right) \times \boldsymbol{\omega}_j = \left(\sum_i^N \mathbf{x}_i - N \frac{\sum_k^N \mathbf{x}_k}{N} \right) \times \boldsymbol{\omega}_j \\
&= \left(\sum_i^N \mathbf{x}_i - \sum_k^N \mathbf{x}_k \right) \times \boldsymbol{\omega}_j = \mathbf{0} \times \boldsymbol{\omega}_j = \mathbf{0}
\end{aligned} \tag{B.61}$$

(B.61). It might not seem intuitive at first that requiring the sum of the rotation vectors for the indivdual atoms to be the zero vector implies that the full rotation vector is orthogonal to the translation vectors. Any translation vector (or linear combination of translation vectors) consists of the same vector of displacement per atom (otherwise the nuclei would not be displaced in the same direction by the same magnitude). Therefore we may represent any linear combination of translation vectors as shwon in Eq. (B.62). The resulting dot product of an arbitrary translation vector with a rotation vector will produce the expression given in Eq. (B.63). In the second line, we have broken up the individual displacement vectors for

$$\mathbf{u}^t = a\mathbf{u}^{tx} + b\mathbf{u}^{ty} + c\mathbf{u}^{tz} = (a, b, c, a, b, c, a, b, c, ...a, b, c) \tag{B.62}$$

$$\begin{aligned}
\mathbf{u}^{r\omega_j} \cdot \mathbf{u}^t &= \sum_i^N \mathbf{u}_i^{r\omega_j} \cdot (a, b, c) \\
&= \sum_i^N \left(a u_{ix}^{r\omega_j} + b u_{iy}^{r\omega_j} + c u_{iz}^{r\omega_j}\right) = a \sum_i^N \left(u_{ix}^{r\omega_j}\right) + b \sum_i^N \left(u_{iy}^{r\omega_j}\right) + c \sum_i^N \left(u_{iz}^{r\omega_j}\right) \\
&= a \cdot 0 + b \cdot 0 + c \cdot 0 = 0
\end{aligned} \tag{B.63}$$

the ith atom in the displacement vector into the x, y, and z components to break the sum up in the remaining line. The last line immediately follows from Eq. (B.61). If the individual displacement vectors for the atoms sum to the zero vector for the rotation displacement vector, then it follows that the x, y, and z components sum to zero separately, and the dot product is zero. Hence constructing the rotational vectors in this way yields vectors that are internally orthogonal (to one another) and vectors that are orthogonal to the translation vectors.

Furthermore we can show that constructing rotation vectors using any center as a rotation point yields a vector that is a linear combination of rotation vectors constructed in the way discussed above and translation vectors. To construct such a displacement vector, we first need to calculate the position vectors of the atoms relative to the center as before. We will do so in such a way that we add a vector $\mathbf{s}$ to the geometric center $\mathbf{r}_{gc}$ to produce the desired arbitrary center of rotation (Eq. (B.64)). We then construct the rotation vector as we have done before–this time using the eigenvectors of the matrix $\tilde{\mathbf{S}} = \sum_i^N \left(\tilde{\mathbf{R}}_i^T \cdot \tilde{\mathbf{R}}_i\right)$, where the matrix $\tilde{\mathbf{R}}_i$ is the matrix form of the cross product of $\tilde{\mathbf{r}}_i$ with another vector. The

$$\tilde{\mathbf{r}}_i = \mathbf{x}_i - (\mathbf{r}_{gc} + \mathbf{s}) = \mathbf{x}_i - \mathbf{r}_{gc} - \mathbf{s} \tag{B.64}$$

new eigenvectors for $\tilde{\mathbf{S}}$, $\tilde{\boldsymbol{\omega}}_l$, can be written as linear combinations of the eigenvectors for $\mathbf{S}$, $\boldsymbol{\omega}_j$ (Eq. (B.65)). The sum can be over 2 or 3 rotation eigenvectors if the molecule is linear

$$\tilde{\boldsymbol{\omega}}_l = \sum_j^{2\text{or}3} c_{lj}\boldsymbol{\omega}_j \tag{B.65}$$

or nonlinear respectively. We will drop the upper bounds for the sum in the equations to follow for convenience. We can now construct a rotation vector in Eq. (B.66), as we have done previously in Eq. (B.52). Here, $\mathbf{a} = -\mathbf{s} \times \sum_j c_{lj}\boldsymbol{\omega}_j$, since this vector is constant and does not depend on the atom index. In the last line, it is clear that the resulting rotational displacement vector is a linear combination of the rotation vectors about the geometric center plus a vector containing $\mathbf{a}$ for every atom position. As stated previously, any such displacement vector where the displacement is constant for every atom can be written as a linear combination of the basal translation vectors. Therefore we have shown that any displacement vector constructed as a rotation vector about any point can be written as a linear combination of translation vectors and rotation vectors formed by rotating about the geometric center. Therefore any such set of linearly independent rotation and translation vectors will necessarily occupy the same space, and after an internal orthogonalizing scheme, can be projected out from the eigenvectors of the Hessian. The remaining vectors will contain only vibrations. This is of course only true for infinitesimal displacements as any vibrational motion of the system will change the rotation and hence vibrational vectors. For the purposes of this work, we are only concerned with the field derivatives of the displacement at zero field, and thus we are not concerned with large system strains.

$$
\begin{aligned}
\mathbf{u}^{\tilde{r}\tilde{\omega}_l} &= (\tilde{\mathbf{r}}_1 \times \tilde{\boldsymbol{\omega}}_l, \tilde{\mathbf{r}}_2 \times \tilde{\boldsymbol{\omega}}_l, \tilde{\mathbf{r}}_3 \times \tilde{\boldsymbol{\omega}}_l, ..., \tilde{\mathbf{r}}_N \times \tilde{\boldsymbol{\omega}}_l) \\
&= \left((\mathbf{x}_1 - \mathbf{r}_{gc} - \mathbf{s}) \times \sum_j c_{lj}\boldsymbol{\omega}_j, ..., (\mathbf{x}_N - \mathbf{r}_{gc} - \mathbf{s}) \times \sum_j c_{lj}\boldsymbol{\omega}_j \right) \\
&= \left((\mathbf{x}_1 - \mathbf{r}_{gc}) \times \sum_j c_{lj}\boldsymbol{\omega}_j - \mathbf{s} \times \sum_j c_{lj}\boldsymbol{\omega}_j, ..., (\mathbf{x}_N - \mathbf{r}_{gc}) \times \sum_j c_{lj}\boldsymbol{\omega}_j - \mathbf{s} \times \sum_j c_{lj}\boldsymbol{\omega}_j \right) \\
&= \left(\sum_j c_{lj}\mathbf{r}_1 \times \boldsymbol{\omega}_j + \mathbf{a}, ..., \sum_j c_{lj}\mathbf{r}_N \times \boldsymbol{\omega}_j + \mathbf{a} \right) \\
&= \sum_j c_{lj} \left(\mathbf{r}_1 \times \boldsymbol{\omega}_j, ..., \mathbf{r}_N \times \boldsymbol{\omega}_j \right) + (\mathbf{a}, ..., \mathbf{a})
\end{aligned}
\tag{B.66}
$$

APPENDIX C

SUPPORTING INFORMATION REGARDING CHAPTER 5

C.1 CALCULATING VOLUMETRIC STRAIN

As presented in 5.3, the definition for volumtric strain is given by Eq. (C.1). so this section

$$\nu = lim_{V_0 \to 0} \frac{(V - V_0)}{V_0} = \frac{dV}{dV_0} - 1, \tag{C.1}$$

focuses mostly on calculating $\frac{dV}{dV_0}$ for a given point in a continuum body. Recall that from a point in a continuum body we may draw in any three directions material lines that extend from the point. If we zoom in on the point, the material lines before and after deformation apper to be straight at the infinitesimal scale. We shall condsider the directions of the material lines in the undeformed body to be the basis for which we describe deformations around the point. We should pick three directions which are linearly independent so that we may describe deformations in any direction under a transformation. For our purposes it is easiest to choose material lines that coincide witht the basis for the representation of the coordinates of points in the undeformed body $\mathbf{X}$.

Fig. 32 shows the infinitesimal volume elements formed by three such material lines for the undeformed (a) and deformed bodies (b). The volume for the undeformed volume element is clearly given by Eq. (C.2). from our choice of basis. dV can be calculated from

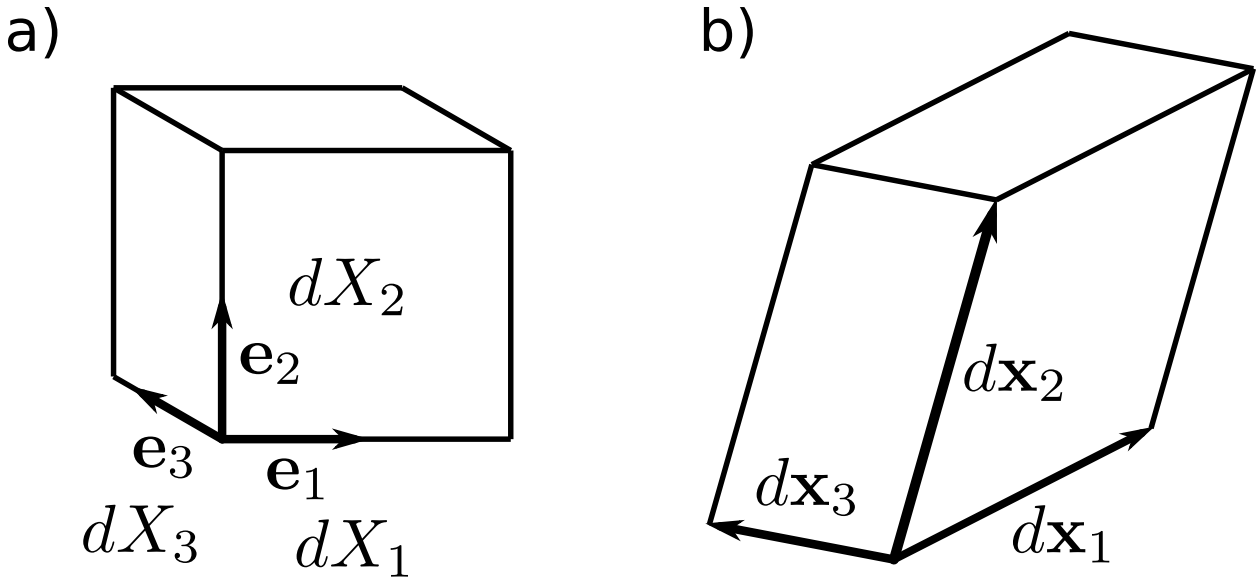

Figure 32: Infinitesimal volume elements formed at the intesection of three material lines in a) the undeformed body and b) the deformed body.

$$dV_0 = dX_1 dX_2 dX_3 \tag{C.2}$$

the determinant of the three vectors in the deformed body $d\mathbf{x}_i$ organized into a matrix. To calculate these vectors recall that the position of any point in the deformed body can be written as the position of that point in the undeformed body plus the displacement vector for that point after deformation, $\mathbf{x} = \mathbf{X} + \mathbf{u}$. We can then write $d\mathbf{x}$ as a differential (Eq. (C.3)). In element form Eq. (C.3) is written as Eq. (C.4). where we have used the Identity matrix or kroeneker delta and the displacement tensor, $\mathbf{A}$ where appropriate. It is then clear that to obtain $d\mathbf{x}_i$, where i now corresponds to the corresponding deformed vector in the deformed body, one merely sets the corresponding dX_i value equal to itself in the differential and the other values of dX_j equal to zero. Hence the columns of the matrix $\mathbf{I} + \mathbf{A}$, where each column is scaled by the appropriate dX_i, is the matrix that houses the three column

$$d\mathbf{x} = \frac{\partial \mathbf{X}}{\partial X_j} dX_j + \frac{\partial \mathbf{u}}{\partial X_j} dX_j = \mathbf{I} d\mathbf{X} + \mathbf{A} d\mathbf{X} \tag{C.3}$$

$$dx_i = \frac{\partial X_i}{\partial X_j} dX_j + \frac{\partial u_i}{\partial X_j} dX_j = \delta_{ij} dX_j + A_{ij} dX_j, \tag{C.4}$$

vectors, $d\mathbf{x}_i$, in the deformed body (Eq. (C.5)). Therefore dV is given by Eq. (C.6). $\frac{dV}{dV_0}$ is

$$\begin{pmatrix} d\mathbf{x}_1 & d\mathbf{x}_2 & d\mathbf{x}_3 \end{pmatrix} = \begin{pmatrix} (\mathbf{I} + \mathbf{A})_{col_1} dX_1 & (\mathbf{I} + \mathbf{A})_{col_2} dX_2 & (\mathbf{I} + \mathbf{A})_{col_3} dX_3 \end{pmatrix} \tag{C.5}$$

$$dV = det(\mathbf{I} + \mathbf{A}) dX_1 dX_2 dX_3, \tag{C.6}$$

then given by Eq. (C.7). Volumetric strain is given by Eq. (C.8).

$$\frac{dV}{dV_0} = \frac{det(\mathbf{I} + \mathbf{A}) dX_1 dX_2 dX_3}{dX_1 dX_2 dX_3} = det(\mathbf{I} + \mathbf{A}), \tag{C.7}$$

$$\nu = det(\mathbf{I} + \mathbf{A}) - 1 \tag{C.8}$$

C.2 REMOVING ROTATIONS FOR PERIODIC SYSTEM CALCULATIONS

For periodic systems, we need to construct the rotational vectors to project out of $3N + 9$ dimensional Hessian and $3N + 9 \times 3$ dipole derivative matrices. So in a fashion similar to B.6, we will consider a periodic system under infinitesimal rotation. A given position of a nucleus, $\mathbf{x}$ can be specified by four indices i, j, k, l (Eq. (C.9)). $\mathbf{r}_i$ is the position of the

$$\mathbf{x}_{ijkl} = \mathbf{r}_i + j\mathbf{a} + k\mathbf{b} + l\mathbf{c} \tag{C.9}$$

corresponding nucleus in the original unit cell, and the index i runs from 1 to N for the number of atoms in the unit cell. The indices j,k, and l are integers and correspond to how many unit cells over from the base cell in the directions of the unit cell vectors $\mathbf{a}, \mathbf{b}, \mathbf{c}$, the nucleus is shifted from the base nucleus. In this case we will choose the indices to run from -J to J, -K to K and -L to L respectively. Hence the base unit cell occurs when $j, k, l = 0$. We will also have the geometric center of the base cell be positioned at the origin, and hence we have Eq. (C.10).

The total geometric center in this system is then also at the origin (Eq. (C.11)). In the last line we have used the fact that $\sum_1^N \mathbf{r}_i = \mathbf{0}$ as well as $\mathbf{a}\sum_{j=-J}^{J} j = \mathbf{0}$, as well as for all of the other indices. So all of the position vectors given are the same as the vectors relative to the geometric center.

Rotating the whole system is equivalent to rotaing the base unit cell and then rotating

$$\begin{aligned} \mathbf{r}_{gc} &= \frac{\sum_1^N \mathbf{r}_i}{N} = 0 \\ \sum_1^N \mathbf{r}_i &= \mathbf{0} \end{aligned} \tag{C.10}$$

$$\begin{aligned} \mathbf{x}_{gc} &= \frac{\sum_{i,j,k,l=1,-J,-K,-L}^{N,J,K,L} (\mathbf{r}_i + j\mathbf{a} + k\mathbf{b} + l\mathbf{c})}{N(2J+1)(2K+1)(2L+1)} \\ &= \frac{(2J+1)(2K+1)(2L+1)\sum_1^N \mathbf{r}_i + (2K+1)(2L+1)\mathbf{a}(\sum_{j=-J}^{J} j) + ...}{N(2J+1)(2K+1)(2L+1)} \\ &= \mathbf{0} \end{aligned} \tag{C.11}$$

the the unit cell vectors. If we construct a vector (similar to Eq. (B.52) in B.6) of the N positions for the unit cell and the 3 unit cell parameters of dimension 3N+9, we form the displacement vector we need from crossing the position and unit cell vectors with some angular velocity vector as done in B.6 (Eq. (C.12)). Just as we have done in B.6, to form

$$\mathbf{u}^{r\omega} = (\mathbf{r}_1 \times \boldsymbol{\omega}, \mathbf{r}_2 \times \boldsymbol{\omega}, \mathbf{r}_3 \times \boldsymbol{\omega}, ..., \mathbf{r}_N \times \boldsymbol{\omega}, \mathbf{a} \times \boldsymbol{\omega}, \mathbf{b} \times \boldsymbol{\omega}, \mathbf{c} \times \boldsymbol{\omega}) \tag{C.12}$$

3 orthogonal vectors, we take the dot product of two displacement vectors formed with two different angular velocity vectors ω_j and ω_k and set the result equal to 0. Just as before if we convert the positions and unit cell vectors into matrices ($\mathbf{R}_i$, $\mathbf{A}$, $\mathbf{B}$, and $\mathbf{C}$ which perform the cross product when acting on the $\boldsymbol{\omega}$ vectors, we obtain Eq. (C.13). Just as before,

$$\mathbf{u}^{r\omega_j} \cdot \mathbf{u}^{r\omega_k} = \boldsymbol{\omega}_j^T \cdot \left(\sum_i^N \left(\mathbf{R}_i^T \cdot \mathbf{R}_i \right) + \mathbf{A}^T \cdot \mathbf{A} + \mathbf{B}^T \cdot \mathbf{B} + \mathbf{C}^T \cdot \mathbf{C} \right) \cdot \boldsymbol{\omega}_k. \tag{C.13}$$

the matrix in parentheses is symmetric and when diagonalized produces three orthogonal angular velocity vectors which produce three orthogonal displacement vectors when used in Eq. (C.12). The translation vectors are formed in the same way as B.6 and only the postions are translated (not the unit cell vectors). Shifting components of the unit cell vectors will create a net strain between adjacent images and so is not incuded. A Gram-schmidt procedure can then be used to orthonormalize the translation and Rotation vectors within this subspace.

BIBLIOGRAPHY

[1] Irgens, F. *Continuum Mechanics*; Springer-Verlag Berlin Heidelberg, 2008.

[2] Shintaku, H.; Nakagawa, T.; Kitagawa, D.; Tanujaya, H.; Kawano, S.; Ito, J. Development of piezoelectric acoustic sensor with frequency selectivity for artificial cochlea. *Sensors and Actuators A: Physical* **2010**, *158*, 183 – 192.

[3] Inaoka, T.; Shintaku, H.; Nakagawa, T.; Kawano, S.; Ogita, H.; Sakamoto, T.; Hamanishi, S.; Wada, H.; Ito, J. Piezoelectric materials mimic the function of the cochlear sensory epithelium. *Proceedings of the National Academy of Sciences* **2011**, *108*, 18390–18395.

[4] Mukherjee, N.; Roseman, R. D.; Willging, J. P. The piezoelectric cochlear implant: Concept, feasibility, challenges, and issues. *J. Biomed. Mater. Res.* **2000**, *53*, 181–187.

[5] Dagdeviren, C. et al. Conformal piezoelectric energy harvesting and storage from motions of the heart, lung, and diaphragm. *Proceedings of the National Academy of Sciences* **2014**, *111*, 1927–1932.

[6] Lu, B.; Chen, Y.; Ou, D.; Chen, H.; Diao, L.; Zhang, W.; Zheng, J.; Ma, W.; Sun, L.; Feng, X. Ultra-flexible Piezoelectric Devices Integrated with Heart to Harvest the Biomechanical Energy. *Scientific Reports* **2015**, *5*, 16065.

[7] Esashi, M.; Ono, T. From MEMS to nanomachine. *Journal of Physics D: Applied Physics* **2005**, *38*, R223–R230.

[8] Kim, K.; Guo, J.; Xu, X.; Fan, D. L. Recent Progress on Man-Made Inorganic Nanomachines. *Small* **2015**, *11*, 4037–4057.

[9] Kremer, F.; Skupin, H.; Lehmann, W.; Gebhardt, E.; Zentel, R. Ferroelectric liquid crystalline elastomers: from the analysis of the molecular dynamics to the design of nanomachines. *Macromol. Symp.* **2001**, *175*, 247–248.

[10] Jianhua Tong,; Tianhong Cui,; Peige Shao,; Liding Wang, Piezoelectric micromotor based on the structure of serial bending arms. *IEEE Transactions on Ultrasonics, Ferroelectrics, and Frequency Control* **2003**, *50*, 1100–1104.

[11] Kornbluh, R.; Pelrine, R.; Eckerle, J.; Joseph, J. Electrostrictive polymer artificial muscle actuators. Proceedings. 1998 IEEE International Conference on Robotics and Automation (Cat. No.98CH36146). 1998; pp 2147–2154 vol.3.

[12] Ribeiro, C.; Sencadas, V.; Correia, D. M.; Lanceros-Mndez, S. Piezoelectric polymers as biomaterials for tissue engineering applications. *Colloids and Surfaces B: Biointerfaces* **2015**, *136*, 46 – 55.

[13] Sodano, H. A.; Inman, D. J.; Park, G. Comparison of Piezoelectric Energy Harvesting Devices for Recharging Batteries. *Journal of Intelligent Material Systems and Structures* **2005**, *16*, 799–807.

[14] Elfrink, R.; Kamel, T. M.; Goedbloed, M.; Matova, S.; Hohlfeld, D.; van Andel, Y.; van Schaijk, R. Vibration energy harvesting with aluminum nitride-based piezoelectric devices. *Journal of Micromechanics and Microengineering* **2009**, *19*, 094005.

[15] Yang, J. *Analysis of Piezoelectric Devices*; WORLD SCIENTIFIC, 2006.

[16] McCallum, J. J. Piezoelectric devices for mass and chemical measurements: an update. A review. *Analyst* **1989**, *114*, 1173–1189.

[17] Cooper, M. A. et al. In *Piezoelectric Sensors*; O. S. Wolfbeis, A. J., C. Steinem, Ed.; Springer, 2007.

[18] Vijaya, M. S. *Piezoelectric Materials and Devices*; CRC Press, 2016.

[19] Schellin, R.; Hess, G.; Kuehnel, W.; Sessler, G. M.; Fukada, E. Silicon subminiature microphones with organic piezoelectric layers-fabrication and acoustical behavior. *IEEE Transactions on Electrical Insulation* **1992**, *27*, 867–871.

[20] Wei, H.; Wang, H.; Xia, Y.; Cui, D.; Shi, Y.; Dong, M.; Liu, C.; Ding, T.; Zhang, J.; Ma, Y.; Wang, N.; Wang, Z.; Sun, Y.; Wei, R.; Guo, Z. An overview of lead-free piezoelectric materials and devices. *J. Mater. Chem. C* **2018**, *6*, 12446–12467.

[21] Rybyanets, A. N. Porous Piezoelectric Ceramics - A historical overview. 2010 IEEE International Symposium on the Applications of Ferroelectrics (ISAF). 2010; pp 1–4.

[22] Uchino, K. *Advanced Piezoelectric Materials: Science and Technology 2nd ed.*; 2017.

[23] Yang, J. In *An Introduction to the Theory of Piezoelectricity*; David Y. Gao, I. K. R. T. R. W. Y., Ray W. Ogden, Ed.; Springer, 2005.

[24] Sessler, G. M. Piezoelectricity in polyvinylidenefluoride. *The Journal of the Acoustical Society of America* **1981**, *70*, 1596–1608.

[25] Kepler, R. G.; Anderson, R. A. Piezoelectricity and pyroelectricity in polyvinylidene fluoride. *Journal of Applied Physics* **1978**, *49*, 4490–4494.

[26] Broadhurst, M. G.; Davis, G. T.; McKinney, J. E.; Collins, R. E. Piezoelectricity and pyroelectricity in polyvinylidene fluorideA model. *Journal of Applied Physics* **1978**, *49*, 4992–4997.

[27] *IEEE Standard on Piezoelectricity*; The Institute of Electrical and electronics Engineers, Inc, 1988.

[28] Martin, R. M. Piezoelectricity. *Phys. Rev. B* **1972**, *5*, 1607–1613.

[29] Cohen, R. E. *Piezoelectricity*; Springer Berlin Heidelberg: Berlin, Heidelberg, 2008; pp 471–492.

[30] Wang, J. *Nanomachines*; Wiley-VCH, 2013.

[31] Ozin, G. A.; Manners, I.; Fournier-Bidoz, S.; Arsenault, A. Dream Nanomachines. *Adv. Mater.* **2005**, *17*, 3011–3018.

[32] Popov, V. L. Nanomachines: Methods to induce a directed motion at nanoscale. *Phys. Rev. E* **2003**, *68*, 026608.

[33] Pisani, C.; Maschio, L.; Casassa, S.; Halo, M.; Schtz, M.; Usvyat, D. Periodic local MP2 method for the study of electronic correlation in crystals: Theory and preliminary applications. *J. Comput. Chem.* **2008**, *29*, 2113–2124.

[34] Suo, Z.; Kuo, C.-M.; Barnett, D.; Willis, J. Fracture mechanics for piezoelectric ceramics. *Journal of the Mechanics and Physics of Solids* **1992**, *40*, 739 – 765.

[35] You, Y.-M. et al. An organic-inorganic perovskite ferroelectric with large piezoelectric response. *Science* **2017**, *357*, 306–309.

[36] Electroactive polymers: current capabilities and challenges. 2002.

[37] Pelrine, R.; Kornbluh, R.; Pei, Q.; Joseph, J. High-Speed Electrically Actuated Elastomers with Strain Greater Than 100%. *Science* **2000**, *287*, 836–839.

[38] Zhang, Q. M.; Li, H.; Poh, M.; Xia, F.; Cheng, Z.-Y.; Xu, H.; Huang, C. An all-organic composite actuator material with a high dielectric constant. *Nature* **2002**, *419*, 284–287.

[39] Marvin, C.; Quan, X.; Seebald, L.; Hutchison, G. Single-Molecule Piezoelectric Deformation: Rational Design from First-Principals Calculations. *J. Phys. Chem. C* **2013**, *117*, 16783–16790.

[40] Paturle, A.; Graafsma, H.; Sheu, H.-S.; Coppens, P.; Becker, P. Measurement of the piezoelectric tensor of an organic crystal by the x-ray method: The nonlinear optical crystal 2-methyl 4-nitroaniline. *Phys. Rev. B* **1991**, *43*, 14683–14691.

[41] DiBenedetto, S. A.; Frattarelli, D.; Ratner, M. A.; Facchetti, A.; Marks, T. J. Vapor phase self-assembly of molecular gate dielectrics for thin film transistors. *J. Am. Chem. Soc.* **2008**, *130*, 7528–7529.

[42] Facchetti, A.; Annoni, E.; Beverina, L.; Morone, M.; Zhu, P.; Marks, T. J.; Pagani, G. A. Very large electro-optic responses in H-bonded heteroaromatic films grown by physical vapour deposition. *Nature Mat.* **2004**, *3*, 910–917.

[43] Frattarelli, D.; Schiavo, M.; Facchetti, A.; Ratner, M. A.; Marks, T. J. Self-assembly from the gas-phase: design and implementation of small-molecule chromophore precursors with large nonlinear optical responses. *J. Am. Chem. Soc.* **2009**, *131*, 12595–12612.

[44] Johal, M. S.; Cao, Y. W.; Chai, X. D.; Smilowitz, L. B.; Robinson, J. M.; Li, T. J.; McBranch, D.; Li, D. Spontaneously Self-Assembled Polar Asymmetric Multilayers Formed by Complementary H-Bonds. *Chem. Mat.* **1999**, *11*, 1962–1965.

[45] Ward, M. D.; Raithby, P. R. Functional behaviour from controlled self-assembly: challenges and prospects. *Chem. Soc. Rev.* **2013**, *42*, 1619–1636.

[46] Zhu, P.; Kang, H.; Facchetti, A.; Evmenenko, G.; Dutta, P.; Marks, T. J. Vapor phase self-assembly of electrooptic thin films via triple hydrogen bonds. *J. Am. Chem. Soc.* **2003**, *125*, 11496–11497.

[47] Werling, K. A.; Hutchison, G. R.; Lambrecht, D. S. Piezoelectric Effects of Applied Electric Fields on Hydrogen-Bond Interactions: First-Principles Electronic Structure Investigation of Weak Electrostatic Interactions. *J. Phys. Chem. Lett.* **2013**, *4*, 1365–1370.

[48] Munn, R. W. Theory of piezoelectricity, electrostriction, and pyroelectricity in molecular crystals. *J. Chem. Phys.* **2010**, *132*.

[49] Riley, K. E.; ; Hobza*, P. Assessment of the MP2 Method, along with Several Basis Sets, for the Computation of Interaction Energies of Biologically Relevant Hydrogen Bonded and Dispersion Bound Complexes. *The Journal of Physical Chemistry A* **2007**, *111*, 8257–8263, PMID: 17649987.

[50] Hanwell, M. D.; Curtis, D. E.; Lonie, D. C.; Vandermeersch, T.; Zurek, E.; Hutchison, G. R. Avogadro: An advanced semantic chemical editor, visualization, and analysis platform. *J. Cheminformatics* **2012**, *4*, 17.

[51] Shao, Y. et al. Advances in molecular quantum chemistry contained in the Q-Chem 4 program package. *Molecular Physics* **2015**, *113*, 184–215.

[52] Becke, A. D. Densityfunctional thermochemistry. III. The role of exact exchange. *The Journal of Chemical Physics* **1993**, *98*, 5648–5652.

[53] Lee, C.; Yang, W.; Parr, R. Development of the Colle-Salvetti correlation-energy formula into a functional of the electron density. *Phys. Rev. B, Condens. Matt.* **1988**, *37*, 785–789.

[54] Vosko, S. H.; Wilk, L.; Nusair, M. Accurate spin-dependent electron liquid correlation energies for local spin density calculations: a critical analysis. *Canadian Journal of Physics* **1980**, *58*, 1200–1211.

[55] Stephens, P. J.; Devlin, F. J.; Chabalowski, C. F.; Frisch, M. J. Ab Initio Calculation of Vibrational Absorption and Circular Dichroism Spectra Using Density Functional Force Fields. *J. Phys. Chem.* **1994**, *98*, 11623–11627.

[56] Weigend, F.; Hser, M.; Patzelt, H.; Ahlrichs, R. RI-MP2: optimized auxiliary basis sets and demonstration of efficiency. *Chemical Physics Letters* **1998**, *294*, 143 – 152.

[57] Hehre, W. J. Self—Consistent Molecular Orbital Methods. XII. Further Extensions of Gaussian—Type Basis Sets for Use in Molecular Orbital Studies of Organic Molecules. *J. Chem. Phys.* **1972**, *56*, 2257.

[58] Hariharan, P. C.; Pople, J. A. The effect of d-functions on molecular orbital energies for hydrocarbons. *Chem. Phys. Lett.* **1972**, *16*, 217–219.

[59] Kabel, M.; Valdes, H.; Sherer, E. C.; Cramer, C. J.; Hobza, P. Benchmark RI-MP2 database of nucleic acid base trimers: performance of different density functional models for prediction of structures and binding energies. *Phys. Chem. Chem. Phys.* **2007**, *9*, 5000–5008.

[60] Dahlke, E. E.; Truhlar, D. G. Electrostatically Embedded Many-Body Correlation Energy, with Applications to the Calculation of Accurate Second-Order MllerPlesset Perturbation Theory Energies for Large Water Clusters. *Journal of Chemical Theory and Computation* **2007**, *3*, 1342–1348, PMID: 26633207.

[61] Dunning, T. H. Gaussian basis sets for use in correlated molecular calculations. I. The atoms boron through neon and hydrogen. *J. Chem. Phys.* **1989**, 1007–1023.

[62] Balabin, R. M. Enthalpy difference between conformations of normal alkanes: Intramolecular basis set superposition error (BSSE) in the case of n-butane and n-hexane. *The Journal of Chemical Physics* **2008**, *129*, 164101.

[63] Kendall, R. A.; Dunning, T. H.; Harrison, R. J. Electron affinities of the first-row atoms revisited. systematic basis sets and wave functions. *J. Chem. Phys.* **1992**, 6796–6806.

[64] Ramos-Cordoba, E.; Lambrecht, D. S.; Head-Gordon, M. Charge-transfer and the hydrogen bond: Spectroscopic and structural implications from electronic structure calculations. *Faraday Discuss.* **2011**, *150*, 345–362.

[65] Contreras-Garca, J.; Johnson, E. R.; Keinan, S.; Chaudret, R.; Piquemal, J.-P.; Beratan, D. N.; Yang, W. NCIPLOT: A Program for Plotting Noncovalent Interaction Regions. *J. Chem. Theory Comput.* **2011**, *7*, 625–632.

[66] Stewart, J. J. P. MOPAC: A semiempirical molecular orbital program. *Journal of Computer-Aided Molecular Design* **1990**, *4*, 1–103.

[67] Stewart, J. J. P. Optimization of parameters for semiempirical methods VI: more modifications to the NDDO approximations and re-optimization of parameters. *Journal of Molecular Modeling* **2013**, *19*, 1–32.

[68] Gale, J. D. GULP: A computer program for the symmetry-adapted simulation of solids. *J. Chem. Soc., Faraday Trans.* **1997**, *93*, 629–637.

[69] Gale, J. D.; Rohl, A. L. The General Utility Lattice Program (GULP). *Molecular Simulation* **2003**, *29*, 291–341.

[70] Lipscomb, G. F.; Garito, A. F.; Narang, R. S. An exceptionally large linear electrooptic effect in the organic solid MNA. *J. Chem. Phys.* **1981**, *75*, 1509–1516.

[71] Clark, R.; Romero, A.; Borbulevych, O.; Antipin, M.; Nesterov, V.; Timofeeva, T. 2-amino derivatives of 5-nitrophenylacetamide. *Acta crystallographica. Section C, Crystal structure communications* **2000**, *56 (Pt 3)*, 336–338.

[72] Seidler, T.; Stadnicka, K.; Champagne, B. In *SPIE Organic Photonics + Electronics*; Eich, M., Nunzi, J.-M., Jakubiak, R., Eds.; SPIE, 2013; p 88270Y.

[73] Greeley, J.; Stephens, I. E. L.; Bondarenko, A. S.; Johansson, T. P.; Hansen, H. A.; Jaramillo, T. F.; Rossmeisl, J.; Chorkendorff, I.; Norskov, J. K. Alloys of platinum and early transition metals as oxygen reduction electrocatalysts. *Nature Chem.* **2009**, *1*, 552–556.

[74] Shao, Y. et al. Advances in methods and algorithms in a modern quantum chemistry program package. *Phys. Chem. Chem. Phys. : PCCP* **2006**, *8*, 3172–3191.

[75] Komornicki, A.; McIver, J. W. An efficient abinitio method for computing infrared and Raman intensities: Application to ethylene. *J. Chem. Phys.* **1979**, *70*, 2014–2016.

[76] Quan, X.; Marvin, C. W.; Seebald, L.; Hutchison, G. R. Single-Molecule Piezoelectric Deformation: Rational Design from First-Principles Calculations. *J. Phys. Chem. C* **2013**, *117*, 16783–16790.

[77] Yamabe, T.; Tachibana, A.; Silverstone, H. J. Theory of the ionization of the hydrogen atom by an external electrostatic field. *Phys. Rev. A* **1977**, *16*, 877–890.

[78] Lanczos, C. Zur Intensittsschwchung der Spektrallinien in hohen elektrischen Feldern. *Zeitschrift fr Physik* **1931**, *68*, 204–232.

[79] Lanczos, C. Zur Theorie des Starkeffekts in hohen Feldern. *Zeitschrift fr Physik* **1930**, *62*, 518–544.

[80] Lanczos, C. Zur Verschiebung der Wasserstoffterme in hohen elektrischen Feldern. *Zeitschrift fr Physik* **1930**, *65*, 431–455.

[81] Baroni, S.; Giannozzi, P.; Testa, A. Green's-Function Approach to Linear Response in Solids Stefano. *Physical Review Letters* **1987**, *58*, 1861–1864.

[82] Baroni, S.; Giannozzi, P.; Testa, A. Elastic Constants of Crystals from Linear-Response Theory Stefano. *Phys Rev Lett* **1987**, *59*, 2662–2665.

[83] Gonze, X.; Allan, D. C.; Teter, M. P. Dielectric tensor, effective charges, and phonons in -quartz by variational density-functional perturbation theory. *Physical Review Letters* **1992**, *68*, 3603–3606.

[84] Hebbache, M. Elastic constants of group IV semiconductors : Microscopic theory. *Canadian Journal of Chemistry* **1997**, *458*, 453–458.

[85] Vanderbilt, D. Berry-phase theory of proper piezoelectric response. *J. Phys. Chem. Solids* **2000**, *61*, 147.

[86] Rogers, C. L.; Rappe, A. M. Geometric formulation of quantum stress fields. *Physical Review B - Condensed Matter and Materials Physics* **2002**, *65*, 1–8.

[87] Hamann, D. R.; Wu, X.; Rabe, K. M.; Vanderbilt, D. Metric tensor formulation of strain in density-functional perturbation theory. *Physical Review B - Condensed Matter and Materials Physics* **2005**, *71*.

[88] Erba, A. The internal-strain tensor of crystals for nuclear-relaxed elastic and piezoelectric constants: on the full exploitation of its symmetry features. *Phys. Chem. Chem. Phys.* **2016**, *18*, 13984–13992.

[89] Werling, K. A.; Griffin, M.; Hutchison, G. R.; Lambrecht, D. S. Piezoelectric Hydrogen Bonding: Computational Screening for a Design Rationale. *The Journal of Physical Chemistry A* **2014**, *118*, 7404–7410.

[90] E. Bright wilson, J., Jr.; Cross, P. C. *Molecular Vibrations: The Theory of Infrared and Raman Vibrational Spectra*; Dover Publications, Inc., 1980.

[91] Press, W. H.; Teukolsky, S. A.; Vetterling, W. T.; Flannery, B. P. *Numerical Recipes 3rd Edition: The Art of Scientific Computing*, 3rd ed.; Cambridge University Press: New York, NY, USA, 2007.

[92] Schlegel, H. B. Geometry optimization. *Wiley Interdisciplinary Reviews: Computational Molecular Science* **2011**, *1*, 790–809.

[93] Baker, J. Geometry optimization in Cartesian coordinates: Constrained optimization. *Journal of Computational Chemistry* **1992**, *13*, 240–253.

[94] Komornicki, A.; Jr., J. W. M. An efficient ab initio method for computing infrared and Raman intensities: Application to ethylene. *The Journal of Chemical Physics* **1979**, *70*, 2014–2016.

[95] Daniel, J. W.; Gragg, W. B.; Kaufman, L.; Stewart, G. W. Reorthogonalization and Stable Algorithms for Updating the Gram-Schmidt QR Factorization. *Mathematics of Computation* **1976**, *30*, 772–795.

[96] Ruhe, A. Numerical aspects of gram-schmidt orthogonalization of vectors. *Linear Algebra and its Applications* **1983**, *52-53*, 591 – 601.

[97] Wolfram Research, Inc., Mathematica 8.0. https://www.wolfram.com.

[98] MATLAB, *version 7.10.0 (R2010a)*; The MathWorks Inc.: Natick, Massachusetts, 2010.

[99] others,, et al. SciPy: Open source scientific tools for Python. 2001–; http://www.scipy.org/, [Online; accessed 4/06/2018].

[100] Humphrey, W.; Dalke, A.; Schulten, K. VMD – Visual Molecular Dynamics. *Journal of Molecular Graphics* **1996**, *14*, 33–38.

[101] Stone, J. *An Efficient Library for Parallel Ray Tracing and Animation*. M.Sc. thesis, Computer Science Department, University of Missouri-Rolla, 1998.

[102] Quan, X.; Marvin, C. W.; Seebald, L.; Hutchison, G. R. Single-Molecule Piezoelectric Deformation: Rational Design from First-Principles Calculations. *The Journal of Physical Chemistry C* **2013**, *117*, 16783–16790.

[103] Mulliken, R. S. Electronic Population Analysis on LCAOMO Molecular Wave Functions. I. *The Journal of Chemical Physics* **1955**, *23*, 1833–1840.

[104] Breneman, C. M.; Wiberg, K. B. Determining atom-centered monopoles from molecular electrostatic potentials. The need for high sampling density in formamide conformational analysis. *Journal of Computational Chemistry* **1990**, *11*, 361–373.

[105] Jensen, F. *Introduction to Computational Chemistry*; John Wiley & Sons, 2006.